


THE SCIENCE REPORTS OF GEA No. 2 (1992)

THE
SCIENCE REPORTS
OF
ECONOMIC GEOLOGY RESEARCH PROJECT
UNIVERSITY OF CONCEPCION

No. 2

JICA LIBRARY

J 1130246 [0]

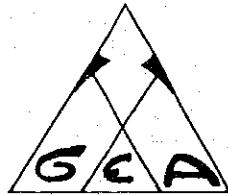
JAPAN INTERNATIONAL COOPERATION AGENCY
(1992)

704
661
J
RARY

JR

THE
SCIENCE REPORTS
OF
ECONOMIC GEOLOGY RESEARCH PROJECT
UNIVERSITY OF CONCEPCION

No. 2



JAPAN INTERNATIONAL COOPERATION AGENCY
(1992)

COPYRIGHT

1992

JAPAN INTERNATIONAL COOPERATION AGENCY

PRINTED BY

EDITORÁ ANÍBAL PINTO S.A.

Maipú 769, Concepción, Chile

PROGRAMA DE GEOLOGIA ECONOMICA APLICADA (GEA)

Universidad de Concepción

Casilla 4107, Concepción 3, Chile

JAPAN INTERNATIONAL COOPERATION AGENCY (JICA)

P. O. Box 216, 48th Floor, Shinjuku Mitsui Building

Nishi-Shinjuku 2-1-1, Shinjuku-ku, Tokyo 163, Japan

(All announcements related with this report should be
addressed to Japan International Cooperation Agency.)



1130246 [0]

Contents

Ore minerals and fluid inclusions from the gold and silver deposits of the Choquelimpie mine, northern Chile Mamoru Enjoji, Asahiko Sugaki, Guillermo Alfaro	1
Gold from Minas del Prado, Región del Biobío, Chile Nobutaka Shimada, Asahiko Sugaki and Guillermo Alfaro	25
Preliminary report on the epithermal gold deposit and ore genesis of the Las Palmas mine, Talca - Chile Arashi Kitakaze, Asahiko Sugaki and Guillermo Alfaro	31
Genesis of skarn ore deposits: A model of skarn-ore forming metasomatic reactions Kiyoshige Ochiai	41
K-Ar dating on rocks and minerals related to ore deposits in Chile (1) Asahiko Sugaki and Nobutaka Shimada	49
Study on the Guinier film reading and calculation method Arashi Kitakaze	57

ORE MINERALS AND FLUID INCLUSIONS FROM THE GOLD AND SILVER DEPOSITS OF THE CHOQUELIMPIE MINE, NORTHERN CHILE

Mamoru Enjoji*, Asahiko Sugaki**, Guillermo Alfaro***

* Institute of Geoscience, University of Tsukuba, Tsukuba, Japan. ** Kadan 4-30-503, Aoba, Sendai 980, Japan. *** Instituto GEA, Universidad de Concepción, Casilla 4107, Concepción 3, Chile

Introduction

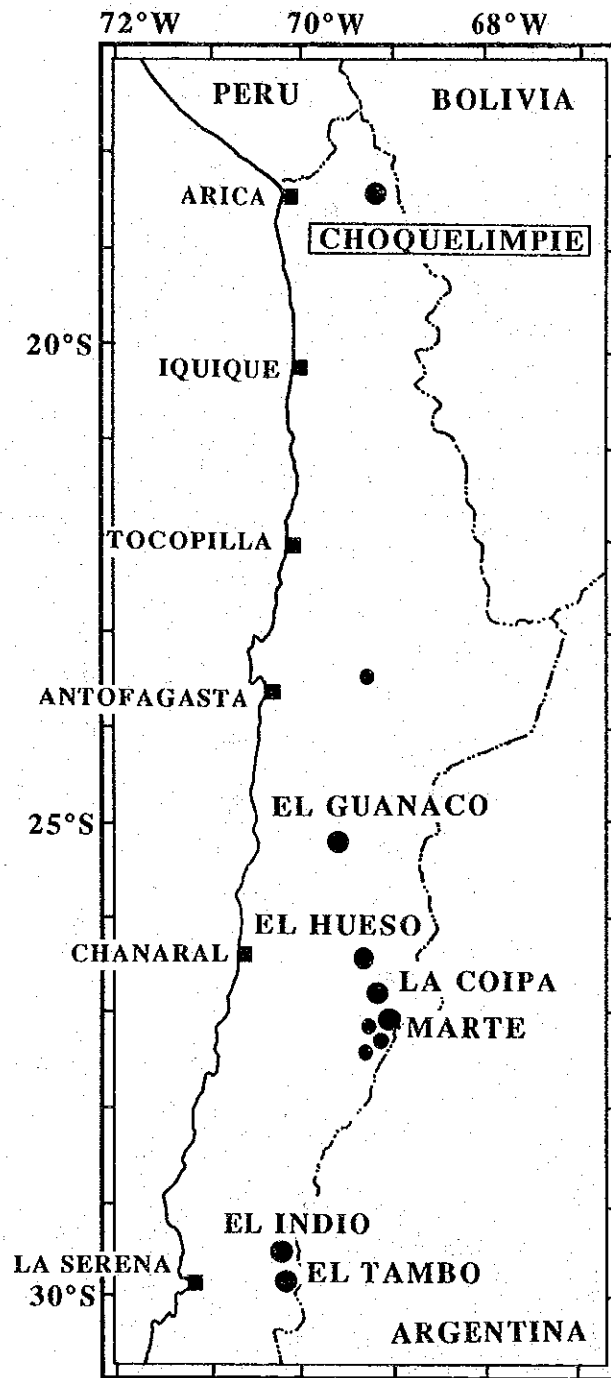
The ore deposits of the Choquelimpie mine (long. 69°16'42"W, lat. 18°18'19"S), northern Chile, are of a series of epithermal deposits which lie in a belt located at an altitude of 3,600 to 4,900 m above sea level and running parallel to the Pacific coast from Perú to Bolivia, and to central Chile (Fig. 1). These epithermal deposits lie east of, and parallel to, a belt of older porphyry copper deposits.

The ore deposits of the Choquelimpie mine are characterized by gold and silver bearing quartz veins and impregnations in the volcanic complex of the late Miocene age. Hydrothermal brecciation, propylitic alteration, silicification and sericitic alteration are characteristic in the mining area. Major ore minerals are sphalerite, galena, pyrite, and argentite. Thus the ore deposits are characterized by the Ag-Au-Pb-Zn assemblage, which contrasts with the Au-Ag-Cu-As provinces of central Chile (Camus, 1985).

In this paper, ore description, mineral chemistry, and fluid inclusion features are preliminarily reported, along with short discussions on the mineralization of gold and silver deposits of the mine.

Geology and ore deposits

Geology around the mine were reported in detail by Gröpper *et al.* (1991). According to the study, the geology and ore deposits of the Choquelimpie mine are briefly cited as follows.



- principal producing mines
- mines in construction

Fig. 1. Index map showing the locality of the Choquelimpie mine, with the epithermal gold and silver deposits in northern Chile.

Choquelimpie is a stratovolcano of roughly circular shape which coalesces to the northeast with the Ajoja twin stratovolcano of similar age. The Choquelimpie volcano measures 4.5 km northeast by 3.8 km northwest. Its central area is deeply eroded, exposing the mineralized core. (See Figs. 2 and 3 in Gröpper *et al.*, 1991) Cerro Choquelimpie, the principal host to mineralization, reaches 4,860 m above sea level. The paleovolcanoes are of andesitic to dacitic composition. The volcanic stratigraphy suggests a rather homogeneous magma production of intermediate composition during the life of the volcano. The K/Ar age of the Choquelimpie volcano has been dated at 6.60 ± 0.20 Ma.

Lithologies at Cerro Choquelimpie, the location of the present open pit, have been hydrothermally altered to such an extent that their original composition and texture are often difficult to determine. The bulk of the rock was originally an andesitic feldspar porphyry, perhaps an intrusive dome. The principal host rocks to mineralization are brecciated and silicified feldspar porphyries, polymictic breccias, and late hydrothermal breccias. These rocks have evolved from the porphyry by successive superimposed phases of brecciation, argillic and siliceous alteration, and supergene leaching. (See Figs. 4 to 7 in Gröpper *et al.*, 1991)

Ore zones are widely distributed in eruptive centers of the caldera. Here, mineralization (> 0.5 g/T Au) occurs beyond the area more than 2 km in diameter (Fig. 2).

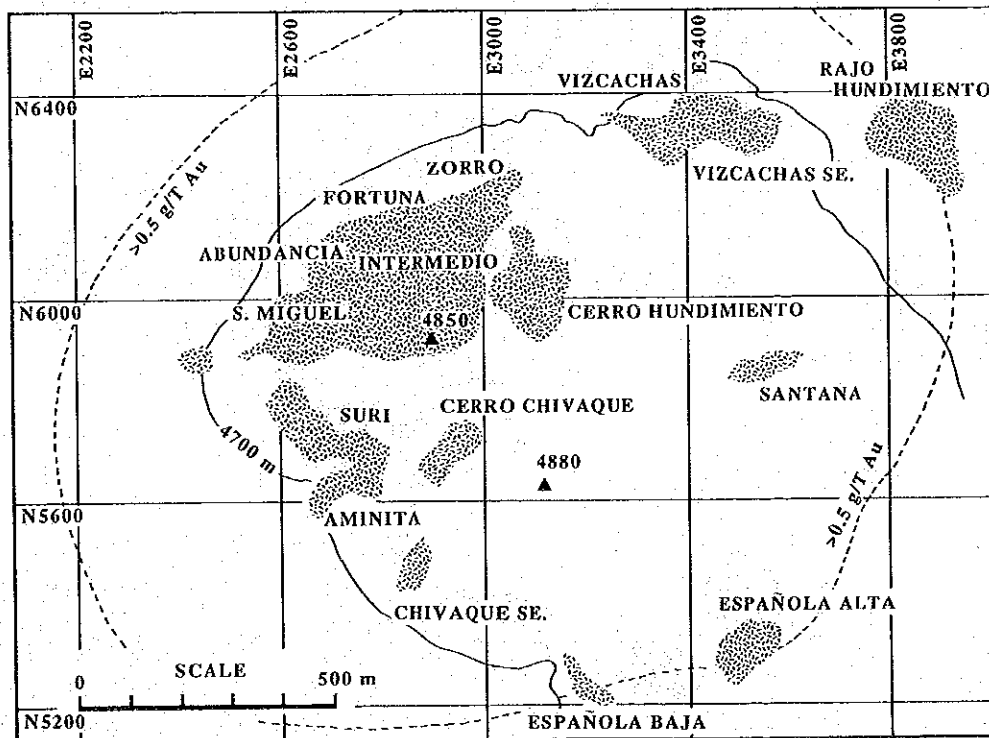


Fig. 2. Location map of the ore deposits in the Choquelimpie mine. (Data after the Sociedad Contractual Minera Vilacollo, 1992)

The main gold-silver mineralization occurs in a fault-controlled belt 2 km long, trending N60°E, and with a maximum width of 200 m. The mineralized breccia bodies typically measure several tens of meters on surface, extend to 150 m depth, and are of irregular shape, often elongated along N60°E and N30°W directions. The principal mineralized bodies are, from west to east, the San Miguel breccia, the Choquelimpie Main orebody comprising five major breccias (Intermedio, Fortuna, Abundancia, Inglesa, and Zorro), the Cerro Hundimiento breccia, the Vizcachas orebody, and the Rajo Hundimiento orebody. Parallel to the main trend occur the mineralized bodies of Animita, Chivaque, and Santana, and is the mineralized Española trend (Fig. 2).

Two types of mineralization have been worked at Choquelimpie, siliceous veins and hydrothermal breccia bodies. All present production comes from oxidized breccia bodies.

Mineralized veins are arranged in a crudely radial pattern around the central sector of the stratovolcano. The veins are generally subvertical and vary in width from a few mm to 1 m, but locally widen to form siliceous breccia bodies several meters thick. The veins were worked to 80 m below the adit level. The vein consists of quartz, kaolinite, barite, pyrite, sphalerite, galena, copper minerals, and silver-bearing minerals including tetrahedrite, pyrargyrite, polybasite, minor argentite, and native silver. Typical richer ore assayed 6.7 percent lead, 0.9 percent copper, 6.6 percent zinc, 490 g/t silver, and traces of gold (in 1926).

Mineralization

Gröpper et al. (1991) reported the mineralization of the district, citing the study by Bisso (1989, unpublished data), as follows.

Hypogene mineralization at Choquelimpie took place in several stages. Stage I caused widespread propylitic and sericitic alterations and produced a calcite-chlorite-pyrite-hematite assemblage. Stage II produced impregnation and fine veining of the central feldspar porphyries with pyrite, sphalerite, galena, and chalcopryrite, and perhaps a little pyrrhotite, some magnetite and arsenopyrite. Kaolinization overprinted the earlier sericite, and barite is an additional gangue mineral. Stage III includes native gold and silver, electrum, argentite, and minerals identified as aramayoite [$\text{Ag}_2\text{S} \cdot (\text{Sb}, \text{Bi})_2\text{S}_3$] and schapbachite [$\text{PbS} \cdot \text{Ag}_2\text{S} \cdot \text{Bi}_2\text{S}_3$], associated with plentiful pyrite and lesser enargite, tennantite, stibnite, and traces of lead sulfosalts. The accompanying gangue minerals are barite, quartz, chalcedony, kaolinite, dickite, and a small amount of alunite. Stages II and III are associated with episodes of hydrothermal brecciation and silicification. Native gold occurs in interstices, or as inclusions within the sulfide, particularly enargite, and sulfosalts, such as liveingite [$5\text{PbS} \cdot 4\text{As}_2\text{S}_3$] and guanajuatite [Bi_2Se_3], but also in stibnite, forming particles of generally less than 10 μm but which reach

a maximum of 70 μm . Late tabular barite, a few millimeters to 6 cm in size, formed in open spaces contemporaneously with stage III. Stage IV appears to be the latest event associated with the hypogene mineralization process, forming rare, narrow, subvertical veins along fractures trending N75°E which clearly cut the hydrothermal breccias. The veins contain near-massive sphalerite and minor galena but no pyrite and carry both gold and silver values. It is not known whether these post-breccia veins are of the same age as the veins formerly exploited around the periphery of the breccia bodies.

Oxidation of the deposits is thought to have been caused by weathering although some observations have kept open the possibility that part of the abundant jarosite associated with the stage III gold-silver mineralization may be hypogene origin. The oxidized zone normally contains traces of unoxidized pyrite encapsulated in silicified breccia fragments. The native gold and silver are more common in the oxide than in the sulfide zone. Native gold occurs as inclusions of up to 20 μm in goethite and jarosite, which is concentrated in fractures and open spaces in siliceous breccias. Traces of gold selenides have been observed in a goethite matrix. Chlorargyrite is found exclusively in the oxide zone and there are also arsenic-, lead-, and copper-bearing silver sulfosalts.

The mineralization stages of the deposits by Gröpper *et. al.*, (1991) are summarized in Table 1.

Table 1. Mineralization stage of the hypogene process and the minerals in the Choquelimpie mine.

	Mineralization	Ore minerals	Gangue minerals
Stage I	propylitic alteration sericitic alteration	pyrite hematite	calcite chlorite
Stage II	hydrothermal brecciation silicification impregnation fine veining	pyrite sphalerite galena (Ag-) chalcopyrite pyrrhotite magnetite arsenopyrite gold and silver	barite kaolinite
Stage III	hydrothermal brecciation silicification	native Au and Ag electrum argentite aramayoite $\text{Ag}_2\text{S} \cdot (\text{Sb}, \text{Bi})_2\text{S}_3$ schapbachite $\text{PbS} \cdot \text{Ag}_2\text{S} \cdot \text{Bi}_2\text{S}_3$ pyrite enargite tennantite stibnite lead-sulfosalts	barite quartz chalcedony kaolinite dickite alunite
Stage IV	narrow, subvertical veins	sphalerite galena gold and silver	

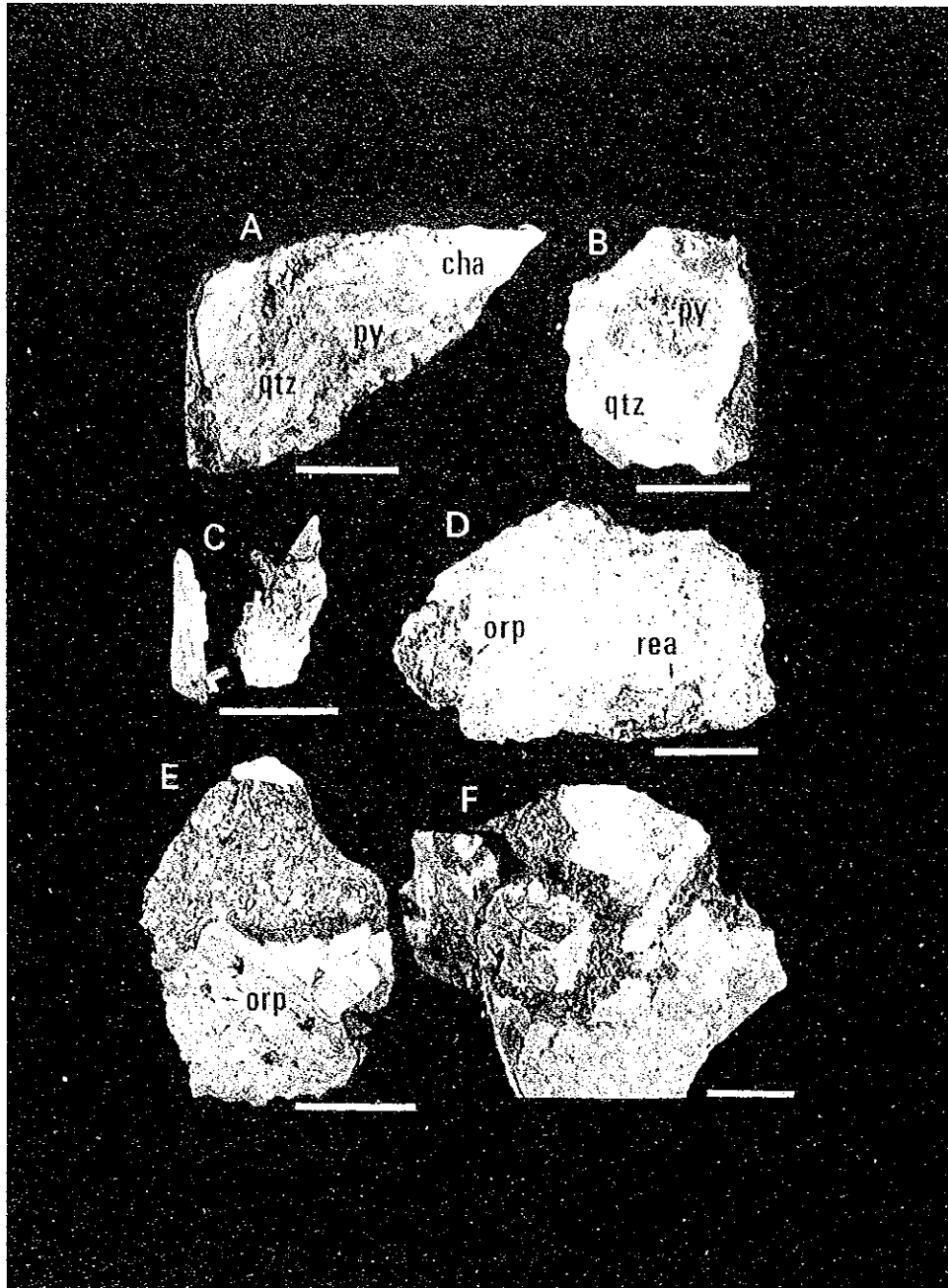


Fig. 3. Photographs showing the typical ore samples from the Choquelimpie mine. A: Massive aggregates of sulfides (py), quartz (qtz), and chalcedonic quartz (cha). Sample CL#1. B: Aggregates of quartz (qtz) and pyrite (py) grown over an altered host rock. Sample CL#2. C: Film of silver sulfide? (arrow) on the surface of single quartz crystals. Sample CL#3. D: Realger (rea) and orpiment (orp) in cavities of altered feldspar porphyry. Sample CL#4. E: Crystals of orpiment (orp) in the cavities of kaolinized rock in altered feldspar porphyry. Sample CL#5. F: Sulfide network vein in brecciated altered rock. Sample CL#6. Scale bars show 2 cm.

Description of ore

Several samples were collected from the mining site. As mentioned above, the mineralization of the deposits is rather complicated by the overprinting events of alteration and mineralization over several stages. Hence, unfortunately, the mineralization stages of each sample are not always certain. Here the samples collected during the survey are briefly described. Photographs of some typical ores are shown in Figs. 3 and 4.

Sample CL#1 (Figs. 3A and 4B) is from the Choquelimpie orebody at N-6070, E-2780, N705 bench. The rock consists of aggregates of massive sulfide (mainly fine grained pyrite) and several crystals of quartz (3-5 mm in width), grown over chalcedonic quartz. The ore is drusy and loose.

Sample CL#2 (Fig. 3B) is from the Choquelimpie orebody at N-6800, E-2810, N715 bench. The rock consists of aggregates of coarse grained quartz and pyrite, grown over the altered feldspar porphyry.

Sample CL#3 (Fig. 3C) is from the Suri orebody at N-5740, E-2640, N710 bench. It is several single crystals of quartz, 20-30 mm in length. On the surface of the crystal, film of silver sulfide (?) can be recognized.

Sample CL#4 (Figs. 3D and 4E) is from the Vincachas orebody at N-6350, E-3340, N685 bench. Realger and orpiment occur in cavities of highly altered feldspar porphyry. Sulfide veins occur in small scale. Boundaries between sulfide veins and the host rock are highly ambiguous by the silicification of the rock. Pyrite and other sulfide minerals disseminate in the rock.

Sample CL#5 (Fig. 3E) is from the Vincachas orebody at N-6350, E-3340, N685 bench. Aggregates of orpiment crystals occur in the cavities of kaolinized rock in altered feldspar porphyry. Relics of phenocrysts in the latter are also kaolinized.

Sample CL#6 (Fig. 3F) is from the Choquelimpie orebody at N-6090, E-2780, N705 bench. Network veins (~10 mm in width) cut brecciated altered rock. Relics of phenocrysts can be recognized though ambiguous. Veins are composed from pale-colored sphalerite, galena, and barite crystals.

Samples CL01 and CL06-10 are mineralized ore in the highly altered host rock (feldspar porphyry), from the Choquelimpie orebody (Intermedio and Cerro Hundimiento).

Sample CL01 (Fig. 4A) is from the Choquelimpie orebody (Intermedio). It is an altered and siliceous igneous rock, in which sulfide minerals (mainly pyrite) occur. The phenocrysts of the igneous rock (feldspar porphyry) are soluted or replaced seriously. Most cavities are filled with euhedral pyrite and quartz, often with small amounts of barite. Pyrite is octahedral in shape. It is considered to belong stage I mineralization by the classification of Gröpper et al. (1991). The cavities are up to 1 mm in length. They might have formed by the solution and/or replacement of the phenocrysts of feldspar porphyry. It is

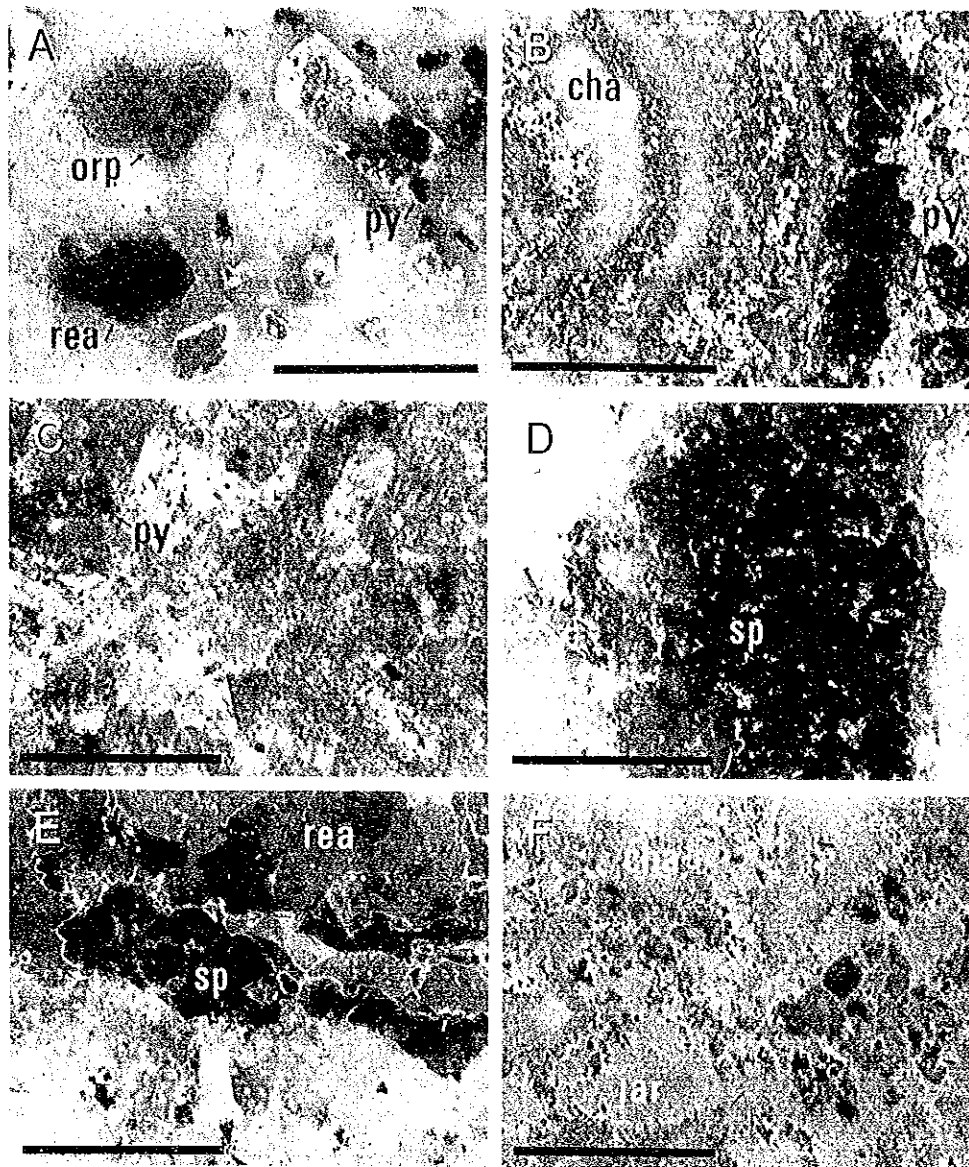


Fig. 4. Photomicrographs showing the typical ore samples (on polished surfaces). A: Altered and mineralized feldspar porphyry. Cavities are filled with euhedral pyrite (py), quartz, orpiment (orp), and realgar (rea). Sample CL01-A. B: A part of vein composed of chalcedonic quartz (cha) and sulfides (py) showing crustal banding structure. Sample CL#1-A. C: A part of brecciated ore impregnated by pyrite (py). Sample CL09-C. D: A veinlet composed of sphalerite (sp) and galena in silicified feldspar porphyry. Sample CL07-1A. E: A veinlet composed of sphalerite (sp) and realgar (rea), in altered feldspar porphyry. Sample CL#4-A. F: Fine aggregates of jarosite (jar) and other minerals filling the cavities of the rock altered by chalcedonic quartz (cha). Sample CL10-3A. Scale bars show 2 mm.

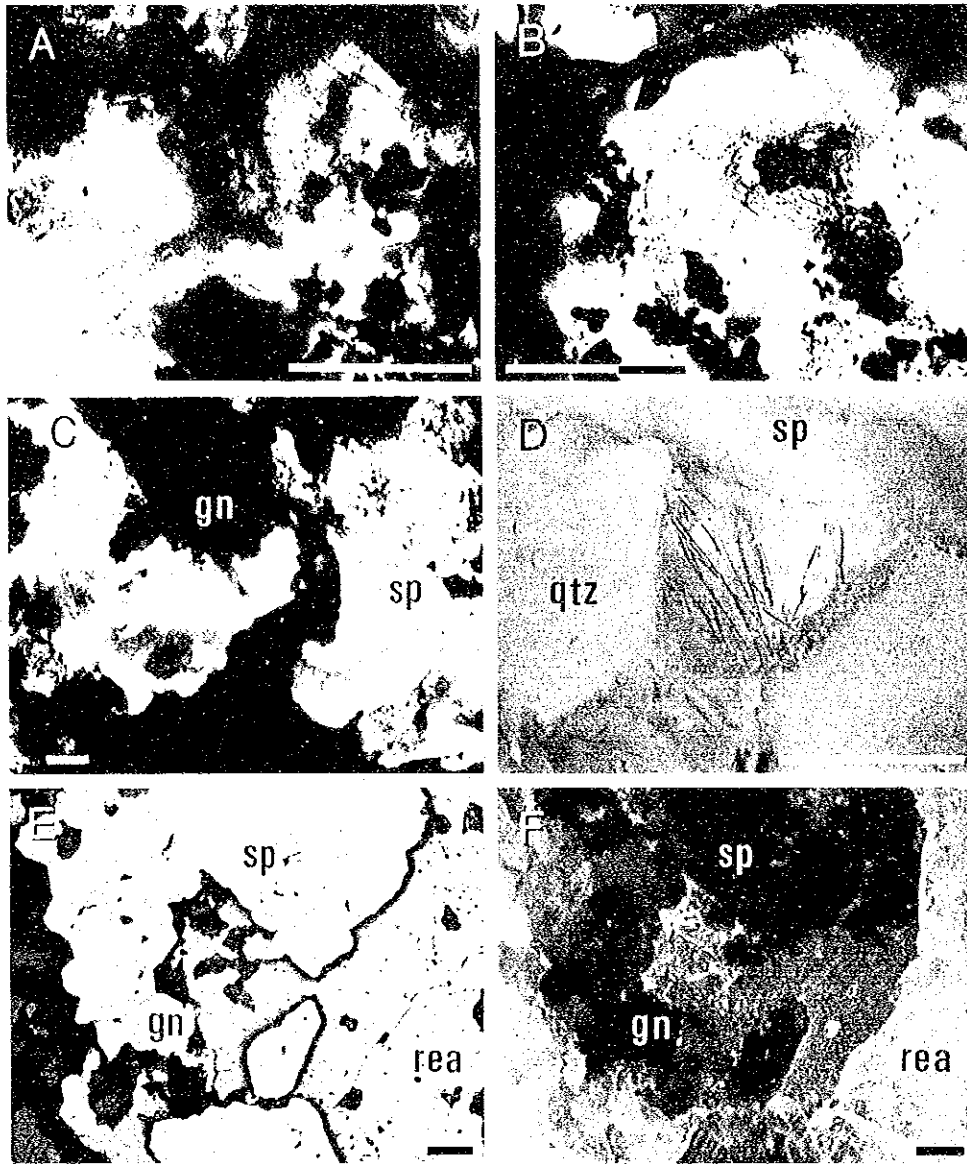


Fig. 5. Photomicrographs showing several textures of the ore. A: «Disease» texture by chalcopyrite? in sphalerite. Sample CL08-B. B: Linear arrangements of minute needles and dots (chalcopyrite?) in sphalerite. Sample CL08-B. C: Color zoning of sphalerite (sp) associated with galena (gn). Sample CL#1-B. D: Needles of hematite (arrow) in sphalerite overgrown to quartz (qtz). Sample CL07-1A. E and F: Realgar (rea) filling cavities between sphalerite (sp) and galena (gn). Sample CL#4-A. A-C; by transmitted, open nicol. D and F; by reflected light, crossed nicols. E, by reflected light, open nicol. Scale bars show 100 μm .

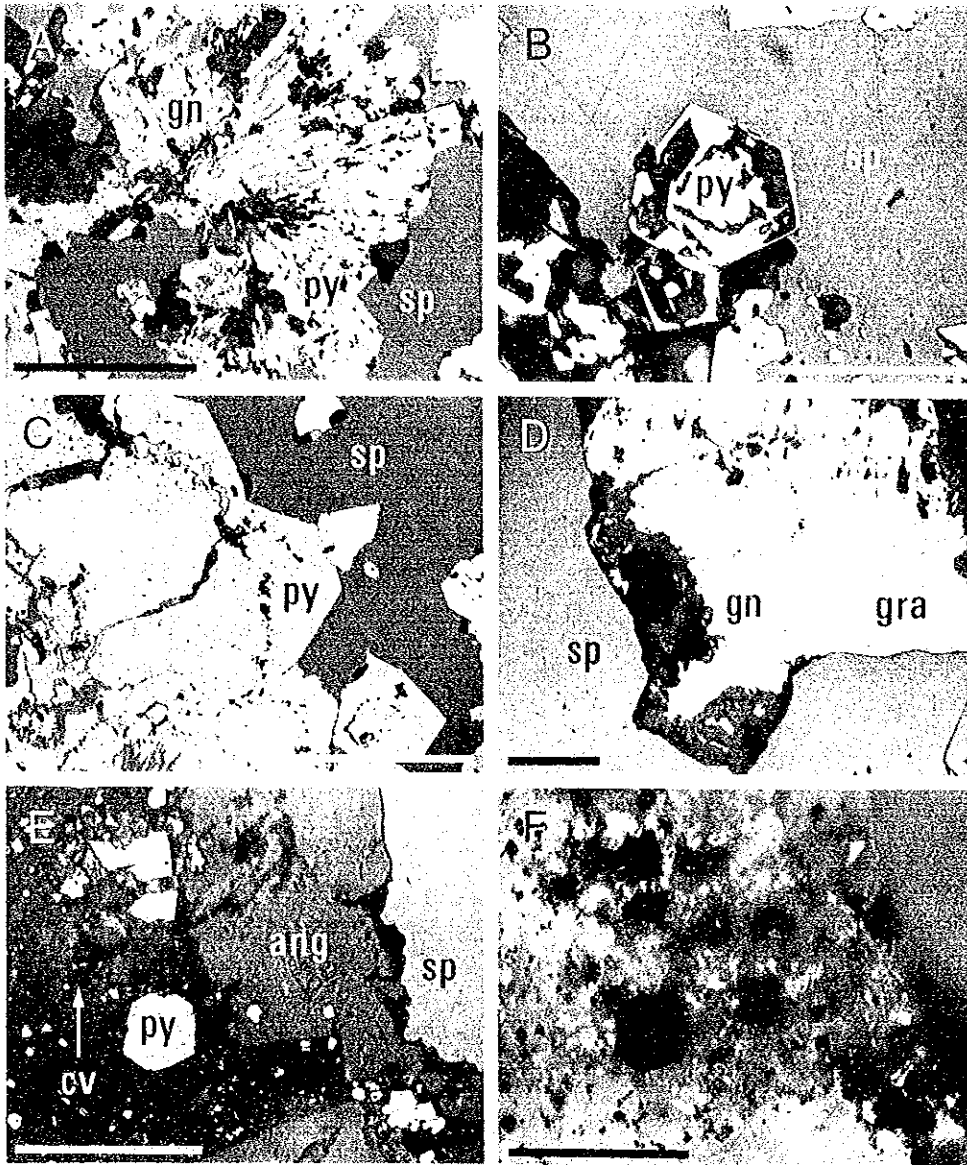


Fig. 6. Photomicrographs showing the modes of occurrence of sulfide and sulfate minerals. Sample CL08-2A. A: Galena (gn) replaced by pyrite (py). Later sphalerite (sp) fills the cavity. B: Skeletonized pyrite (py), in sphalerite (sp). C: pyrite (py) overgrown on galena. Cavities are filled with later sphalerite (sp). D: Galena (white, gn) and gratonite? (grayish white, gra) associated with sphalerite (sp). E and F: anglesite (ang) in cavities of rock with disseminated sphalerite (sp). Left to pyrite (py) crystal, covellite (cv) is recognized. A-E; by reflected light, open nicol. F; by reflected light, crossed nicols. Scale bars show 100 μm .

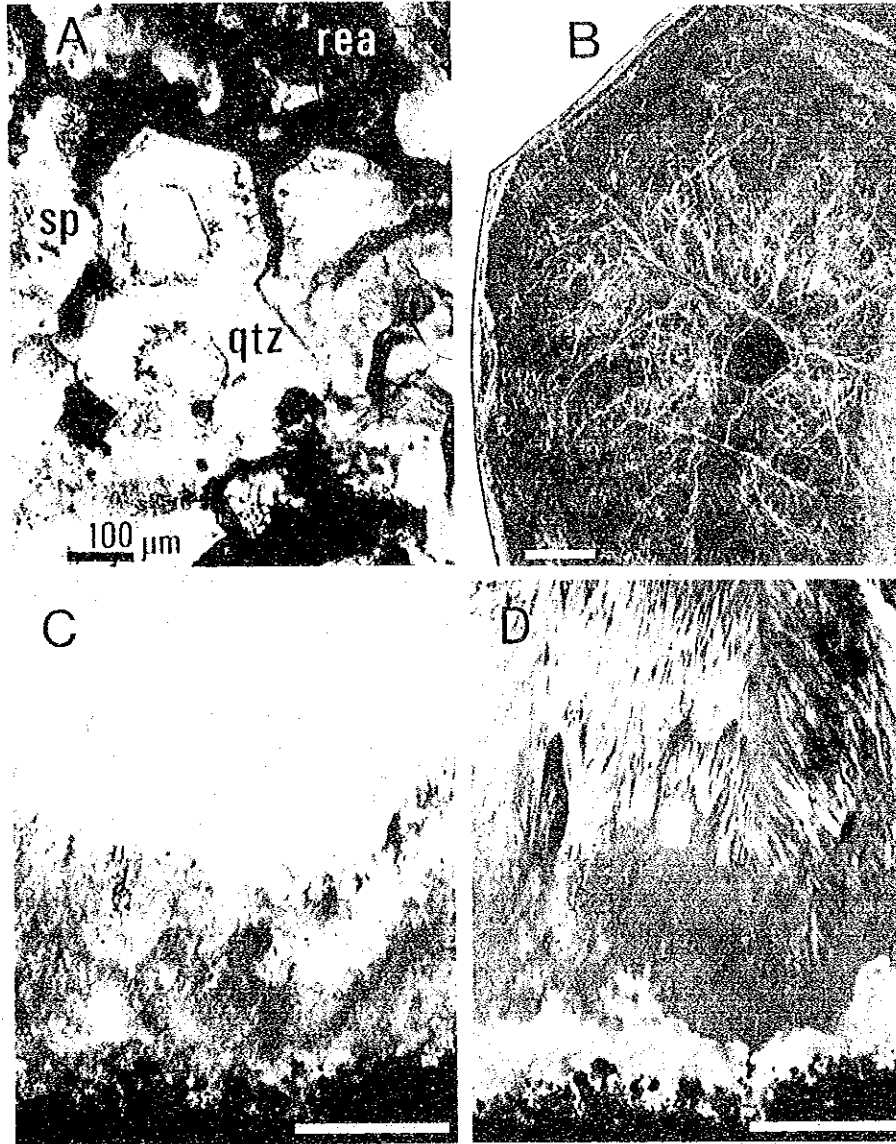


Fig. 7. Photomicrographs showing the growth pattern of quartz. A: Growth zoning in euhedral quartz (qtz) associated with sphalerite (sp) and realgar (rea) in druse. Sample CL#4-B. B: Growth zoning in quartz. The planes parallel to the crystal faces are composed of primary fluid and dusty inclusions. Irregular, curved, lace-like pattern are by the alignments of fluid inclusions of secondary and/or pseudosecondary in origin. Sample CL#1-B. C and D: A root portion of quartz crystal showing a dendritic texture by dusty inclusions and the aggregates of orientated fine grained quartz in one "single" crystal. Sample CL#2-A. A-C; by transmitted light, open nicol. D; by transmitted light, crossed nicols. B-D; scale bars show 500 μm .

overprinted by the later mineralization. Clayey minerals, pale yellowish brown in color, fill the interstice of the rock.

Sample CL06 is from the Choquelimpie orebody (Cerro Hundimiento). It is aggregates of large barite crystals, up to 15 mm in length and 1-3 mm in width, formed in a vug of the fine grained altered rock composed mainly of jarosite. Surfaces of barite are coated with fine grained black minerals.

Sample CL07 (Fig. 4D) is from the Choquelimpie orebody (Cerro Hundimiento). Veins and veinlets composed of sphalerite, galena and pyrite occur in silicified feldspar porphyry impregnated by pyrite. Boundaries between veins and the host rock are ambiguous.

Sample CL08 is from the Choquelimpie orebody (Cerro Hundimiento). It is network veins composed of sulfide minerals, in the brecciated altered rock. The host rock is highly altered and very loose, light gray in color. Relics of phenocrysts can be recognized as white spots up to about 2 mm in size. Veins and veinlets are irregular in shape, 0-1 cm in width, partly drusy. Major sulfide minerals are sphalerite (pale brown) and pyrite. Gangue minerals such as quartz and/or barite cannot be seen. Boundaries between veins and the host rock are fairly sharp.

Sample CL09 (Fig. 4C) is from the Choquelimpie orebody (Cerro Hundimiento). Black colored minerals (aggregates of pyrite, marcasite, sphalerite and galena) impregnate in brecciated and altered feldspar porphyry (dark gray in color). Quartz and barite also occur in small cavities.

Sample CL10 (Fig. 4F) is from the highly oxydised zone of the Choquelimpie orebody (Intermedio). Fine aggregates of jarosite and other minerals fill the cracks and cavities of feldspar porphyry, which altered to the rock rich in chalcedonic quartz. Minute holes are embedded by crystals of barite(?).

Mineralogy

Major sulfide minerals in the ore are pyrite, sphalerite, and galena, with a small amount of marcasite, realgar, orpiment, chalcopyrite, pyrrotite and Pb-As sulfosalts. Besides, hematite, goethite and native gold are found. Quartz, barite jarosite and anglesite are common gangue minerals.

Pyrite: Throughout the ores, pyrite is the most common ore mineral. It distributes widely as impregnated forms in the rock, and fills the cavities and veins. In silicified rocks, the phenocrysts of the rock is a good reservoir for pyrite (Fig. 4A). Usually pyrite fills the cavities formed by dissolution of phenocrysts, where most of pyrite has octahedron in shape, and grows from the border of the cavity with quartz. Those cavities are often filled with minute crystals of arsenic sulfides such as orpiment and realgar. In the highly altered rock, pyrite impregnates as minute crystals in matrix.

The modes of occurrence of pyrite in the vein are rather complicated. Major

pyrite is scattered in veins as euhedral crystals which may be relics of the crystals of the earlier stage. Often pyrite is highly skeletonized in sphalerite (Fig. 6B) or shows neck-ring like lace. Some crystals of pyrite replace sphalerite and/or galena and lead sulfosalt, and filled by later sphalerite (Figs. 6A and 6C). Pyrite also fills the vein as crustal banding with chalcedonic quartz (Fig. 4B).

Sphalerite: Sphalerite is the major ore mineral and fills cavities and veins. Usually it is transparent and shows honey color. It is associated well with galena and lead sulfosalts. Minute spots or dots of galena, chalcopryrite and pyrrhotite are included. In some cases, sphalerite has a "disease" texture by chalcopryrite(?) (Figs. 5A and 5B). Weak color zoning (brown to reddish brown) is commonly recognized (Fig. 5C). Often sphalerite includes fine aggregates of needle or fibrous minerals (Fig. 5D), which might be hematite from the optical and chemical characteristics.

Table 2. Representative chemical compositions of sphalerite from the ore deposit of the Choquelimpie mine

Anal. no.	21	23	24	27	37	38	39	mean
Zn wt.%	66.57	66.26	66.87	67.33	66.71	66.01	66.38	66.59
Fe	0.96	0.42	0.31	0.00	0.12	0.01	0.10	0.27
Cd	0.44	0.67	0.30	0.40	0.09	0.35	0.10	0.34
Pb	0.00	0.25	0.35	0.52	0.00	0.00	0.01	0.16
S	32.67	32.39	32.54	32.61	33.07	32.99	32.40	32.67
Total	100.63	99.99	100.36	100.87	99.99	99.35	98.98	
Zn atom.%	49.47	49.72	49.96	50.16	49.66	49.45	50.06	49.78
Fe	0.84	0.37	0.27	0.00	0.10	0.00	0.09	0.24
Cd	0.19	0.29	0.13	0.17	0.04	0.15	0.04	0.14
Pb	0.00	0.06	0.08	0.12	0.00	0.00	0.00	0.04
S	49.51	49.56	49.56	49.54	50.20	50.40	49.81	49.80

Chemically sphalerite is almost pure ZnS, and has 0.0-1.0 mole % FeS and 0.0-0.3 mole % CdS. In some samples, a small amount of Mn is detected. Representative chemical compositions of sphalerite, obtained by EPMA analyses, are listed in Table 2.

Galena: Galena occurs as small grains, associated well with Pb-As sulfosalts, and the both with sphalerite (Figs. 5C, 5E, 6A and 6D). Often galena is replaced and overgrown by pyrite (Fig. 6D).

Galena consists of almost pure PbS. Small amount of Zn may be derived from small inclusion of sphalerite in the mineral. 0.1-0.3 atomic % of Cd, and 0.0-0.3 atomic % of Fe are also included. Often small amounts of rhenium are detected. Representative chemical compositions of galena are listed in Table 3.

Pb-As sulfosalt: Three kinds of Pb-As sulfosalt are recognized. The minerals

occur as small grains in galena. Optically they are very similar with each other. One is greyish white with greenish tint, and shows weak pleochroism (Fig. 6D). It shows weak but distinct anisotropism. Polishing hardness is nearly the same as galena. No inner reflection can be seen. It consists of 32.2-33.1 atomic % of Pb, 12.6-13.3 atomic % of As, 53.5-54.9 atomic % of S, hence, resemble to gratonite $[9\text{PbS} \cdot 2\text{As}_2\text{S}_3]$ chemically (Table 4). Often small amounts of rhenium are detected.

One is optically resemble to galena and gratonite(?). It is also greyish white with greenish tint, slightly darker than gratonite. It shows weak anisotropism.

Table 3. Representative chemical compositions of galena from the ore deposit of the Choquelimpie mine

Anal. no.	8	11	12	16	18	30	31	mean
Pb wt.%	85.99	86.76	85.23	86.00	85.06	86.94	86.32	86.04
Zn	0.01	0.00	0.01	0.02	0.49	0.06	0.04	0.09
Fe	0.01	0.12	0.06	0.04	0.09	0.06	0.00	0.05
Cd	0.18	0.17	0.09	0.07	0.08	0.30	0.10	0.14
S	13.51	13.49	13.70	13.39	13.57	13.79	13.59	13.58
Total	99.70	100.54	99.09	99.52	99.29	101.13	100.05	
Pb atom.%	49.52	49.66	48.93	49.75	48.67	49.13	49.48	49.31
Zn	0.01	0.00	0.01	0.04	0.89	0.10	0.07	0.16
Fe	0.02	0.25	0.12	0.09	0.19	0.12	0.00	0.11
Cd	0.19	0.18	0.10	0.08	0.09	0.31	0.10	0.15
S	50.26	49.91	50.84	50.04	50.16	50.34	50.35	50.27

Table 4. Representative chemical compositions of Pb-As sulfosalt A from the ore deposit of the Choquelimpie mine.

Anal. no.	2	3	13	28	29	41	42	mean
Pb wt.%	70.84	70.87	72.13	72.83	70.58	70.80	71.15	70.78
As	9.79	10.37	10.18	10.48	10.10	10.39	10.45	10.56
Zn	0.05	0.34	0.15	0.12	0.05	0.81	0.22	0.23
Fe	0.01	0.01	0.00	0.02	0.03	0.00	0.01	0.01
Cd	0.12	0.15	0.23	0.14	0.09	0.16	0.20	0.15
S	18.12	18.39	18.11	18.57	18.60	18.19	18.33	18.41
Total	98.94	100.14	100.79	102.17	99.45	100.35	100.37	
Pb atom.%	32.88	32.24	33.06	32.73	32.21	32.19	32.40	32.18
As	12.56	13.05	12.90	13.02	12.75	13.06	13.16	13.26
Zn	0.08	0.49	0.22	0.17	0.07	1.17	0.32	0.34
Fe	0.02	0.02	0.00	0.04	0.04	0.01	0.01	0.06
Cd	0.10	0.13	0.19	0.11	0.08	0.13	0.17	0.13
S	54.35	54.07	53.63	53.93	54.85	53.45	53.94	54.08

Table 5. Representative chemical compositions of Pb-As sulfosalts B (Anal. no. 6) and C (Anal. no. 7) from the ore deposit of the Choquelimpie mine

Anal. no.	6	7
Pb wt. %	69.06	56.06
As	12.65	20.27
Fe	0.00	0.04
Cd	0.12	0.05
S	19.15	22.55
Total	100.98	98.97
Pb atom. %	30.29	21.72
As	15.35	21.72
Fe	0.00	0.06
Cd	0.09	0.04
S	54.28	56.47

It consists of 21.7 atomic % of Pb, 21.7 atomic % of As, and 56.5 atomic % of S, hence, near to dufrenoyite [$2\text{PbS} \cdot \text{As}_2\text{S}_3$] in chemical composition (Table 5, Anal. no. 7). However, the optical properties of the minerals are slightly different from the data reported in previous articles. Therefore, there is a possibility that the mineral is unreported face of the Pb-As sulfosalts.

The other is very similar to gratonite(?). The optical property is so similar

Table 6. Representative chemical compositions of realgar from the ore deposit of the Choquelimpie mine

Anal. no.	32	34	35	36	mean
As wt. %	67.93	66.82	67.15	65.30	66.80
Zn	0.64	1.61	1.20	1.66	1.28
Cd	0.04	0.04	0.01	0.02	0.03
S	31.17	31.34	31.21	31.72	31.36
Total	99.78	99.81	99.57	98.70	
As atom. %	48.01	47.09	47.47	46.21	47.19
Zn	0.52	1.30	0.97	1.35	1.04
Cd	0.02	0.02	0.01	0.01	0.02
S	51.45	51.59	51.55	52.44	51.76

that it is difficult to distinguish under the microscope. It consists of 30.3 atomic % of Pb, 15.4 atomic % of As, and 54.3 atomic % of S (Table 5, Anal. no. 6). Therefore, it is near to $[4\text{PbS} \cdot \text{As}_2\text{S}_3]$. Up to present, the name is not known. Though it is not certain by the small size, there is a possibility that the mineral is also an unreported phase of the Pb-As sulfosalts.

Chalcopyrite and pyrrhotite: Chalcopyrite and pyrrhotite are found as small dots in sphalerite. Some of them might form the disease texture in sphalerite.

Realgar: Realgar is the products in the vug or small hole produced in the small cavity of the phenocrysts of the host igneous rock (Figs. 3D, 4D, 4E, 5E and 5F). Often it grow up to 1 centimeter in length. It is reddish yellow to yellow in color. The polishing surface is slightly rough by the soft hardness (H=1.5). It consists of 52.5-53.2 atomic % of As and 45.0-46.8 atomic % of S, and 1.2-2.1 atomic % of Zn is also included. Zn contents may be derived from minute sphalerite often visible in the mineral. Representative chemical compositions of realgar are listed in Table 6.

Table 7. Representative chemical compositions of orpiment from the ore deposit of the Choquelimpic mine

Anal. no.	43	44	45	46	47	48	50	mean
As wt.%	59.96	60.24	59.42	60.65	60.04	60.60	60.10	60.14
Zn	0.04	0.00	0.01	0.00	0.03	0.00	0.00	0.01
Cd	0.01	0.00	0.08	0.00	0.00	0.05	0.04	0.03
S	39.74	39.82	39.33	39.88	39.66	39.67	40.82	39.85
Total	99.75	100.06	98.84	100.53	99.73	100.32	100.96	
As atom.%	39.23	39.30	39.25	39.43	39.31	39.53	38.65	39.24
Zn	0.03	0.00	0.01	0.00	0.02	0.00	0.00	0.01
Cd	0.00	0.00	0.03	0.00	0.00	0.02	0.02	0.01
S	60.74	60.70	60.70	60.57	60.66	60.45	61.33	60.74

Orpiment: Orpiment is also the products in the vug or small hole produced in the small cavity of the phenocrysts of the host igneous rock (Figs. 3E, 4A and 5F). Often it grow up to 1 centimeter in length. It is reddish yellow in color. The polishing surface is also rough by the soft hardness (H=1.5), having minute cracks by the cleavage of the specimen (Fig. 9F). Representative chemical compositions of realgar are listed in Table 7.

Anglesite: Anglesite has been recognized only under the microscope. It occurs in matrix of the brecciated and altered ore with sphalerite (Figs. 6E and 6F). Chemical analysis shows that it is almost pure anglesite.

Native gold: Native gold, or electrum, is recognized as tiny grains (less than 2 μm) in aggregates of jarosite. Unfortunately, the grains large enough for the

EPMA analyses are not found yet. From the color it is considered to be rich in gold contents.

Quartz and Barite : Both minerals are found in the small cavity of the phenocrysts of the host igneous rock as small crystals, and in drusy veins as large crystals. Quartz often shows a clear growth zoning (Figs. 7A and 7B) and numerous healed cracks (Fig. 7B) occupied by various types of inclusions. The root portion of quartz crystals often shows the aggregation of fine fibrous crystal (Figs. 7C and 7D). These patterns probably show the rapid growth of the crystal. Barite is usually transparent crystal, with a growth zoning composed of various kinds of minute inclusions. Often it is as large as several centimeters.

Hematite: Hematite is found as needle or as small dots in sphalerite (Fig. 5D). The diameter of the needle is often smaller than 1 μm . Hematite also occurs on the surface of barite crystals.

Jarosite: Jarosite fills the cavities in altered feldspar porphyry (Fig. 4F). It is yellowish brown in color, and composed of aggregates of fine crystals. It occurs in the highly oxidized ore, filling cracks or vugs of the host rock.

Fluid inclusion

Fluid inclusions were observed in quartz, sphalerite, barite, and realgar. Some are primary in origin judging from the modes of occurrence such as an arrangement to the euhedral crystal plane and a scattered presence without any spacial relationship with the other inclusions.

In quartz: In an euhedral crystal of quartz, 4 mm in width and 18 mm in length (Sample CL#3-A), several types of fluid inclusions are observed. In the root part of the single crystal, there are many small inclusions on the curved planes which construct network or honeycomb structure (Fig. 8E). They consist of liquid and gas phases (Fig. 8F). The volume ratio of the liquid to the fluid inclusion (filling degree) is 70-80 vol.%. Though they are very small and highly irregular in shape, their modes of occurrence suggest that these inclusions are primary in origin.

At the central part, the crystal has a few but large gaseous fluid inclusions. They distribute on planes which are parallel to the present crystal face with other crystal aggregates of clayey minerals (Fig. 8C). This is also strong criterion for the primary origin. Filling degree is less than 5 vol.% (Fig. 8D).

In the zone near to the crystal face or at the summit part of the crystal, primary inclusions arranged in a growth plane (Fig. 8A). Filling degree of the fluid inclusions is more than 75 vol.% (Fig. 8B).

Thus, the features of the fluid inclusions suggest the history during the growth of the single crystal of quartz; from the rapid growth in dilute solution at the beginning, via the growth in gaseous condition, to the slow growth in liquid

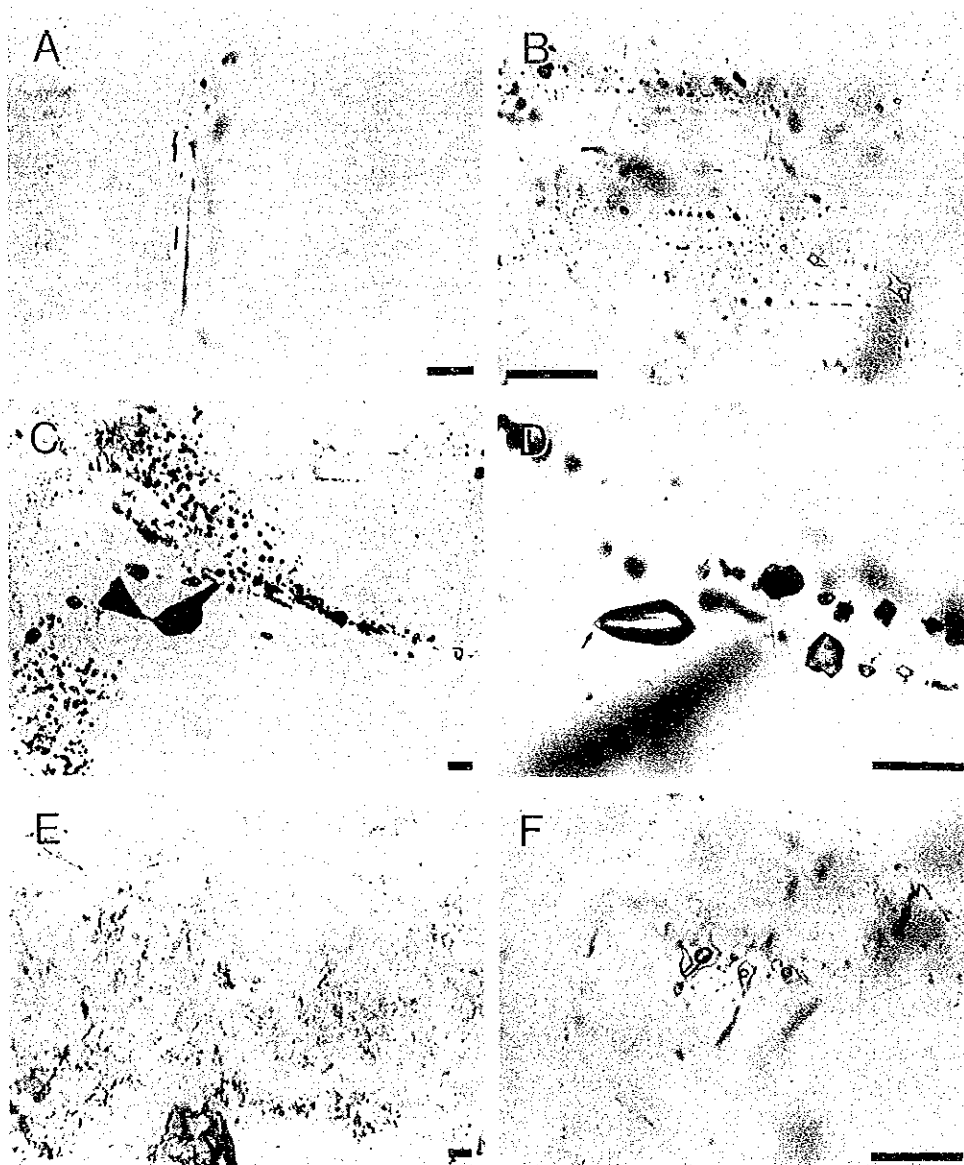


Fig. 8. Photomicrographs of fluid inclusions in a single quartz crystal. A and B: Fluid inclusions at the summit part of the crystal, distributing on the plane parallel to the euhedral crystal face. C: Fluid inclusions at the central part of the crystal. They show the growth banding, parallel to the euhedral crystal face, with other crystal aggregates of clayey minerals (black dots). Central two large inclusions were destroyed during the sample preparation. D: Fluid inclusions in C, composed of essentially gaseous phase with small amount of liquid phase (arrow). E: Fluid inclusions at the root part of the crystal. They distribute on the curved planes of network or honeycomb structure. F: A group of fluid inclusions in E. Sample CL#3-A. Scale bars show 100 μm .

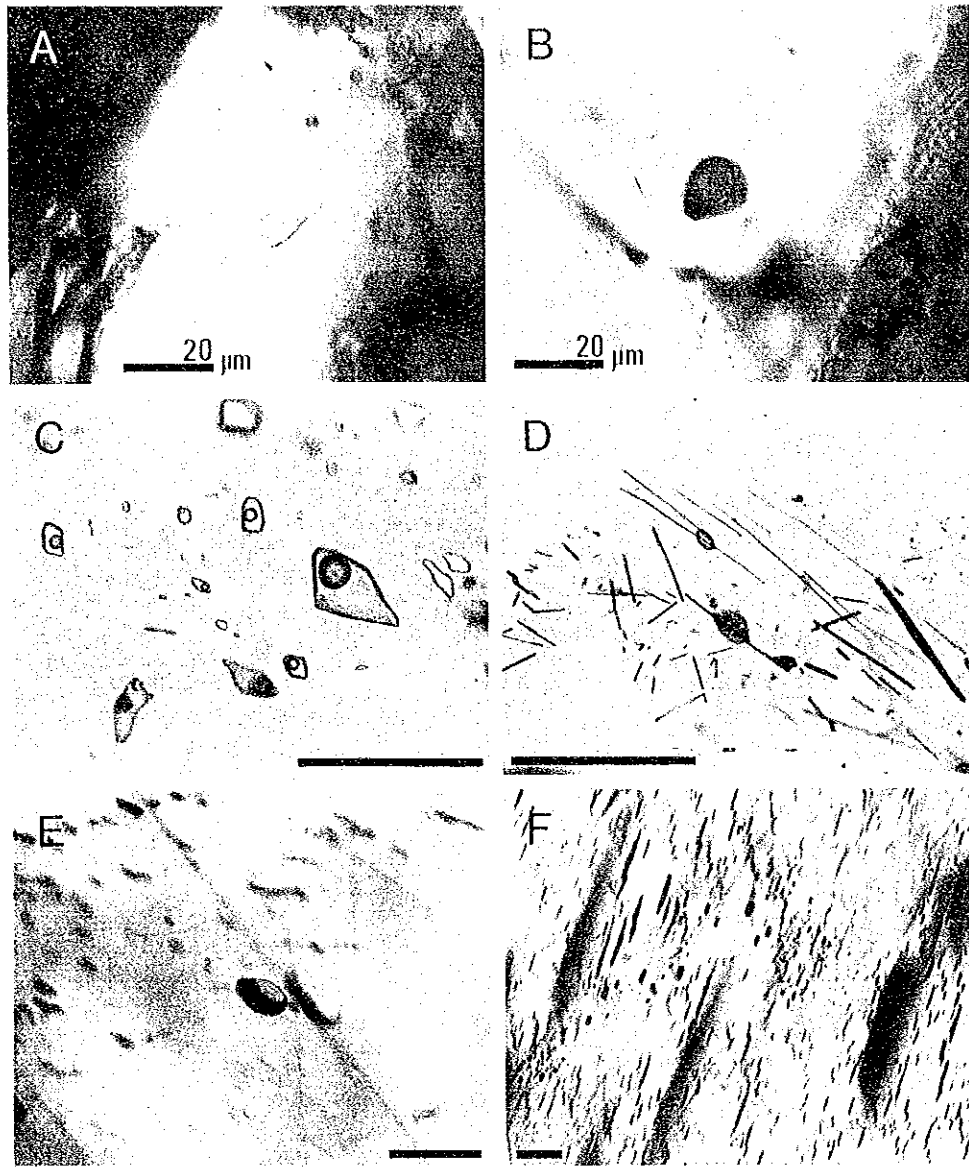


Fig. 9. Photomicrographs of fluid inclusions in other minerals. A and B: Primary fluid inclusions in sphalerite. Many fluid inclusions in sphalerite look like solid opaque minerals. Sample CL#6-B. C: Two-phase fluid inclusions in barite. Sample CL06-A. D: Fibrous to needle-like crystals as solid inclusions in barite, which often accompanied with fluid inclusions. Sample CL06-A. E: A fluid inclusion in orpiment, having a negative tabular shape. Phase component is not certain by the high refractive index of the host mineral. Sample CL#5-B1. F: Arrangement of the fluid inclusions in orpiment. Minute cracks, parallel to the cleavage plane, are difficult to avoid during polishing. Sample CL#5-B1. C-F; scale bars show 100 μm .

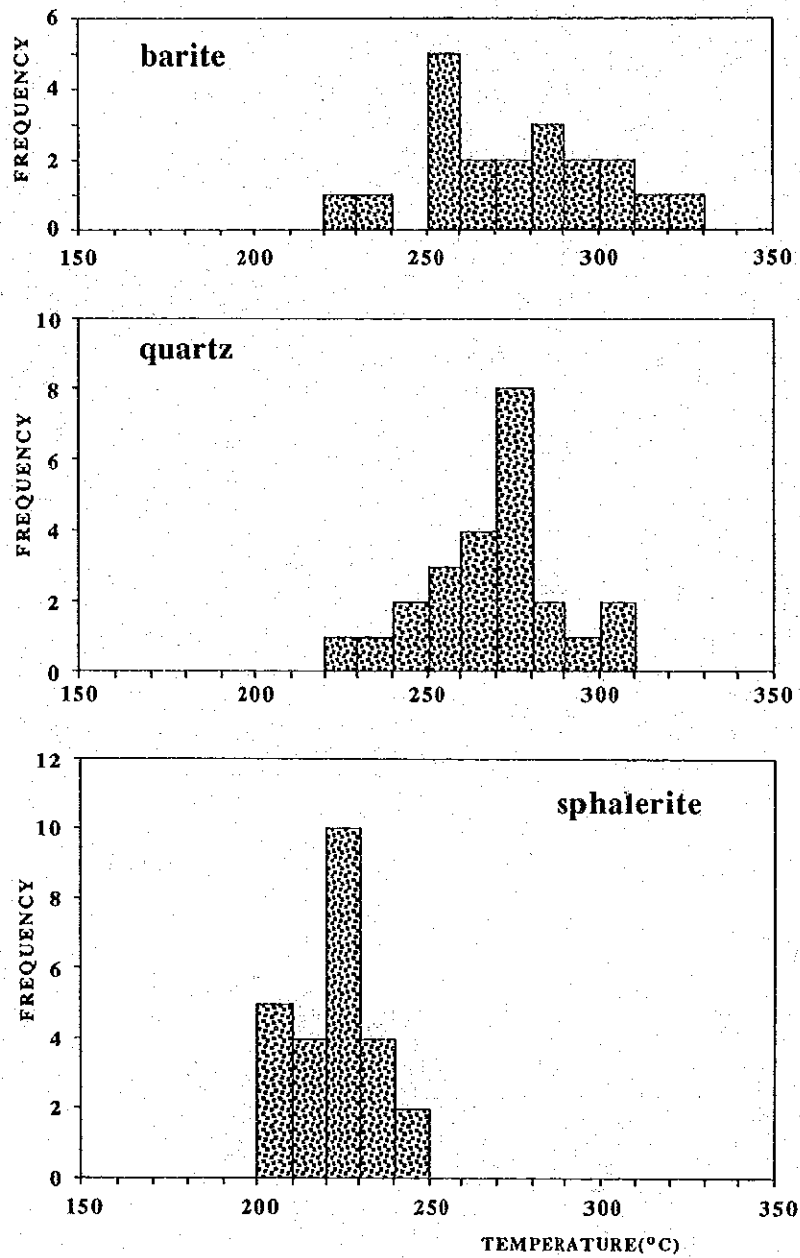


Fig. 10. Homogenization temperatures of fluid inclusions in barite, quartz, and sphalerite from the Choquelimpie mine.

dominant condition at the later stage. Mineral forming media might be largely changed during the stage of mineralization.

Gröpper *et al.* (1991) reported the coexisting of two types of primary inclusions, one rich in vapor (<25% liquid) and one rich in liquid (<20% vapor), in quartz from a breccia matrix at Animita, suggesting that the sample was formed under boiling conditions. As the necking down of fluid inclusions is very common phenomena, it is very difficult to conclude whether the boiling was occurred or not, even if the fluid inclusions having the different filling degrees coexist. The presence of the inclusions having different modes of filling in one crystal, however, suggests that the presence of "boiling in a broad sense" occurred during the mineralization. Similar phenomena were also reported by Nakayama and Enjoji (1987) for the gold-silver vein of the Nebazawa mine, central Japan.

Fluid inclusions in quartz homogenize in a range of 310-220°C (Fig. 10). However, there are many fluid inclusions which have very small filling degree (gaseous inclusions) and whose homogenizing temperature could not be measured. Homogenization temperatures are in good agreement with the values (305-213°C) obtained by Gröpper *et al.* (1991). The salinities estimated from depression of the freezing temperatures are very low, 1.5-0 wt.% (NaCl equiv.). The data are slightly lower than those (4.5-0.5 wt.%) given by Gröpper *et al.* (1991).

Throughout the observation, fluid inclusions containing halite crystals as solid phases and those containing liquid carbon dioxide at room temperature are not found. Often fluid inclusions contain solid crystals as small grains or fibrous minerals. From the modes of occurrence, however, they might be trapped minerals at the time of formation of fluid inclusions. Rather they might contribute for the formation of the fluid inclusions.

In sphalerite: Sphalerite occurs with the other sulfides and sulfosalts, which are closely related to the formation of gold and silver. Fluid inclusions composed of liquid and vapor phases are often found in pale colored sphalerite (Fig. 9A). However, many inclusions look like opaque minerals by the high refractive index of the mineral (Fig. 9B). Fluid inclusions in sphalerite homogenize in fairly narrow range of 250-200°C (Fig. 10).

In barite: Many and fairly large fluid inclusions in barite show negative crystal shapes (Fig. 9C). They consist of liquid and vapor phases in various volume ratios. Even fluid inclusions without vapor are also included. Fibrous solid crystals are often included. Small amounts of liquid are trapped with the solid (Fig. 9D). Fluid inclusions containing halite crystals as solid phases are not found.

As the result, fluid inclusions in barite homogenize in wider range (Fig. 10). However, the data from many inclusions having obviously higher homogenization temperatures, or very low ones, even one-phase liquid inclusions at room temperature, are not shown here.

The presence of the fluid inclusions with various filling degrees, is one of the evidence showing the boiling phenomena at the time of the mineral formation. However, the wide presence of the phenomena in barite crystal have been considered to be curious to the investigators. Roedder (1984) reported the uncertainty of the use of the fluid inclusions in barite as the study of mineral forming media, because of the wide range in the homogenization temperatures of the mineral. Enjoji (1975) also reported the similar phenomena for the fluid inclusions in barite from the kuroko deposits of the Fukazawa mine, northern Japan. The feature of the fluid inclusions in barite crystals should be treated carefully.

In realgar: Fluid inclusions are also found in realgar. Some may be primary in origin (Fig. 9E), from the modes of occurrence. However, it is very difficult to know the phase constituents, because of its high refractive index. Most of the inclusions in realgar may consist of vapor dominant phase by the observation from various directions.

Concluding remarks

Already Gröpper et al. (1991) reported the features of ore deposits of the Choquelimpie mine. The present results are generally similar to those obtained by them. Some additional informations are obtained in this study. From the modes of occurrence of the ore-forming minerals, their chemical compositions, and features of fluid inclusions was following results are preliminarily obtained on the mineralization at the Choquelimpie mine.

(1) Ores in the mine are aggregates of veins and veinlets, and impregnation into feldspar porphyry. The phenocrysts of the rock, mainly feldspar, were soluted, and replaced by pyrite and quartz, often by sphalerite, galena, realgar and orpiment.

(2) Sphalerite is the major ore mineral in impregnated ore and veins. It is pale brown in color. Color zoning and "disease" texture by chalcopyrite? are often observed. Needles of hematite are also recognized in sphalerite. Sphalerite include 0-1.5 mole % FeS. Small amounts of Mn and Re are detected.

(3) Galena is well accompanied with sphalerite. It includes 0.1-0.3 atomic % of Cd. Gratonite(?) $[9\text{PbS} \cdot 2\text{As}_2\text{S}_3]$ is well associated with galena. Dufrenoyite(?) $[2\text{PbS} \cdot \text{As}_2\text{S}_3]$ and unknown mineral $[4\text{PbS} \cdot \text{As}_2\text{S}_3]$ are also recognized.

(4) Electrum occurs as minute grains in jarosite. However, they are very small (less than $2 \mu\text{m}$) and not enough to analyze by EPMA.

(5) Orpiment and realgar are common as the impregnation and film vein forming minerals. Anglesite occurs as fissure filling minerals of the later stage.

(6) Fluid inclusions in sphalerite, quartz, and barite were observed. They

consist of liquid and vapor phases. Essential gaseous inclusions are also included, especially in the middle stage of the growth of quartz. Thus, boiling phenomena in a broad sense might have occurred during the formation of the ore deposits. Fluid inclusions containing liquid carbon dioxide or solid phases as halite are not found.

(7) The homogenization temperature of fluid inclusions in sphalerite, quartz, and barite are in the ranges of 250-200° C, 310-220° C, and 330-220° C, respectively. The salinities of inclusion fluids in quartz, estimated from depression of the freezing temperature, are very low, 1.5-0 wt.% (NaCl equiv.)

Acknowledgments

The authors wish to express their gratitude to Mr. J. H. Akkerman of the Sociedad Contractual Minera Vilacollo for his invaluable guidance and explanation in the field survey at the mine. Present research was done as a part of activities of Project GEA (Geología Económica Aplicada, Universidad de Concepción, Chile) financially supported by JICA (Japan International Cooperation Agency).

References

- Camus, F. (1985) : Geología de los yacimientos epitermales de oro en Chile y posible modelo idealizado. in *Geología y Recursos Minerales de Chile, Tomo II* (Eds. J. Frutos, R. Oyarzun and M. Pincheira), Universidad de Concepción, 923, 653-689 (in Spanish with English abstract)
- Enjoji, M. (1975) : Fluid inclusions in barite from the kuroko deposit of the Fukazawa mine, Japan. in *Report on the Project of the Mineral Paragenesis and the Formation Condition of the Hydrothermal Ore Deposits of the Neogene Tertiary, Japan*, 13-19 (in Japanese).
- Gröpper, H., Calvo, M., Crepsio, H., Bisso, C. R., Cuadra, W. A., Dunkerley, P.M., and Aguirre, E. (1991) : The epithermal gold-silver deposit of the Choquelimpic, Northern Chile. *Econ. Geol.*, 86, 1206-1221.
- Nakayama, E., and Enjoji, M. (1985) : Gold and silver bearing quartz vein of the Nebazawa mine, Central Japan. in *Gold and Silver Ores in Japan. Vol. 3, Nippon Kogyokai*, 228, 89-112 (in Japanese)
- Roedder, E., 1984, *Fluid Inclusions*, Reviews in Mineralogy, Vol. 12, Mineralogical Society of America, p. 644.

11/11/2019 10:11:11 AM

11/11/2019 10:11:11 AM

GOLD FROM MINAS DEL PRADO, REGION DEL BIOBIO, CHILE

Nobutaka Shimada*, Asahiko Sugaki** and Guillermo Alfaro***

* Faculty of science, Kyushu University, Hakozaki 6-10-1, Fukuoka 812, Japan. ** Kadan 4-30-503, Aoba, Sendai 980, Japan. *** Instituto GEA, Universidad de Concepción, Casilla 4107, Concepción 3, Chile.

Abstract

The gold bearing quartz veins of Minas del Prado occur in hydrothermally altered dacite and andesite lavas and pyroclastic rocks belonging to the Pierna Blanca Series (Lower Miocene). They are principally composed of quartz and clay minerals as chlorite (chamosite) and smectite (montmorillonite) in association with pyrite, hematite, calcite, plagioclase (albite), kaolin and goethite. However, no silver mineral was found in the gold ores.

Gold appears as native gold and electrum in globular, granular, botryoidal, massive and irregular forms, less than 0.1mm to 0.4mm in size, in assemblage with quartz, pyrite and goethite. Gold contains fairly amounts of silver (Table 1). The composition range of gold is from 74 to 100 wt% Au, but is mostly limited to 74 to 82 wt% Au. Gold with the compositions of Nos. 1 to 5 in Table 1 corresponds to electrum. The composition images (Fig. 2-C, D) of EPMA for gold showed that gold (or electrum) grains occasionally are constitutively heterogeneous so as to have a marginal rim of higher gold contents. Copper is not almost included in gold.

Introduction

Gold in general occurs primarily as native element or electrum in ores, and are commonly composed of gold and silver with some amounts of copper and iron, rarely bismuth, tin, lead, platinum group metals etc., as alloy. The compositions of gold or electrum are controlled by circumstantial conditions of the mineralization as temperature and sulfur fugacity (Barton & Toulmin, 1964). Therefore, it is certainly necessary to determine the compositions of gold or electrum when we like to know the data on conditions of formation of the ore deposits. Under such significance, gold and electrum in the ore from Minas del Prado was investigated by means of ore microscopy, scanning electron microscopy, SEM (Secondary electron image of EPMA) and electron probe microanalysis

(EPMA), and as a result the composition data of gold from this mine were obtained as will be described below.

2. Geological outline

The area of Minas del Prado, which is located at about 50 km east of Chillán, Región del Biobío (Fig. 1), consists principally of dacite and andesite lavas and lapilli tuff, tuff breccia and volcanic breccia corresponding to the Pierna Blanca Series of Neogen Tertiary (Ambrus & Araya, 1981; IIG-MMAJ, 1981; Alfaro, 1984; Collao & Frutos, 1991). The K/Ar ages of two andesites were 17.05 ± 0.60 Ma and 19.71 ± 1.37 Ma in whole rock analyses (Alfaro, 1984), indicating to Early Miocene. These rocks of the Pierna Blanca Series suffered hydrothermal alterations such as silicification, argillization and propylitization.

The volcanic lavas and pyroclastic rocks of the Pierna Blanca Series are covered with the formation, being composed of basic lavas of andesite and basalt, their pyroclastic rocks and semiconsolidated conglomerate etc. corresponding to the Cola de Zorro Formation (0.5 to 1.5 Ma, IIG-MMAJ, 1981).

Gold bearing veins and stockwork in Minas del Prado occur in hydrothermally altered dacitic and andesitic lavas and their pyroclastic rocks of the Pierna Blanca Series. The gold veins such as San Lorenzo, Rudemil Pérez, Pedernales, Las mellizas,

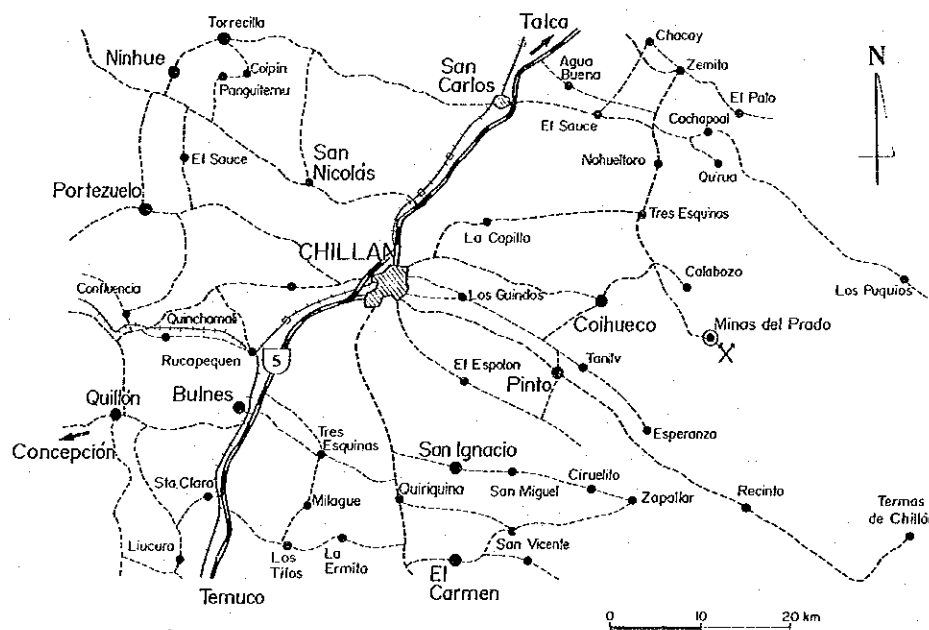


Fig. 1. Location of Minas del Prado.

Urra, and Moreno, running generally to N60° to 70°E direction and dipping to 70° to 90°S, are usually 5 to 40cm in width, rarely 120cm including gangue rock and 30 to 60m in length, sometimes about 70 to 120m. Gold contents in the quartz and quartz-chlorite veins are normally 1 to 4 g/t, rarely 12 to 16.5 g/t, but those of clay (chlorite-smectite) veins are in general less than 1 g/t (Alfaro, 1984).

The gold veins are composed principally of quartz and clay minerals such as chlorite (chamosite) and smectite (montmorillonite) with some amounts of pyrite, plagioclase (albite), hematite, calcite and goethite. They sometimes accompany with small amounts of kaolin mineral. Gold appears as native gold and electrum on fine grains assembled with quartz and pyrite, and occasionally goethite. However, no silver mineral was observed under ore microscope.

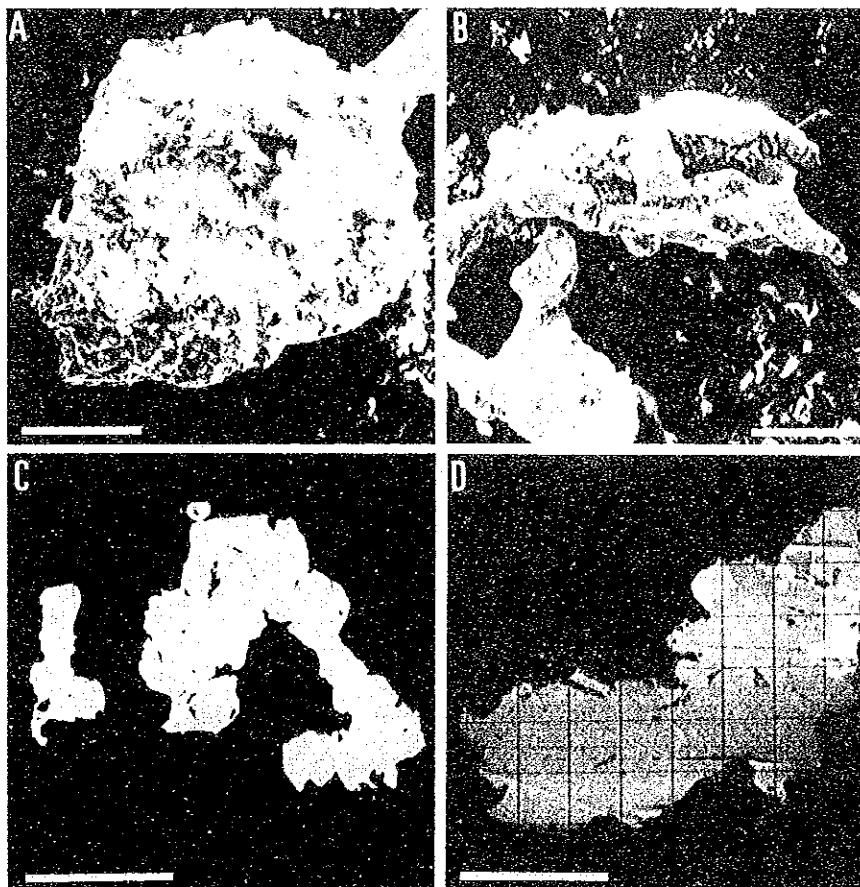


Fig. 2. Photomicrographs of gold (and electrum) from Minas del Prado. Scal bar indicates 100 microns.

A, B: Secondary electron images of gold by EPMA (JEOL, JCSA-733 type).
C, D: Composition images of gold by backscattered electron of EPMA (JEOL, JXA-5A type).

3. Occurrence of gold

As mentioned above, gold occurs as globular, granular, and botryoidal, massive and irregular forms, 0.4mm to less than 0.1mm across, in association with quartz, pyrite and goethite. Gold often fills up an interstice of aggregate of quartz and pyrite.

Photomicrographs of the secondary electron image by electron probe microanalyzer (EPMA) for gold described above are shown in Fig. 2-A, B. The photomicrographs were taken by using JEOL JXA 733 type EPMA with 25kV in accelerating voltage. The photographs correspond to those of SEM. As seen in the photographs, gold is roundly massive or globular forms (A), 0.3 x 0.35mm in size, and irregular shape (B) 0.1 x 0.3mm in size. Gold also appears as botryoidal form as shown in the photographs of the backscattered electron images of EPMA (JEOL, JXA-5 type). Such forms of gold are thought to have been controlled by forms of crystal and its aggregate of quartz and pyrite crystallized previously.

4. Compositions of gold

To know the chemical compositions, gold from Minas del Prado was analyzed with JEOL JXA-5 type EPMA. After the sample with gold was mounted in resin at room temperature and then polished very well, a polished surface was done a vacuum evaporation with carbon. The analytical measurement was carried out under condition as follows (Taguchi & Hirowatari, 1976): accelerating voltage: 20kV, current on pure iron: 0.02mA, take-off angle: 40°, used characteristic X-rays: Ag-L α , Au-M α , Cu-K α . analyzing crystal: PET for Ag-L α , LIF for Cu-K α . The measurement at a point on the sample (gold) was performed for 10 sec. per a time and repeated 5 times at same point. Pure gold and silver and chalcopyrite CuFeS₂ were used as standard materials for Au, Ag and Cu, respectively. The correction for the measurement values depended on the Bence-Albee method (Bence & Albee, 1968).

The analytical data for gold obtained by EPMA as mentioned above are given in Table 1. According to this table, gold contains fairly amounts of silver except one of

Table 1. Analytical data of gold and electrum from Minas del Prado by EPMA

	Weight percent				Atomic percent		
	Au	Ag	Cu	Total	Au	Ag	Cu
1	73.4	25.2	0.0	98.6	61.5	38.5	0.0
2	74.5	24.7	0.0	99.2	62.3	37.7	0.0
3	77.6	22.1	0.0	99.7	65.8	34.2	0.0
4	79.4	20.5	0.1	100.0	67.9	32.1	0.0
5	79.9	20.6	0.0	100.5	68.0	32.0	0.0
6	82.6	18.2	0.0	100.8	71.3	28.7	0.0
7	100.0	0.7	0.0	100.7	98.8	1.2	0.0

No. 7. Composition range of gold is from 74 to 100 wt% Au, but being limited to 74 to 82 wt% Au except No. 7. Gold with compositions of Nos. 1 to 5 corresponds to electrum. The composition images of backscattered electron by EPMA are shown in Fig. 2-C, D. As seen in the photomicrographs of the figure, gold (or electrum) grains occasionally are constitutively heterogeneous so as to have a marginal rim of higher gold content, although gold (or electrum) within a single grain usually has homogeneous composition. Copper is not almost included in gold (or electrum) except No. 4.

5. Summary

The gold bearing quartz veins of Minas del Prado occur in hydrothermally altered dacite and andesite lavas and pyroclastic rocks belonging to the Pierna Blanca Series (Lower Miocene). Occurrence, shape, size, mineral assemblage, chemical composition and homogeneity of gold from Minas del Prado were investigated by means of field observation, ore microscopy and electron probe microanalysis (EPMA). As results of these investigations, the valuable data on gold from this mine were obtained as follows:

1) Gold veins such as San Lorenzo, Rudemil Pérez, Pedernales, Las Mellizas, Urra, and Moreno are composed principally of quartz and clay minerals as chlorite (chamosite) and smectite (montmorillonite) associated with pyrite, hematite, calcite, plagioclase, kaolin and goethite.

2) Gold appears native gold and electrum in globular, granular, botryoidal, massive and irregular forms, 0.4mm to less than 0.1mm across, in association with quartz, pyrite and goethite. Gold fills up an interstice of aggregate of quartz and pyrite. However, no silver mineral was found under ore microscope.

3) Gold contains fairly amounts of silver as given in Table 1. Its composition range is from 74 to 100 wt% Au, but is mostly limited to 74 to 82 wt% Au. Gold with compositions of Nos. 1 to 5 in Table 1 corresponds to electrum.

4) The composition images (Fig. 2-C, D) of back scattered electron by EPMA for gold showed that gold (or electrum) grains occasionally are constitutively heterogeneous so as to have a marginal rim of higher gold contents. Copper is not almost included in gold (or electrum).

References

- Alfaro, G. (1984): Study on metallic ore deposits of central-south region in Chile. Ph. D. Thesis Tohoku University, Japan. p. 268.
- Ambrus, J. & Araya, M. (1981): Notes on the geology of Minas del Prado, Chile. (Unpublished report)
- Barton, P. B. Jr. & Toulmin, P. III (1964): The electrum-tarnish method for the determination of the fugacity of sulfur in laboratory sulfide systems. *Geochim. Cosmochim. Acta*, 28, 619-640.

- Bence, A. E. & Albee, A. L. (1968): Empirical correction factor for the electron microanalysis of silicates and oxides. *Jour. Geol.*, 76, 382-403.
- Collao, S. & Frutos, J. (1991): Mineralogía, alteración hidrotermal e inclusiones fluidas del yacimiento aurífero de Minas del Prado, Región del Biobío, Sur de Chile. Congr. Geol. Chile, 1991, Actas Vol. 1, Resum. Expand., 343-346.
- IIG-MMAJ (1981): Informe de reconocimiento geológico de la región andina situada al este de la ciudad de Concepción.
- Taguchi, S. & Hirowatari, F. (1976): Quantitative electron microanalysis of electron by Bence and Albee method. *Jour. Miner. Soc. Japan.* 12, Special Issue, 82-85. (in Japanese).

PRELIMINARY REPORT ON THE EPITHERMAL GOLD DEPOSIT AND ORE GENESIS OF THE LAS PALMAS MINE, TALCA - CHILE

Arashi Kitakaze*, Asahiko Sugaki** and Guillermo Alfaro***

* Faculty of Science, Tohoku University, Aramaki-Aoba, Sendai 980, Japan.

** Kadan 4-30-503, Aoba, Sendai 980, Japan. *** Instituto GEA, Universidad de Concepción, Casilla 4107, Concepción 3, Chile.

Abstract

Epithermal gold deposit of the Las Palmas mine, Talca, Chile, was studied by field observation, microscopic observation, EPMA analysis, fluid inclusion experiment, measurement of sulfur isotope. Ore veins in the Las Palmas mine are fissure filling type of gold-silver bearing quartz vein developed in Jurassic andesitic rock. The Valencia and Quillay veins are mainly working. Ore veins are mainly composed of quartz accompanied with chlorite, pyrite, sphalerite, galena, chalcopyrite, hematite, magnetite. In the Valencia vein, pyrite occurs as the most dominant sulfide. It associates with sphalerite, chalcopyrite, hematite and galena, rarely tetrahedrite. In the Quillay vein, galena, sphalerite and pyrite occur as common sulfide minerals. They are found in close association accompanied with chalcopyrite, hematite and magnetite. Univariate assemblage of pyrite-magnetite-hematite often occurs. Gold bearing mineral cannot be found.

Chemical compositions of sphalerite obtained by EPMA analysis are in the range from 4.0 to 6.2 mole % FeS. Homogenization temperatures of fluid inclusion in quartz from the Valencia and Quillay veins are in the ranges from 264 to 325°C, and 267 to 314°C, respectively. The $\delta^{34}\text{S}$ values of sulfur isotope for pyrite, sphalerite and galena are -1.47 to -0.19, -2.48 to -1.90, and -5.03 to -4.33‰, respectively.

From FeS content of sphalerite, homogenization temperature of fluid inclusion, sulfur isotope fractionation temperature, ore forming conditions for the Quillay vein are estimated as temperature; 265-330°C, sulfur activity; $10^{-11.7} - 10^{-7.5}$.

1. Introduction

Las Palmas mine (Latitude: 35° 09.6' South, Longitude: 71° 36.2' East) is situated at approximately 200 km south from Santiago, and at 30 km northeast of the Talca city which is regional capital of region VII (Fig. 1). Production of this mine is approximately 9,500t per month as crude ore containing about 4-5 g/t of gold and 20 g/t of silver in 1991. There are found some amounts of lead and zinc, but both metals

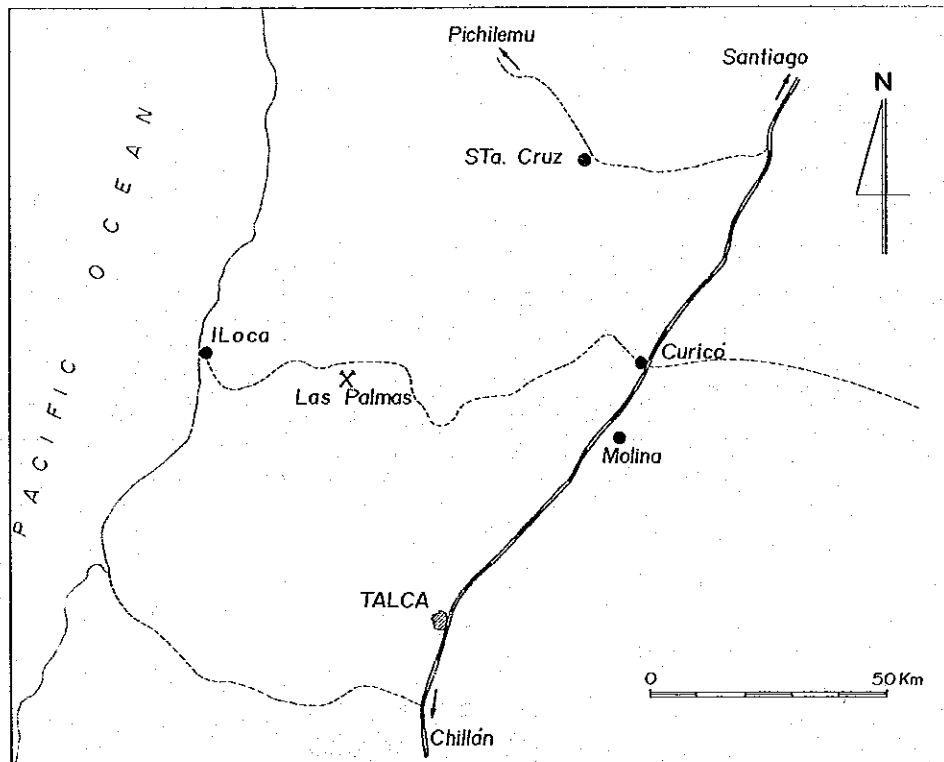


Fig. 1. Location map of the Las Palmas mine.

are not produced because of their mineral processing of cyanization. The number of working people in this mine was 180 men in 1991.

Outline of the geology and ore deposits of this mine were described by Frizsche (1930), Camus & Duhalde (1981), Camus (1986). The area of the mine is mainly composed of andesitic rock containing small amount of marine sediments (sandstone or shale) of middle Jurassic. But studies on the ore minerals and their mineralization have not been reported. Therefore, the present authors would like to describe about occurrence, paragenesis and mineral assemblage, and condition of mineralization in this paper.

Some part of andesitic rock is affected by propyltization, silicification, sericitization or agrillization. Near Quillay vein, sandstone or shale is affected by contact metasomatism by Cretaceous granodiorite, and change to biotite hornfels. After mineralization, the veins are cut by andesite dike and move by some faults.

K-Ar ages for sericite from alteration zone of country rock, biotite from biotite hornfels, and sericite from fault are 113 ± 6 , 105 ± 5 and 103 ± 5 Ma, respectively (Sugaki & Shimada, unpublished data) and correspond to middle Cretaceous. These data are also close to age of granodiorite related to mineralization.

2. Ore deposits

The ore deposits of Las Palmas mine are fissure filling type of epithermal gold-silver bearing quartz veins developed mainly in Jurassic andesitic rock. There are found several veins such as Valencia, Gody (Valencia branch), Esperanza and Quillay, in the mine. The veins generally tend to be northwest to N-W of strikes. The Valencia and Quillay veins are working at present time.

Valencia vein

This vein is main working one having the scale of 150m in depth, 1,500 m in length, and 1-6 m in width. It generally strikes N80-90°E, and dips 50-60°S. This vein contains 5-6 g/t of gold, more the 25 g/t of silver, 0.8 to 1.0% Zn and 0.5% Pb. It is composed mainly of various colored quartzes and some amounts of chlorite, pyrite, sphalerite, hematite and small amounts of galena, chalcopryrite, tetrahedrite and magnetite, and show crustified banding structure which bands of dark gray to white colored quartz, chlorite and sulfide minerals. Amount of ore mineral is less than those for the Quillay vein.

Esperanza vein

This vein is almost parallel to Valencia vein and shows crustified banding about same to Valencia vein. It contains 2-2.5 g/t of gold and about 5% of lead + zinc.

Another about 5 veins similar to Valencia and Esperanza were known but no working in this time.

Quillay vein

This vein is also main working one having scale of 130m in depth 150m in length, and about 3 m in width. It generally strikes N70-80°W and dips 50-70°S. This vein from outcrop (410 m in sea level) to 70 depth is strongly oxidized, and sulfide minerals are not found. The primary minerals are found in lower part than 340 ml. This vein is mainly composed of quartz, pyrite, sphalerite, galena, chalcopryrite and small amounts of magnetite and hematite. This vein does not show the crustified banding and sulfide minerals distribute as irregular form in the vein. Amount of sulfide minerals in the vein is rather than those of the Valencia vein. Some parts of the vein contain more than 10% Pb, and 1-30 g/t Au. Some part of andesitic rock as country rock is strongly affected by sericitization.

3. Ore and minerals

The gold-silver bearing ore from the Las Palmas mine is composed mainly of banded quartz associated with some amounts of ore and gangue minerals. Ore minerals such as pyrite, sphalerite, galena, chalcopyrite, hematite, magnetite and tetrahedrite are found. Some amounts of chlorite, sericite and calcite as gangue minerals are accompanied by quartz. Mineral paragenesis and assemblage for the Valencia and Quillay veins are somewhat different because the Quillay vein is nearly situated with granodiorite that is thought to be related closely with mineralization.

Ores from the Valencia vein show the crustified banding structure by quartz of various colors or grain size. Chlorite bands (about 5 mm in width) occur between quartz band (1-2 cm in width). Ore minerals of pyrite, sphalerite, galena, chalcopyrite and hematite commonly occur in chlorite band. Pyrite and sphalerite are macroscopically found as the most common ore minerals associating with microscopic size of galena, chalcopyrite, hematite and sometimes magnetite as silver bearing mineral, tetrahedrite occurs very rarely associated with chalcopyrite. Gold bearing mineral cannot be found microscopically. Sometimes, euhedral pyrite, quartz and hematite are found in the bug of central part of the vein.

Meanwhile, ores from the Quillay vein do not show the banding structure. Ore minerals occur irregularly in quartz and more dominant than the Valencia vein. Galena, sphalerite and pyrite are macroscopically occur as common minerals. They are closely assembled with each other. They are usually associated with chalcopyrite, microscopically. Hematite and magnetite are found as inclusion in sphalerite, associated with pyrite and chalcopyrite. Sometimes, sphalerite includes chalcopyrite dots. Gold or silver bearing minerals have not been found microscopically.

4. EPMA analysis of sphalerite

Chemical composition of sphalerite associated with pyrite from the Valencia and Quillay vein was obtained using EPMA. Analytical results are shown in Table 1. Fe content of sphalerite from the Valencia vein is in the range from 2.18 to 2.54 atomic %. Meanwhile, that from the Quillay vein is 2.02 to 3.15 atomic %. Both values are very similar.

Cd content of sphalerite from the Valencia vein is 0.16 to 0.17 atomic %. Meanwhile, Cd content from the Quillay vein is 0.15 to 0.40 atomic %, and more high value and wide range than that from the Valencia vein. Cu and Mn contents are less than 0.02 and 0.11 atomic %, respectively.

Histogram for FeS content as mole % is given in Fig. 2. Sphalerite from the Las Palmas mine contains 4.0 to 6.2 mole % FeS.

Table 1. Analytical results of sphalerite from the Las Palmas mine

	Weight %						Atomic %						
	Zn	Fe	Cu	Mn	Cd	S	Total	Zn	Fe	Cu	Mn	Cd	S
911401722 (V. Valencia)													
64.55	2.51	0.02	0.04	0.40	33.05	100.57	47.75	2.18	0.02	0.03	0.17	49.85	
63.92	2.62	0.00	0.08	0.39	32.88	99.87	47.58	2.28	0.00	0.07	0.17	49.90	
64.00	2.88	0.02	0.07	0.37	32.63	99.96	47.68	2.51	0.01	0.06	0.16	49.57	
63.44	2.92	0.00	0.05	0.36	32.81	100.08	47.53	2.54	0.00	0.05	0.16	49.73	
91101703 (V. Quillay, 360 ml)													
63.17	3.08	0.01	0.11	0.40	32.41	99.18	47.41	2.70	0.01	0.10	0.17	49.60	
63.43	3.15	0.00	0.10	0.42	32.93	100.03	47.11	2.74	0.00	0.09	0.18	49.87	
62.96	3.20	0.03	0.12	0.35	33.03	99.69	46.94	2.79	0.02	0.11	0.15	50.09	
63.05	3.56	0.02	0.12	0.44	32.73	99.92	46.92	3.10	0.02	0.11	0.19	49.67	
91101706 (V. Quillay, 350 ml)													
63.32	2.72	0.00	0.00	0.93	32.99	99.97	47.14	2.37	0.00	0.00	0.40	50.08	
63.13	2.80	0.00	0.02	0.77	32.15	98.86	47.67	2.47	0.00	0.02	0.34	49.50	
63.06	2.45	0.01	0.02	0.85	32.68	99.08	47.38	3.15	0.01	0.02	0.37	50.06	
64.02	2.30	0.02	0.00	0.80	32.43	99.56	48.03	2.02	0.01	0.00	0.55	49.60	
91101708 (V. Quillay, 345 ml)													
63.62	2.70	0.00	0.01	0.77	32.22	99.31	47.86	2.38	0.00	0.01	0.33	49.42	
63.39	2.95	0.00	0.02	0.67	32.00	99.02	47.84	2.60	0.00	0.01	0.29	49.24	
63.77	2.70	0.00	0.01	0.69	32.93	100.11	47.42	2.35	0.00	0.01	0.30	49.93	
63.42	3.07	0.00	0.02	0.68	32.50	99.69	47.44	2.68	0.00	0.02	0.30	49.56	

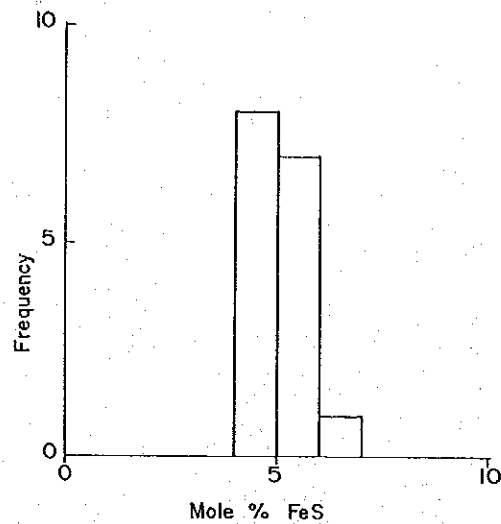


Fig. 2. Histogram of FeS content of sphalerite from the veins of the Las Palmas mine.

5. Fluid inclusion

Fluid inclusions in quartz from the Las Palmas mine are two phases, vapor and liquid. Most of them are very fine, less than 5 μm in size, then measurements of homogenization temperature and salinity for them are selectively observed on larger than 5 μm in size. Homogenization temperatures of fluid inclusion were measured using a heating and cooling stage of the Linkam TH-600 type under heating rate of 2°C per minute. The experimental results on the homogenization temperature of fluid inclusions in quartz from the Valencia and Quillay veins are shown as histogram in Fig. 3. According to these data, the homogenization temperatures are in the ranges from 264 to 325°C (average 295°C) for the Valencia vein, and 267 to 314°C (average 293°C) for the Quillay vein. Both values are very similar.

6. Sulfur isotope

The $\delta^{34}\text{S}$ values for pyrite, sphalerite and galena from the Valencia and Quillay veins are shown in Table 2. Their histogram is given in Fig. 4. The values for pyrite, sphalerite and galena are in the very narrow ranges from -1.47 to -0.19 ‰, -2.48 to -1.90 ‰ and -5.03 to -4.33 ‰, respectively.

The differences of $\delta^{34}\text{S}$ values for associated minerals as pyrite-sphalerite and sphalerite-galena assemblages from the Quillay vein are 1.03 (91101703), 2.18 (91101706), 2.76 (91101708) and 2.56 (91101710), respectively. Isotopic fractionation temperatures are calculated from these values using formula given by

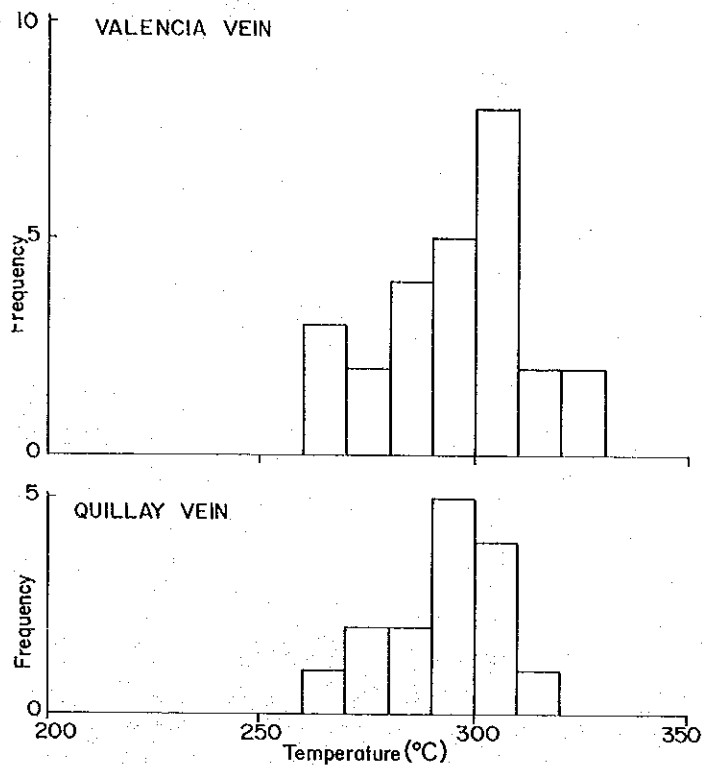


Fig. 3. Histogram of homogenization temperature of fluid inclusion in quartz from the Valencia and Quillay veins of the Las Palmas mine.

Kajiwara & Krouse (1971) for pyrite-sphalerite and sphalerite-galena assemblages. Their temperatures are given as 267°C for pyrite-sphalerite assemblage, and 333, 265 and 286°C for sphalerite-galena assemblage. These values are in the range from 265 to 333°C, which is about same range (265 to 313°C) for homogenization temperature of fluid inclusion from the Quillay vein.

7. Mineralization

From occurrence of ore and gangue minerals as above, mineralization in the Valencia and Quillay veins are thought to be somewhat different, but relations between both veins are not clear. Then, mineralization in the Las Palmas mining area cannot be estimated. More detailed study on this point is necessary.

Sphalerite associated with pyrite contains 4.0 to 6.2 mole % FeS (Table 1 and Fig. 2). Homogenization temperature of fluid inclusion in quartz from the mine is in the range from 264 to 325°C. Also, isotopic fractionation temperature between pyrite,

Table 2. Sulfur isotope composition ($\delta^{34}\text{S}$) of pyrite, sphalerite and galena from the Las Palmas mine

	Pyrite (‰)	Sphalerite (‰)	Galena (‰)
Valencia vein			
91101718	-0.19	-	-
91101722	-1.47	-	-
Quillay vein			
91101703	-1.19	-2.22	-
91101706	-	-2.48	-4.66
91101707	-	-	-4.33
91101708	-	-1.90	-4.66
91101710	-	-2.47	-5.03

sphalerite and galena ranges from 265 to 333°C. Both temperature ranges are very similar values, then these values are thought to correspond to ore forming temperature at least for the Quillay vein. In the temperature (T) - sulfur activity (a_{S_2}) diagram given in Fig. 5, dotted area from ranges of sphalerite composition and forming temperature is obtained. In this range, pyrite and chalcopyrite exist as stable phases. In the high sulfur activity region, three-phase assemblage of magnetite, hematite and pyrite is found stably. These mineral assemblages are very close to those found in the ore from the Las Palmas mine. From these facts, temperature and sulfur activity values of forming condition of the Quillay vein are estimated as follows:

Temperature; 265 to 330°C,

Sulfur activity: $10^{-11.7}$ to $10^{-7.5}$.

FeS content in sphalerite and homogenization temperature of fluid inclusion in quartz from the Valencia vein are about same to those for the Quillay vein. However, this vein shows the crustified banding of quartz and chlorite as normally found in epithermal quartz vein. Therefore forming temperature is estimated to be lower than that of the Quillay vein and more detailed study is necessary for this problem.

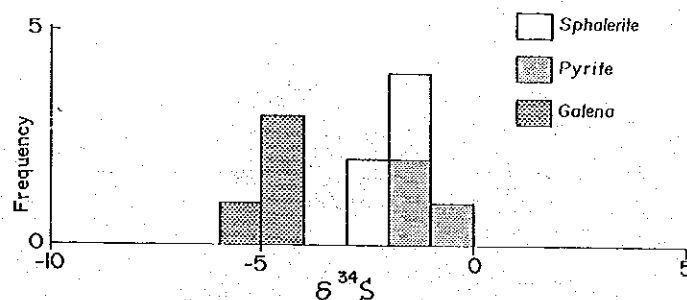


Fig. 4. Histogram of sulfur isotope compositions for pyrite, sphalerite and galena from the Las Palmas mine.

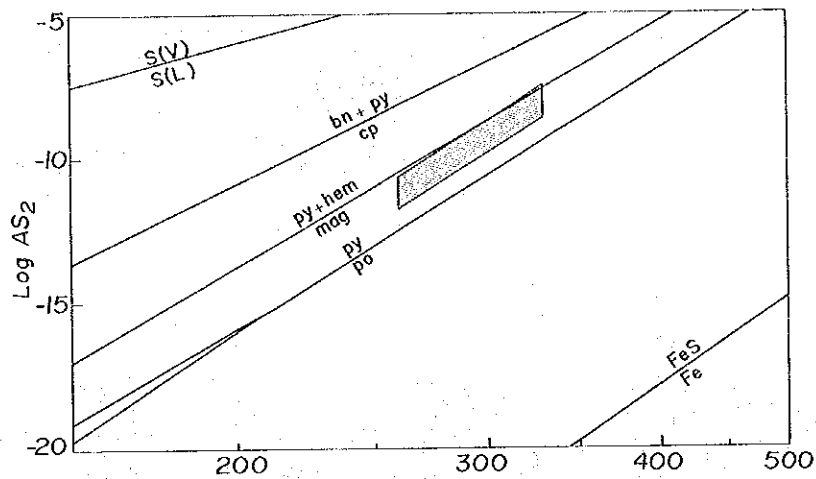


Fig. 5. Temperature and sulfur activity of mineralization for the Quillay vein of the Las Palmas mine (dotted area). bn: bornite, cp: chalcopyrite, hm: hematite, mag: magnetite, po: pyrrhotite, py: pyrite.

Acknowledgment

We would like to thank to Dr. Katsuo Kase, Okayama University for EPMA analysis of sphalerite and useful suggestion. We also want to express heartily to Drs. Isao Kusachi, Okayama University, Masatoshi Shiba, Hirosaki University and Satoshi Nakano, Shiga University for analysis of sulfur isotopic ratios of some sulfide minerals.

References

- Camus, F. & Duhalde, M.A. (1981) Evaluación Geológica del Distrito Minero Las Palmas, VII Región. Informe Inédito, 3.
- Camus, F. (1986) Geología de los yacimientos epitermales de oro en Chile y posible modelo idealizado. In *Geología y Recursos Minerales de Chile*, eds., J. Furutos et al., pp. 651-689, Editorial de la Universidad de Concepcion.
- Frizsche, F.H. (1930) Informe sobre el mineral de oro de "Las Palmas" del Departamento de Talca. *Bol. soc. Nac. Min.*, 42, 618-621.
- Kajiwara, Y. & Kröuse, H.R. (1971) Sulfur isotope partitioning in metallic sulfide systems. *Can. Jour. Earth. Sci.*, 8, 1379-1408.

GENESIS OF SKARN ORE DEPOSITS: A MODEL OF SKARN- ORE FORMING METASOMATIC REACTIONS

Kiyoshige Ochiai

Science Education Institute, Karita 4-13-23, Sumiyoshi, Osaka 558,
Japan.

Skarn deposits are formed by metasomatic reaction between hydrothermal fluid and limestone, which produce concentration and deposition of metallic elements. Hydrothermal fluid reaction with carbonate rocks is an essential characteristic which distinguishes skarn deposits from most other types of hydrothermal ore deposits. A quantitative reaction model was formulated for the formation of the metasomatic skarn zones between the marble and the quartz dioritic stock in the Nippo deposit of the Kamaishi mine, Japan (Figs. 1, 2, 3 and 4). The reaction model reveals the following features of the reaction (Figs. 5, 6 and 7).

Hydrothermal fluids containing Si, Fe, S, Cu, Zn, Ni and Co flowed primarily at the reaction sites where CO_2 or H_2O was released. There was a positive correlation between mass addition and the loss of CO_2 or H_2O . About 90 mole percent of the mass addition was concentrated at the contact of the skarn with the marble. Release of CO_2 or H_2O promoted the introduction of hydrothermal fluids, because production of volatiles temporarily increased fluid pressure, which caused pores and fractures, thus increasing permeability. The hydrothermal fluids followed the release of volatiles from the wall rocks, forming a single flow system at the reaction sites. Furthermore, Ca or alkalies were liberated and sulfide minerals were precipitated at the same devolatilization sites. This supports the conclusion that crystallization of the sulfide minerals was promoted by the neutralization of acid hydrothermal fluids reacting with carbonate minerals of feldspar. Thus, devolatilization, especially decarbonation, dominated the process of skarn ore formation from the introduction of hydrothermal fluids to the precipitation of ore minerals. The reaction model explains the location of ore pods within the Nippo skarn. The fluid-rock ratio (volumetric) was estimated to be 2.3-7.3 at the reaction site of contact with the marble, and the concentrations of metallic elements in the fluids were more than Cu = 5909, Zn = 130, Ni = 120, Co = 30 ppm, and Fe = 8.8 %.

Crystallization varying mineral paragenesis with time occurred locally in the skarns due to increasing chemical potential of CO_2 (Fig. 8). CO_2 behaved as a perfectly mobile component in the early stage, while in the later stage CO_2 became stagnant and locally closed, reflecting a decrease of effusion of fluids. Later formed veins of sulfides, quartz and calcite were also locally precipitated. These minerals filled pores and fractures which had been the channels of fluids and crystallization was ended by the complete closing off of the supply of hydrothermal fluids and a decrease of temperature.

The REE patterns of garnet skarns and garnets show large variations of Eu anomalies from positive to negative on chondrite-normalized REE diagrams (Fig. 9). The $f\text{O}_2$ is the main factor that controls $\text{Eu}^{2+}/\text{Eu}^{3+}$ ratios in minerals, and Eu^{3+} is preferentially taken into garnet relative to Eu^{2+} . The initial hydrothermal fluids with higher $f\text{O}_2$ because of their metasomatic reaction with graphite bearing limestone with lower $f\text{O}_2$.

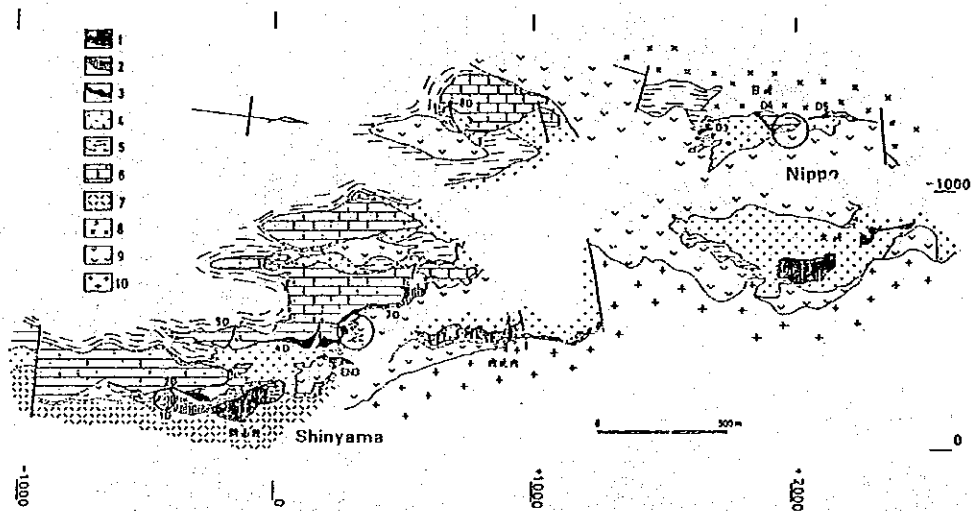


Fig. 1. Geological map of the western side ore deposits of the Kamaishi mine (Hamabe, 1971). The geological map is compiled from geological maps of the Shinyama 450 m level, Sahinai and Ohmine 725 m level, and Nippo 250 m level. 1= iron orebody, 2= iron-copper orebody, 3= copper orebody, 4= skarn, 5= slate and sandstone, 6= limestone, 7= andesitic pyroclastic rocks, 8= the Kurihashi granodiorite, 9= diorite and diorite porphyry, 10= the Ganidake granorite. Three circles represented studied areas in this paper.

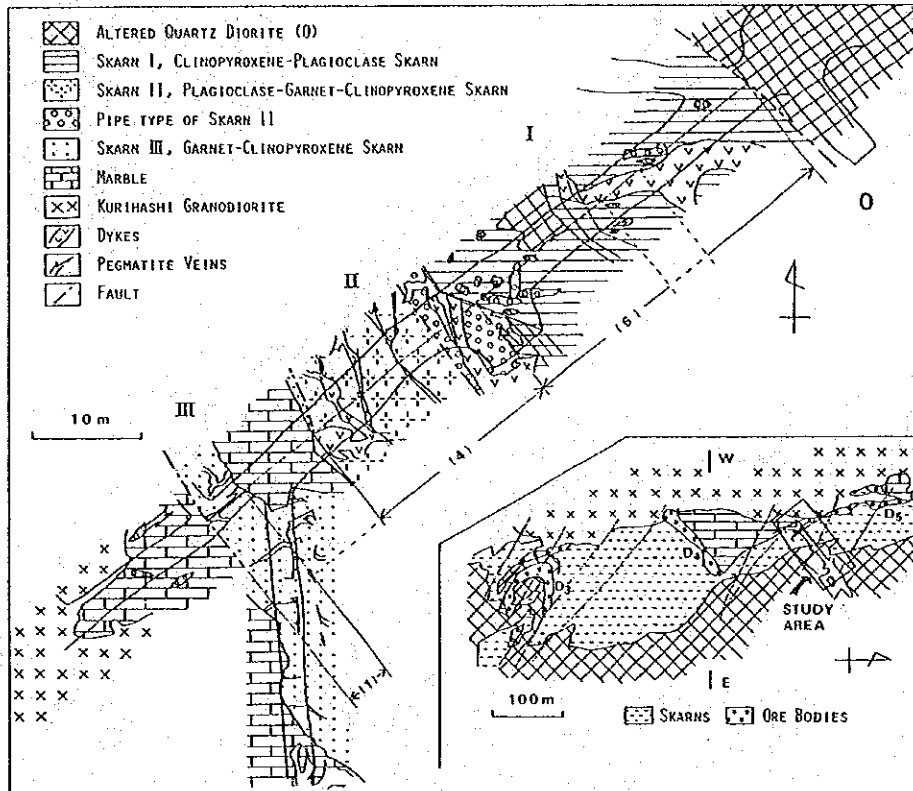


Fig. 2. Geologic sketch map of the zoned skarns on the 250 m level of the Nippo ore deposit. Large copper orebodies D₃, D₄, and D₅ are shown in the lower right map. Although ores are not shown in the sketch map, sulfide ores are concentrated on a small scale mostly in skarn III, particularly at the contact with the marble, and secondly in skarn I.

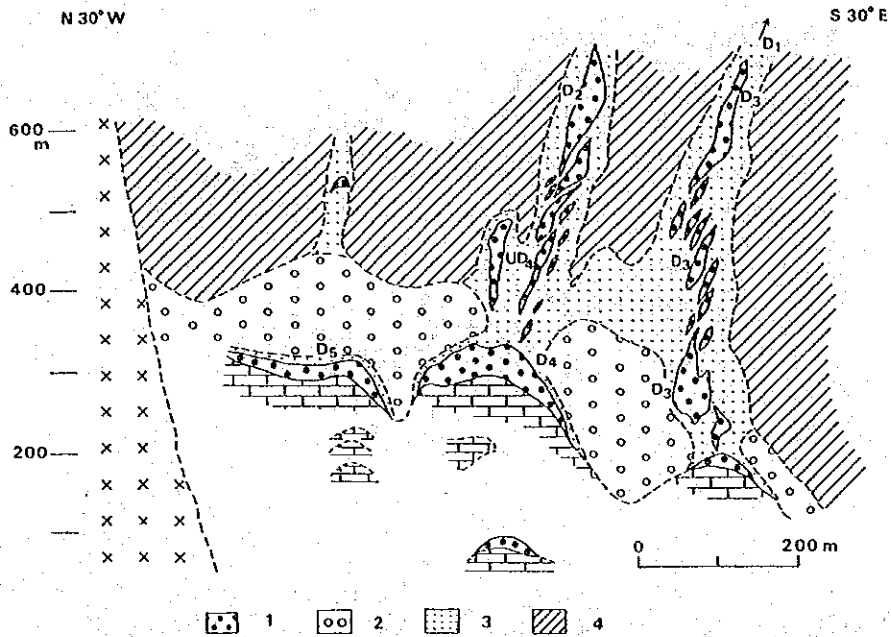


Fig. 3. Schematic perspective drawing of orebodies projected on a N 30° W cross section (adapted from unpublished data of the Lasa Industrial Company, Ltd., Tono). Orebodies are aligned over each marble body. 1= ore bodies, 2= garnet-predominant skarn, 3= clinopyroxene-predominant skarn, 4= slate and sandstone.

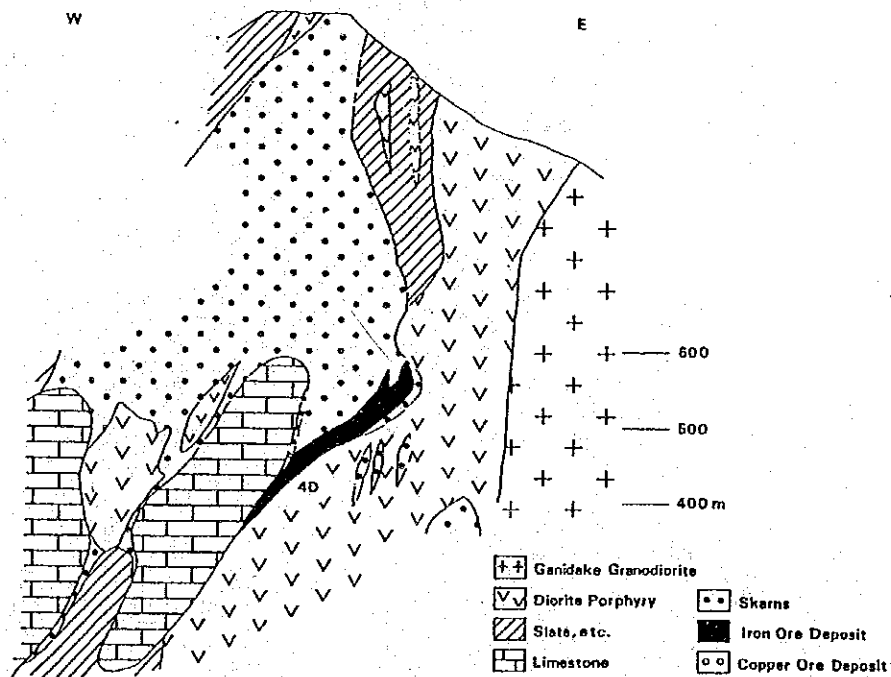


Fig. 4. East-west geological section (N310) of the Shinyama 4D orebody (after the Kamaishi Mining Company, Ltd.). The distribution area of the skarns enlarges from the lower 400 m level to the upper 600 m level.

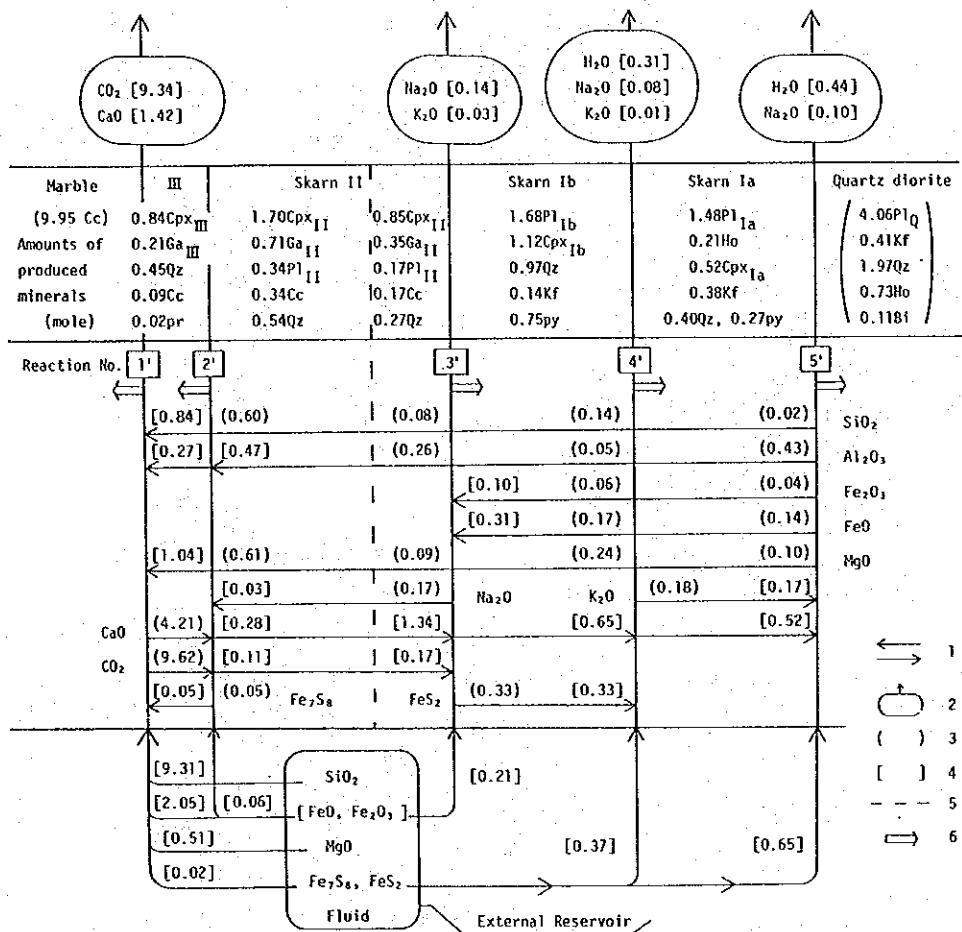


Fig. 5. Reaction model producing the skarn zones at the constant volume reference frame and a schematic representation of mass transfer in the skarn zones. The reaction between the marble and quartz diorite starts with the introduction of hydrothermal fluids at their initial boundaries. The reaction composed of the five interfacial reactions simultaneously produces the four zones, involving diffusive and infiltrative mass transfer. The production rate of each skarn zone is proportional to the observed zone width. The zones spread out from skarn II, in which the initial boundary is located, with the progress of the reaction. Explanation of symbols: 1= diffusive contributions to mass transfer between marble and quartz diorite, arrows are drawn at the sites where components are consumed, 2= infiltrative contributions to mass transfer by hydrothermal fluids, 3= moles of components which are produced in the reactions, 4= moles of components which are consumed, 5= initial boundary between the marble and quartz diorite, 6= direction in which the site of the reaction moves with the growth of the zones. The width of each skarn zone is drawn in proportion to the amount produced. At the site of reaction (1'), the concentration of sulfide minerals is minimized, but in reality there is a much larger amount, because the sulfide-concentrated part of skarn III was eliminated from the samples for analysis in order to minimize the interference of sulfur.

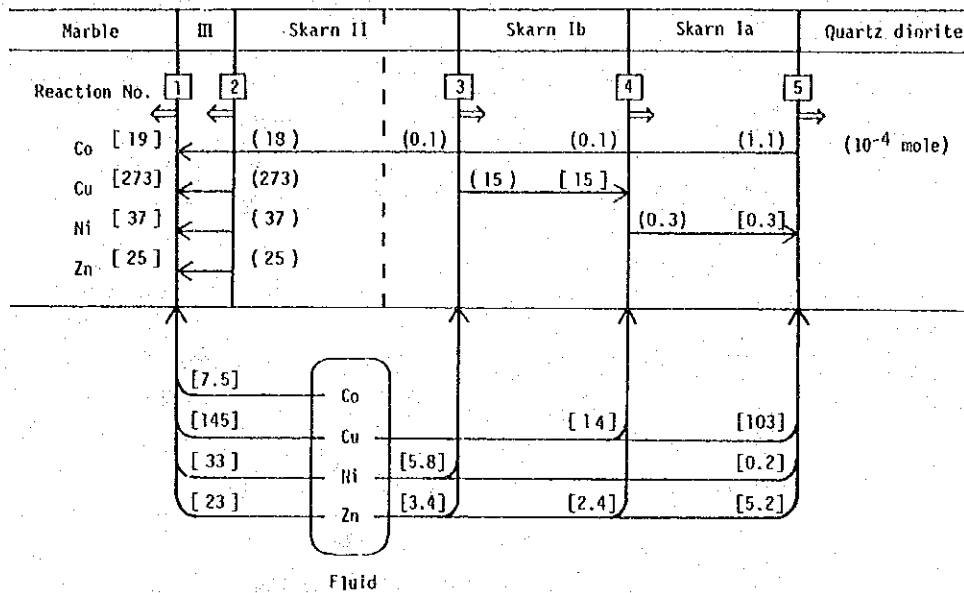


Fig. 6. Behavior of chalcophile or siderophile trace elements in the skarn zones.

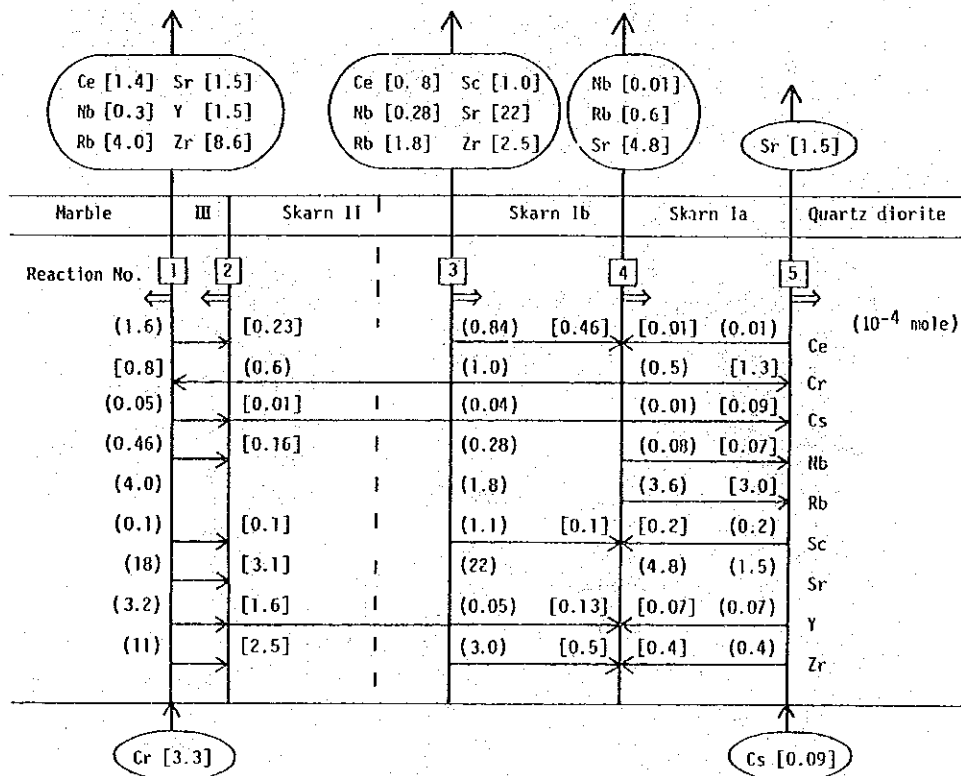


Fig. 7. Behavior of lithophile trace elements in the skarn zones.

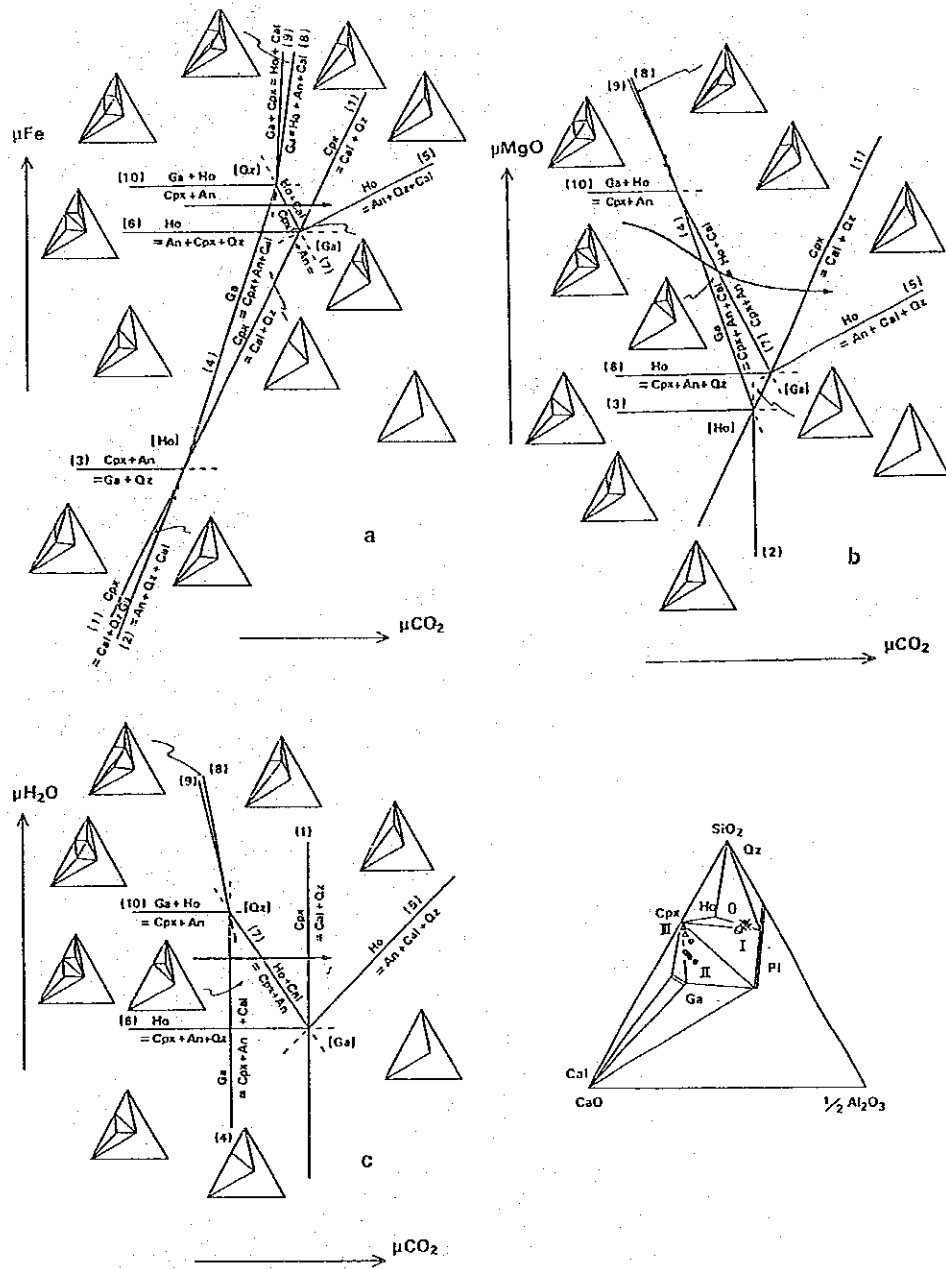


Fig. 8. Chemical potential diagrams for equilibrium reactions among six minerals, garnet, clinopyroxene, hornblende, anorthite, calcite and quartz, of the system $\text{SiO}_2\text{-CaO-Al}_2\text{O}_3$ with perfectly mobile components H_2O , CO_2 , FeO , Fe_2O_3 and MgO for skarn II at the Nippo deposit. a: $\mu_{\text{Fe}} - \mu_{\text{CO}_2}$ diagram, b: $\mu_{\text{MgO}} - \mu_{\text{CO}_2}$ diagram, c: $\mu_{\text{H}_2\text{O}} - \mu_{\text{CO}_2}$ diagram. Arrows indicate the variation of mineral paragenesis observed in skarn II. Mineral abbreviations: Ga = garnet, Cal = calcite, Pl = plagioclase, Cpx = clinopyroxene, Ho = hornblende, Qtz = quartz. Symbols: cross = chemical compositions of quartz diorite, open circle = skarn I, solid circle = skarn II, triangle = skarn III.

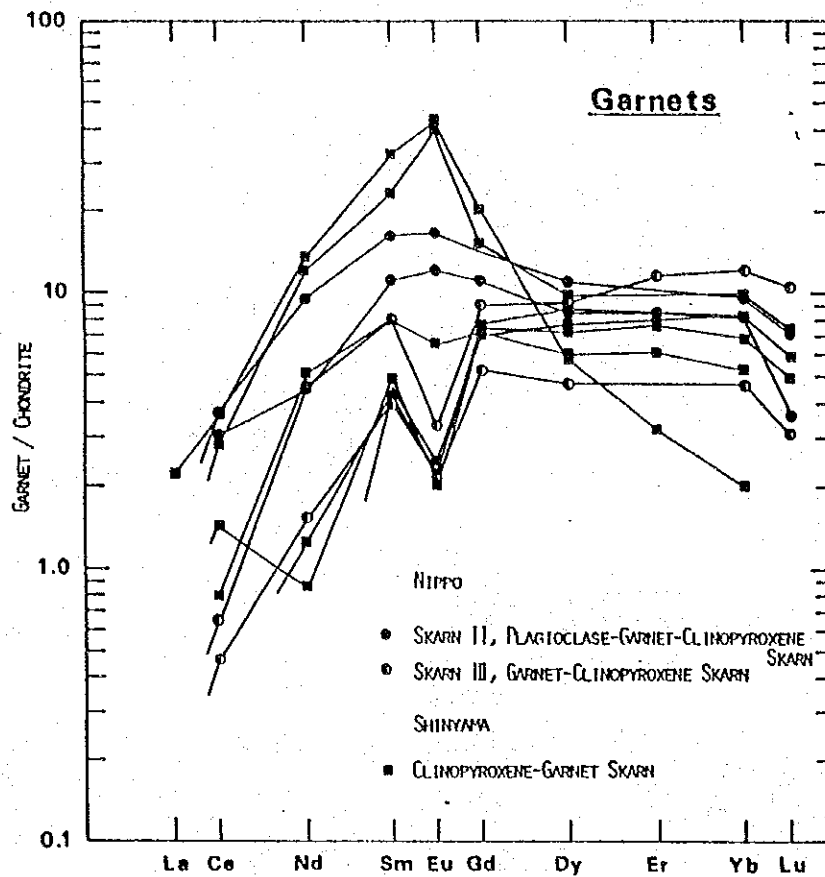


Fig. 9. Chondrite-normalized REE patterns of the analysed ten garnets from the Nippo and Shinyama ore deposits. The large variation of Eu anomalies reflects the fluctuation of fO_2 caused by the metasomatic reaction between hydrothermal fluids with higher fO_2 and graphite-bearing limestone with lower fO_2 .

K-Ar DATING ON ROCKS AND MINERALS RELATED TO ORE DEPOSITS IN CHILE (1)

Asahiko Sugaki* and Nobutaka Shimada**

* Kadan 4-30-503, Aoba, Sendai 980, Japan. ** Faculty of Science, Kyushu University, Hakozaki 6-10-1, Higashi, Fukuoka 812, Japan.

1. Introduction

Until recently, little was known about the absolute ages of the various kinds of mineralizations in Chile, although more than 200 radiometric age data on granitoids in Chile (Aguirre, 1983) and also 800 ones on igneous and metamorphic rocks in the meridional Andean border (Cecioni, 1985) have been presented. This is a preliminary report on K-Ar age determinations that will contribute to define the mineralization epoch on various kinds of ore deposits in Chile. Here are presented seventeen age data which show the hydrothermal alteration epochs of both porphyry copper deposits of Chuquicamata and Escondida and the manto-type copper deposit of Buena Esperanza. They also include several gold deposits such as Andacollo, La Coipa, El Bronce, and Las Palmas, a silver deposit of Choquelimpie, and an iron deposit of Ambiciosa.

All samples analyzed were principally collected during our field surveys in 1991. They were carefully separated into potassium-bearing minerals such as sericite, biotite, hornblende, K-feldspar and alunite at the laboratory of GEA, Geología Económica Aplicada, of the University of Concepcion.

2. K-Ar age determinations

K-Ar dating was carried out for seventeen separated minerals at the Potassium-Argon Laboratory, Teledyne Isotopes, New Jersey, U.S.A. The constants used in age calculation are $\lambda_{\beta} = 4.92 \times 10^{-10}/\text{year}$, $\lambda_{\epsilon} = 0.581 \times 10^{-10}/\text{year}$, and $^{40}\text{K}/\text{K} = 1.167 \times 10^{-2}$ atom% (Steiger and Jäger, 1977). The error was calculated after the method of Cox and Dalrymple (1967).

3. The mode of occurrence

The modes of occurrence on seventeen samples are briefly described as follows:

Choquelimpie (2022507): Greyish white colored, intensely altered andesite, containing abundant quartz and sericite, was collected at the open-pit, 4,715m above sea level, of the Choquelimpie Mine. Clay fractions of sericite for dating were separated by the hydraulic elutriation method. Several veinlets, having reddish brown colored sphalarite with minor amount of galena, barite, and b-axis disordered kaolinite, less than 3mm wide, frequently transect the altered andesite.

Choquelimpie (2022509): This is a grey colored, intensely altered rock, containing abundant quartz with sericite and pyrite. It is characterized by pure white colored, sericitized feldspar phenocrysts, up to 4 mm in size. Fine grained pyrite occurs as disseminations. These features are very close to "feldspar porphyry" described by Gröpper *et al.* (1991). Sericite fractions for dating were obtained in the same way as 2022507.

Choquelimpie (2022518): This sample is an intensely altered and leached rock, showing brecciated structure. White colored powdery breccias, up to 5 cm in size, contain abundant alunite with minor quartz. The groundmass, pale grey colored, consists of vuggy silica. Beautiful crystals of orpiment sometime fill a druse of the rock. Alunite was confirmed by an X-ray powder diffractometer, and used for dating.

Buena Esperanza (1030714): At the adit of the level 285 m in the Buena Esperanza mine, a quartz-sericite-chlorite veinlet, trending N80°E and dipping 80°N, definitely cuts altered andesite, the host rock of manto-type copper ore deposits. The clay fractions were separated from the veinlet and were provided for dating.

Chuquicamata (2022002): This sample was collected at the coordinate of N4100 and E3250 on the level N-1 of the Principal Pit, Chuquicamata. According to the zonal arrangement reported by Alvarez *et al.* (1980), the sampling point belongs to the quartz-sericite zone. The sample is greyish white colored altered granite porphyry with pyrite occurring as disseminations and in fine fractures. The pulverized specimen consists of abundant quartz with subordinate amount of 2M₁ sericite. The elutriated sericite was used for dating.

Chuquicamata (2022011): This was also from the point of N3150-E3300 on the level L-3 in the Principal Pit, Chuquicamata. The site entirely belongs to the potassic alteration zone (Alvarez *et al.*, 1980). Beige colored, large crystals of K-feldspar, up to 8 cm in size, occur in granite porphyry. The numerous hair-cracks developed in the crystals are characteristically filled with chalcopyrite. X-ray powder diffraction indicates that the separated K-feldspar for dating contains subordinate amount of quartz with trace amount of mica and kaolin minerals.

Escondida (2080301): The sample is intensely altered granite porphyry from the open-pit of the Escondida porphyry copper deposit. It belongs to the secondary

sulfide enrichment zone, especially rich in chalcocite ores attaining 5% Cu. Sericite was separated from the altered rock, and used for dating.

Ambiciosa (2051736): The stratified magnetite ore deposits of Ambiciosa occur in the Abundancia-Nantoco Formations, and are thermally metamorphosed by the early Cretaceous plutonic intrusions (Segerstrom *et al.*, 1963). Fresh monzodiorite, a kind of plutonic intrusions (Tilling, 1962), crops out about 500 m east of the mine. Felsic grains of the rock were separated by an isodynamic separator. They contain quartz and K-feldspar, and were provided for age determination (2051736-A). Biotite flakes were separated from the rock, and used for dating (2051736-B). Also hornblende grains were separated from the rock and prepared for K-Ar age determination (2051736-C).

Andacollo (1031301-5): The sample was collected from the primary ores of some gold-bearing sulfide-sericite-quartz veins (ore bodies), developed in the western part of Andacollo Town. Sericite fractions were separated from the sample by the elutriation method, and used for dating.

La Coipa (1031305-2): Copper-rich ores from the secondary sulfide enrichment zone of porphyry copper deposits, developed at the open-pit of the La Coipa mine, located about 500 m west of Andacollo, are actively mined. The ores contain secondary chalcocite and covellite. This zone of the open-pit suffered intense hydrothermal alteration, and sericite, alunite, jarosite and goethite occur as alteration products. Sericite fractions were separated from the altered rock with chalcocite veinlets in this secondary zone, and were provided for dating.

El Bronce (1031504): From the Maria Isabel vein, 25 cm wide, at the Chivato level (1,380m) in the El Bronce mine, this sample was taken. It contains sulfide bands composed of pyrite, chalcopyrite, tetrahedrite, etc. Sericite fractions were separated and utilized for dating.

El Bronce (1031505): A gold-bearing sulfide (pyrite and chalcopyrite) and quartz vein develops as a branch of the above-mentioned vein. Small amounts of sericite fractions, less than 3g, were separated from the vein, and used for dating.

Las Palmas (1101704): Clay-sized fractions composed of sericite were separated from a hydrothermally altered rock with sericite and quartz, adjoined to the Quillay branch vein (a gold bearing quartz vein), at the 345 m level of Las Palmas mine.

Las Palmas (1101712): Biotite fractions were concentrated by means of isodynamic separator from the pulverized sample of biotite hornfels, as the host rock of the gold-quartz vein which may be a contact metamorphic product of granitic intrusion related genetically to formation of the gold veins.

Las Palmas (1101715): Silky white clay, composed of sericite, was elutriated from a clayey sample along the boundary sericite, was elutriated from a clayey sample along the boundary with hanging wall of the Valencia vein of a gold-bearing crustified banding quartz vein with hematite and sulfide, 1.5 m in width, at the 170 m level of the Las Palmas mine.

4. Results and discussions

The results of K-Ar age determinations are shown in Table 1.

The mineralization ages of Choquelimpic, 6.0 ± 0.3 , 5.6 ± 0.3 , and 6.9 ± 0.3 Ma, are compatible to 6.6 ± 0.2 Ma presented by Worner *et al.* (1988) for late stage dacite dykes. They regarded that the latter age postdates the epochs of both hydrothermal alteration and gold mineralization at Choquelimpic.

The genesis of the manto-type copper deposits at Buena Esperanza has been controversial for a long time. Ruiz *et al.* (1971) insisted exhalative sedimentary process, while Losert (1973), Palacio and Definis (1981), and Orquera (1987) laid stress on epigenetic-hydrothermal process. Sato (1984) proposed the dehydration process of burial metamorphism. On the age determinations, three epochs have been known. The La Negra Formation, consisting the host andesites of manto-type copper ores, was dated for 186.5 ± 13.5 Ma as the Rb-Sr whole rock age (Roger, 1985). A gabbroic body which intrudes the La Negra Formation shows K-Ar age of 168 ± 5 Ma (Maksaev, *et al.*, 1988). While, Boric *et al.* (1984) and Rogers (1985) presented 165 ± 3 and 154.7 ± 13.4 Ma, respectively, for a granodiorite pluton, which widely distributes near the manto-type deposits and intrudes apparently the La Negra Formation. The present age, 159 ± 8 Ma, definitely indicates the postdate of the manto-type mineralization. This age is very close to the previously reported ages on the pluton, however, more comprehensive age data are still necessary to discuss the genetical considerations.

The primary alteration epoch at Chuquicamata is defined to be a fixed period between 32.3 ± 1.6 and 33.3 ± 1.7 Ma, and is compatible to those ages of previous studies, for example, 29.6 to 37.0 Ma, compiled by Frutos (1981). It is quite interesting that hydrothermal alteration age of Escondida is here defined to be 34.9 ± 1.7 Ma, which is very close to that of Chuquicamata.

The intrusion age of the monzodiorite body, cropping out near the Ambiciosa, about 30 km south of Copiapo, can be regarded to 102 ± 3 Ma, an averaged value of three data. This is consistent to the previous geologic correlation in the Copiapo (Segerstrom *et al.*, 1963). This age obviously defines the epoch of contact metamorphism to the stratified iron deposits of Ambiciosa.

At Andacollo and La Coipa, the mineralization ages, 101 ± 5 and 104 ± 5 are conformable to those obtained recently by Reyes (1991). He reported 91 ± 6 Ma for the gold-bearing rock, and 98 ± 2 and 104 ± 3 Ma for samples from the porphyry copper deposit in Andacollo.

Two age data of the present study are identical within the errors for the mineralization epoch of the El Bronce epithermal vein system. Recently Camus *et al.* (1991) reported four K-Ar data for alteration zone in the El Bronce area. However, they show the wide range from 79 ± 3 to 109 ± 4 Ma, implying the various stages of mineralizations.

From the field observations, the formation of gold-quartz veins at Las Palmas is

Table 1. K-Ar ages on rocks and minerals related to ore deposits in Chile.

Locality (Mine)	Province	Latitude (South)	Longitude (West)	Sample No.	Material analyzed	K (wt%)	$^{40}\text{Ar rad}$ (10^{-5}cc/g)	$^{40}\text{Ar rad}/\text{Age}$ (%)	Age (Ma)
Choquelimpie	Parinacota	18° 17.0'	69° 14.2'	2022507	sericite	5.85±0.01	0.137 ± 0.002	51.8	6.0 ± 0.3
Choquelimpie	Parinacota	18° 17.0'	69° 14.2'	2022509	sericite	6.81±0.01	0.148 ± 0.005	75.4	5.6 ± 0.3
Choquelimpie	Parinacota	18° 17.0'	69° 14.2'	2022518	alunite	6.19±0.01	0.166 ± 0.003	53.5	6.9 ± 0.3
Buena Esperanza	Tocopilla	22° 09.9'	70° 12.6'	1030714	sericite	4.70±0.03	3.03 ± 0.01	96.1	159 ± 8
Chuquicamata	El Loa	22° 17.5'	68° 54.5'	2022002	sericite	6.95±0.01	0.879 ± 0.007	86.9	32.3 ± 1.6
Chuquicamata	El Loa	22° 17.5'	68° 54.5'	2022011	K-feldspar	7.77±0.04	1.02 ± 0.01	93.1	33.3 ± 1.7
Escondida	Antofagasta	24° 15.2'	69° 05.0'	2080301	sericite	6.51±0.06	0.891 ± 0.002	89.3	34.9 ± 1.7
Ambicosa	Copiapó	27° 37.3'	70° 23.3'	2051736-A	K-feldspar	1.50±0.01	0.577 ± 0.023	79.7	96.7 ± 4.8
Ambicosa	Copiapó	27° 37.3'	70° 23.3'	2051736-B	biotite	5.76±0.01	2.54 ± 0.03	96.4	110 ± 5
Ambicosa	Copiapó	27° 37.3'	70° 23.3'	2051736-C	hornblende	2.61±0.02	1.04 ± 0.01	78.7	100 ± 5
Andacollo	Limarí	30° 13.7'	71° 05.4'	1031301-5	sericite	7.64±0.08	3.10 ± 0.01	94.1	101 ± 5
La Coipa	Limarí	30° 13.7'	71° 04.6'	1031305-2	sericite	4.12±0.03	1.71 ± 0.01	93.8	104 ± 5
El Bronce	Petorca	32° 10.7'	70° 56.2'	1031504	sericite	3.79±0.03	1.33 ± 0.01	93.4	87.9 ± 4.4
El Bronce	Petorca	32° 10.7'	70° 56.2'	1031505	sericite	3.35±0.03	1.17 ± 0.01	92.6	87.3 ± 4.4
Las Palmas	Talca	35° 09.6'	71° 44.0'	1101704	sericite	4.73±0.01	2.14 ± 0.04	94.5	113 ± 6
Las Palmas	Talca	35° 09.6'	71° 44.0'	1101712	biotite	6.30±0.01	2.66 ± 0.01	96.3	105 ± 5
Las Palmas	Talca	35° 09.6'	71° 44.0'	1101715	sericite	5.61±0.01	2.31 ± 0.03	94.6	103 ± 5

considered to be genetically related to granitic intrusion, located under the veins (*e.g.*, Camus, 1985). The present study apparently suggests this idea, because it shows that the contact metamorphic age is defined to be 105 ± 5 Ma, which corresponds to the ages of both wall rock alteration (113 ± 6 Ma) and mineralization (103 ± 5 Ma) within the experimental errors.

Acknowledgements

The authors gratefully acknowledge Dr. Masato Fukuoka, Dr. Mamoru Enjoji, Dr. Masahiko Yamamoto, Dr. Masatoshi Shiba, Dr. Arashi Kitakaze, Mr. Eduardo Campos, Dr. Guillermo Alfaro, and Dr. José Frutos for their kind helps in collecting samples and the field works. We would express our hearty thanks to Dr. Hirotosugu Nishido, Dr. Arashi Kitakaze, Dr. Masatoshi Shiba and Dr. Masahiko Yamamoto for their cooperation in separating potassium-bearing minerals from the samples.

References

- Aguirre, L. (1983): *Granitoids in Chile*. Geol. Soc. Memoir, 159, 293-316.
- Alvarez, O., Miranda, J. and Guzman, P. (1980): Geología del complejo Chuquicamata. *Minería de Cobre Porfídicos*, 2, 314-363.
- Boric, R., Díaz, F. and Maksaev, V. (1984): Compiemento mapa melogenético, II Región, Chile. *SERNAGEOMIN-CORFO*.
- Camus, F. (1985): Geología de los yacimientos epitermales de oro en Chile y posible modelo idealizado. In *Geología y Recursos Minerales de Chile*, Frutos, J. *et al.* eds., Vol 2, 653-689.
- Camus, F., Boric, R., Skewes, M.A., Castelli, J.C., Reichhard, E. and Mestre, A. (1991): Geologic, structural, and fluid inclusion studies of El Bronce epithermal vein system, Pitorca, Central Chile. *Econ. Geol.*, 86, 1317-1345.
- Cecioni, A. (1985): Dataciones radiométricas de rocas ígneas y metamórficas del ámbito andino meridional. In *Geología y Recursos Minerales de Chile*, Frutos, J. *et al.*, eds., Vol. 1, 219-284.
- Cox, A. and Dalrymple, G.B. (1976): Statistical analysis of geomagnetic reversal data and the precision of potassium-argon dating. *J. Geophys. Res.*, 72, 2603-2614.
- Frutos, J. (1981): *Atlas of 1200 Chilean mines and prospects*. Vol. 1, 1-112, A. Sütulov, Inter. Pub.
- Gröpper, H., Calvo, M., Crespo, H., Bisso, C.R., Cuadra, W.A., Dunkerley, P.M. and Aguirre, E. (1991): The epithermal gold-silver deposit of Choquelimpie, Northern Chile. *Econ. Geol.*, 86, 1206-1221.
- Losert, J. (1973): Genesis of copper mineralizations and associated alterations in the Jurassic volcanic rocks of the Buena Esperanza mining area. (Antofagasta Province, Northern Chile). *Dep. Geol., Univ. of Chile*, 40, 1-64.
- Maksaev, V., Boric, R., Zentilli, M. y Reynolds, P. H. (1988): Significado metalogenético de dataciones K-Ar, ^{40}Ar - ^{39}Ar y trazas de fisión de zonas mineralizadas en el Norte Grande de Chile. *V Congreso Chileno, Santiago*, 1, B65-B86.
- Orquera, W. (1985): Geología y geoquímica de alteración en el "Área de Superficie" de la mina de cobre Buena Esperanza, Chile. *Memoria de Título, Depto. Geociencias, Univ. del Norte, Antofagasta*, 1-221.

- Palacios, C.M. (1990): Geology of the Buena Esperanza copper-silver deposit, Northern Chile. In *Stratabound Ore Deposits in the Andes*, Fontobe, L. et al. eds., Springer-V., 313-318.
- Reyes, M. (1991): The Andacollo strata-bound gold deposit, Chile, and its position in a porphyry copper-gold system. *Econ. Geol.*, 86, 1301-1316.
- Roger, G. (1985): A geochemical traverse across the North Chilean Andes. Ph. D. Thesis, *Dept. Earth Sci., The Open Univ., London, UK.*
- Ruiz, C., Aguilar, A., Egert, E., Espinoza, W., Peebles, F., Quezada, R. y Serrano, M. (1971): Strata-bound copper sulphide deposits of Chile. In *IMA-IAGOD 70th Meeting, Tokyo, Japan, 1970, Soc. Mining Geol. Japan, Special Issue, No. 3*, 252-260.
- Sato, T. (1984): Manto-Type copper deposits in Chile - A review. *Bull. Geol. Surv Japan*, 35, 565-582.
- Segerstrom, K., Thomas, H. and Tilling, R.I. (1963): Cuadrángulo Pintadas. Provincia de Atacama, Escala 1:50,000. *Instituto de Investigaciones Geológicas, Chile*, 12, 1-52.
- Steger, R. H. and Jäger, E. (1977): Subcommission on geochronology: Convention on the use of decay constant in geo- and cosmo-chronology. *Earth Planet. Sci. Letters*, 36, 359-362.
- Tilling, R.I. (1962): Batholith emplacement and contact metamorphism in the Paipote-Tierra Amarilla area, Atacama Province, Chile. *Ph D. Thesis, Yale Univ.*, 1-202.
- Wörner, G., Harmon, R.S., Davidson, J., Moorbath, S., Turner, D.L., McMillan, H., Nye, C., López-Escobar, L. and Moreno, H. (1988): The Nevados de Payachata volcanic region (18° S/69° N, Chile), I. Geological, geochemical, and isotopic observations. *Bull. Volcanology*, 50, 287-303.

STUDY ON THE GUINIER FILM READING AND CALCULATION METHODS

Arashi Kitakaze

Faculty of Science, Tohoku University, Aramaki-Aoba, Sendai 980, Japan.

1. Introduction

The X-ray powder diffraction measurement is easily performed by the powder diffractometer, but this method needs an adequate sample quality, and can not be obtained easily with the desired high resolution data. Therefore, various types of X-ray powder diffraction cameras are used. There are three commonly employed instruments, the Debye-Scherrer camera, the Gandolfi camera and the Guinier focusing camera.

The data measured by both Debye-Scherrer and Gandolfi cameras are lacking of resolution. The Guinier focusing camera is commonly employed when measuring the high resolution data. The instruments, principle of measurement, and data collection and calculation methods for the Guinier camera are summarized by Malmros & Thomas (1977), Jenkins (1989), Smith (1989) and Howard & Preston (1989).

The source of error in the Guinier method is mainly raised by important factors as, (1) measurement for distance of reflection lines and (2) geometry of camera, such as camera radius, X-ray beam divergence, film shrinkage, specimen displacement, and absorption of X-ray. These systematic errors caused by themselves are corrected by the use of an internal standard (Jenkins, 1989).

If error by distance measurement due to the reflection lines can be minimized, we will get an accurate X-ray powder diffraction data. Therefore, an automatic reading system for the Guinier film, a computer program for the calculation of the line positions and intensities, using a least-squares fitting of line profile are constructed. Then, d-spacings with high precision can be obtained. Farther more, lattice parameters of the sample can be refined by least-squares calculation using these d-values.

These methods and the use of such techniques are described below.

2. The principle of X-ray powder diffraction by a Guinier method

The principle of the X-ray powder diffraction by the Guinier method is schematically illustrated in Fig. 1.

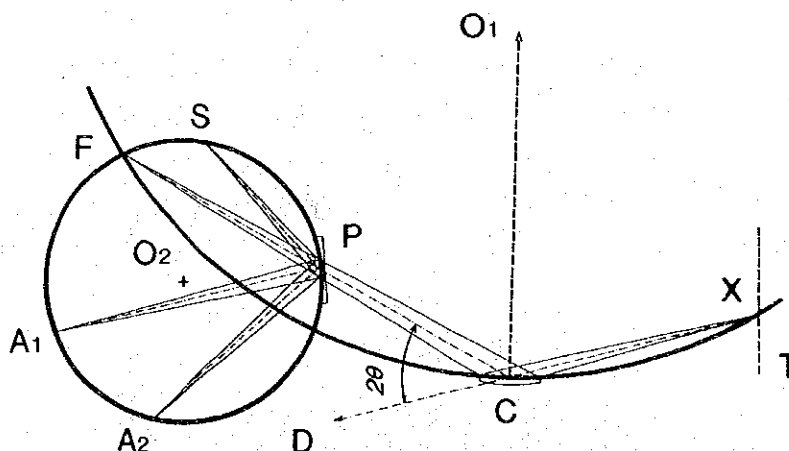


Fig. 1. Diagram showing the principle of the Guinier method.
X: Line focus of X-ray tube, T: Axis of X-ray tube, D: Direction of primary X-ray beam taken out the X-ray tube, C: Monochromator crystal, O_1 : Center of monochromator focussing circle, P: Powder specimen, F: Focal line, O_2 : Center of cylinder in film holder, A_1 , A_2 & S: Example of diffraction lines in the case of "addition" (A) and "subtraction" (S), 2θ : Reflection angle of the monochromator.

The Guinier camera was constructed before the first appearance of line focus of a fine focus X-ray tube and it uses a monochromator of the Johansson type with a bent quartz crystal diffracting from 101 reflection.

The primary scattered X-ray beam X-C-D (Fig. 1) taken out at an angle of about 4.5° to the center of target plane (X) of the X-ray tube is reflected to C-F direction by monochromator crystal. The monochromatized direct beam is translated along the direction C-F passing through the powdered sample (P) until line focus F on the film. The reflection lines by the sample also focus on the film loaded along the film holder such as the case of addition (A_1 , A_2) and subtraction (S).

Sharper diffraction lines are obtained by placing the film holder and employing monochromatized focussing $K\alpha_1$ radiation so that the $K\alpha_2$ component is practically eliminated. In this way, X-ray powder diffraction data of high precision is obtained.

As seen in Fig. 1, powdered specimen (P) is placed inclined towards the direct beam of the monochromatized X-ray radiation. In order to smooth out the diffraction lines, the specimen is rotated in its plane by means of the electric motor. This rotation gives a better smoothing-out effect of translation and orientation of the sample. This requires a much smaller specimen size in order to give an acceptable result.

The Guinier camera (Expectron XDC-1000) has a diameter of 100 mm, giving a dispersion equal to that of a Debye-Scherrer camera with a diameter of 200 mm. So, theoretically, the length of 1 mm on the Guinier film corresponds to 0.57296° in angle 2θ . Usually, the reflection lines can be solved when they are as close as 0.01 mm of the Guinier film of the samples. This corresponds to an ability of separating the lines at 0.005° in 2θ .

As the Guinier method yields a large diffracted intensity, X-ray diffraction data can be obtained by small amount of powdered sample less than 1 mg.

3. Equipment of the system

The instruments for Guinier film reading system consist of (1) a system taking a Guinier film and (2) a Guinier film reading system.

3.1. System for X-ray powder diffraction for Guinier method

The apparatus used for taking the X-ray powder diffraction film by the Guinier method consists of:

- (1) X-ray generator for a Guinier camera
X-ray source power supply: 2 kW.
X-ray tube: fine focus type of Cu or Cr
- (2) Guinier camera
Expectron type XDC-1000
Camera diameter: 100 mm.
Monochromator: Johansson type bent quartz crystal for Cu and Cr radiation.

Using these instruments, the Guinier film will be taken by the method described below.

3.2. Guinier film reading system

The Guinier film obtained by the instruments described above is measured by the X-ray film reading system. This system consists of the following apparatus, which are directly connected among each other so as to read automatically the concentration of the Guinier film during the scanning of the microphotometer stage (Fig. 2), and control it by computer software.

- (1) Personal computer
NEC PC-9801 RX
Memory: 640 kB and 10 MHz of clock time.

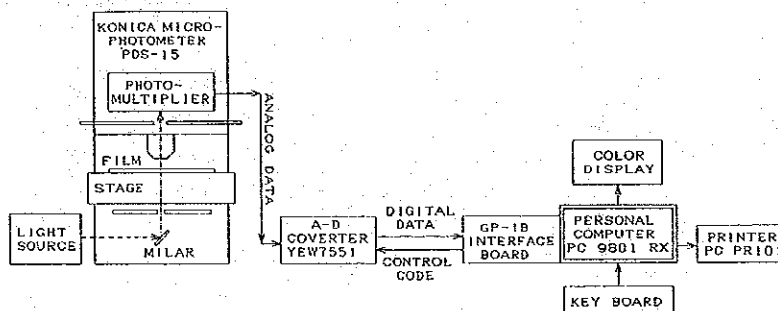


Fig. 2. Schematic block diagram of the Guinier film reading system.

- Floppy disk driver: 2 drivers (A and B).
- Color Display: NEC-PC-KD854N with 14 inches in size.
- (2) GP-IB Interface
NEC-PC-9801-29N GP-IB interface board.
- (3) A-D converter
Yokogawa YEW 7551 digital multimeter with GP-IB interface.
- (4) Serial printer
NEC PC-PR101G2
- (5) Microphotometer
Konica Microphotometer type PDS-15
Measurement range: 0.0 - 4.0 D.

The concentration of a Guinier film on the stage scanned by the electric motor is read by the microphotometer (Konica PDS-15) as analog data. Its values are converted to digital data by digital multimeter (YEW 7551), and automatically inputted into the personal computer (NEC PC-9801 RX) though GP-IB interface (PC-9801-29N), controlled by the computer software.

4. Calculation method and software

The Guinier film reading and calculation programs are used for the automatic data collection of the measured Guinier film, and obtained from the X-ray powder diffraction data of the measured sample. Farther more, if approximate cell parameters of measurement specimen are known, their values can be refined by the least-squares calculation using measured d-values.

These programs were first written by N88BASIC of MS-DOS version 3.3B and converted to the P-code interpreter using by BASIC compiler of MS-DOS. This computer software consists of (1) MAIN, (2) READ-V3, (3) CALC-V3 and (4) XRPD-V3 programs.

At least, two floppy disk drivers are necessary in order to use this software, one is for the program disk (normally drive A or 1), the other is for the data disk (usually drive B).

In this description, input "1", "Y", etc. means push keys of "1" or "Y", etc. in the keyboard and then push "RETURN" key.

4.1. "MAIN" program

The schematic flow chart of the "MAIN" program is shown in Fig. 3. This program consists of the following procedures.

- (1) "READ-V3" program is directly called.
- (2) After selection of file name and data type stored in the data disk, this program changes to "CALC-V3" program.
- (3) After selection of file name saved in the data disk, "XRPD-V3" program is run immediately.
- (4) Setting of the initial parameters for reading and calculation processes like the type of A-D converter, driver name employing as the data disk, measurement method, diameter of used camera, measurement X-ray radiation, its wave

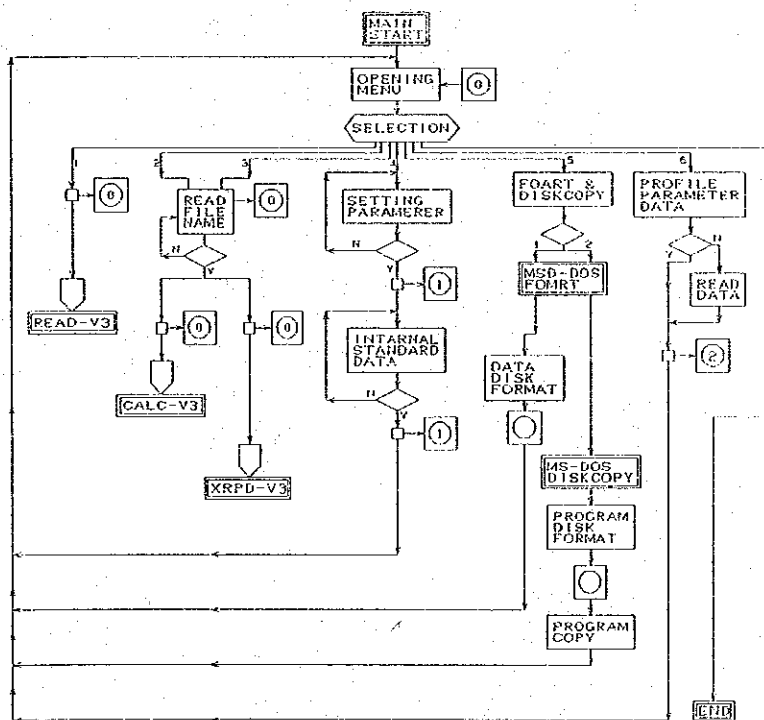


Fig. 3. Schematic flow chart of the "MAIN" program.
Disk data 0, 1 and 2 correspond to "FILE.NAM", "STD.DAT" and "FUNCTION.DAT" file, respectively.

- length, using internal standard, and its reflection position as mm in the Guinier film measured previously are performed.
- (5) MS-DOS commands as disk formatting and program copy are carried out.
 - (6) The profile fitting function as Pearson VII or Gaussian type and parameters using least-squares calculation are selected.

4.2. "READ-V3" program

The Guinier film reading system is controlled by this program of which schematic flow chart is shown in Fig. 4. After the names of the measurement are given as file names, the concentration of a Guinier film as analog data moving the film stage of the microphotometer set in 0.1 mm/sec as scanning speed are converted to digital data by A-D converter, and automatically inputted into the computer passing through the GP-IB interface in 250 msec interval (4 times/sec). This timing is also controlled by the program. The digitalized 6,480 data are collected during measurement of 162 mm length of the film displaying measured values. After data collection during 27 minutes, all reading data are stored into the data disk, and then the program changes to "CALC-V3" program, automatically.

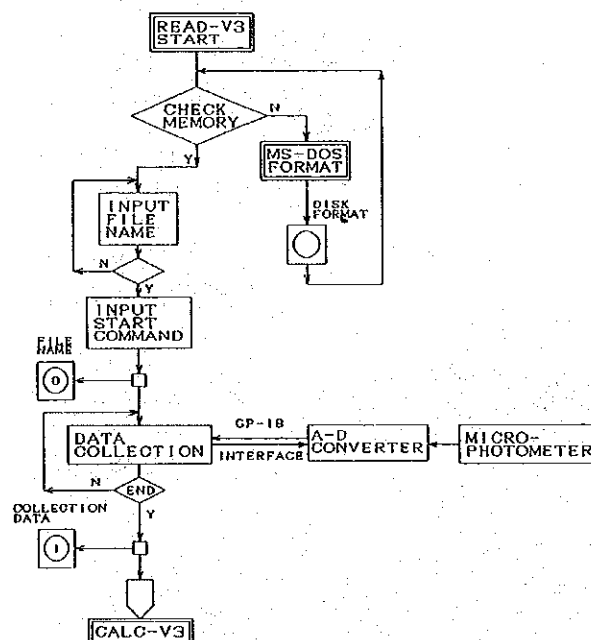


Fig. 4. Schematic flow chart of the "READ-V3" program.
Disk data 0 and 1 is "FILE.NAM" and "...FLM" files, respectively.

4.3. "CALC-V3" program

The schematic flow chart of this program is given in Fig. 5. Four procedures are carried out according to the data type given by "MAIN" program. The most important process is data type No.1 consisting of the following procedures:

- (1) After reading the collected data obtained by "READ-V3" program, back ground subduction is performed using the same method by Sonneveld & Visser (1975) as treatment of following procedures.
 - a. Reading data stepped 20 interval (p_i) is first approximate as back ground.
 - b. Calculate of $m_i = (p_{i+1} + p_{i-1})/2$.
 - c. If $p_i > m_i$ then p_i is replaced by m_i .

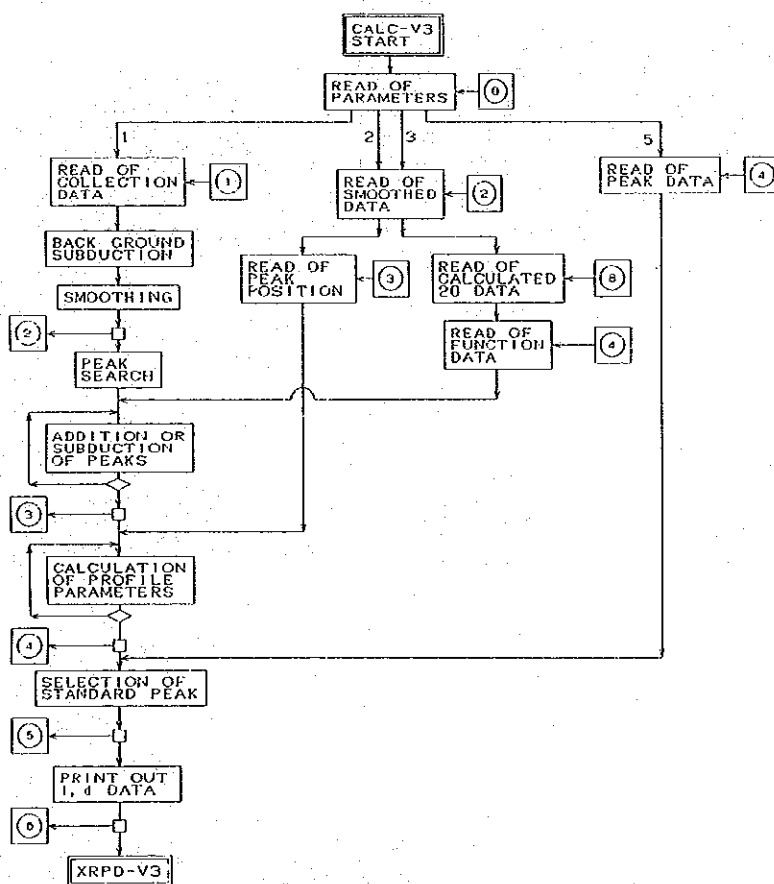


Fig. 5. Schematic flow chart of the "CALC-V3" program.
 Data 0: "FILE.NAM" = "STD.DAT" and "FUNCTION.DAT" files
 1: "...FLM", 2: "...SMT", 3: "...CH", 4: "...MM", 5: "...FNC",
 6: "...ID", 8: "...20" files.

The procedures from b to c are repeated about 8 times, which is a good approximation of the back ground for the Guinier film.

- (2) The intensity data subtracted back ground are smoothed using the filter constants in the Gaussian function for 7 points data, and stored in a data disk.
- (3) Peak search is carried out by means of the top-hat method, and the intensity and position for each reflection as a first approach are calculated. Then addition or subtraction of some peaks are made manually.
- (4) Using these values, the peak profiles are fitted with a Pearson VII function.

The intensity (I_i) at a given point (X_i) in the function can be expressed by:

$$I_i = I_o / [1 + C (X_i - X_o)^2]^m + BG,$$

where I_o : peak intensity

$$C = 4 \cdot (2^{1/m} - 1) / (FWHM \times A)^2$$

m : parameter of exponent for the function

X_o : peak position

A : asymmetry factor

BG : back ground

These parameters as I_o , X_o , FWHM, A and BG for each reflection are refined by the non-linear least squares calculation. If the difference of the positions in a first approach are within 5 times of FWHM, and these reflections are more than two, they are calculated as one group. When the change of each parameter is less than the previously decided value (0.02), the refinement for profile fitting of each reflection or a group of reflections is finished, normally, 5 to 6 times of the calculation. The fitting error (R) as unweighed residual value is determined from the following expression.

$$R = [S(I_i^{obs} - I_i^{calc})^2 / S(I_i^{calc})^2]^{1/2}$$

After profile fitting is carried out all peaks selected by procedure (3), the next procedure, are performed.

- (5) After reflections for the internal standard are selected, a calibration curve for conversion of a length in mm to 2θ is obtained as biquadratic equation. In this calculation, values of 5.43088 Å as standard silicon and 1.540598 Å as wave length of $CuK\alpha_1$ radiation are used. The intensity, and d-values for each reflection are calculated, and printed out.

4.4. "XRPD-V3" program

Flow chart of this program is shown in Fig. 6. This program is ran through the following procedures:

- (1) Read a crystallographic data type as 1: newly inputted or 2: stored value.
- (2) Select to read a type of intensity and d-spacing values obtained by 1: "CALC-V3" program or 2: another.
- (3) Input the crystallographic data such as mineral name, chemical formula,

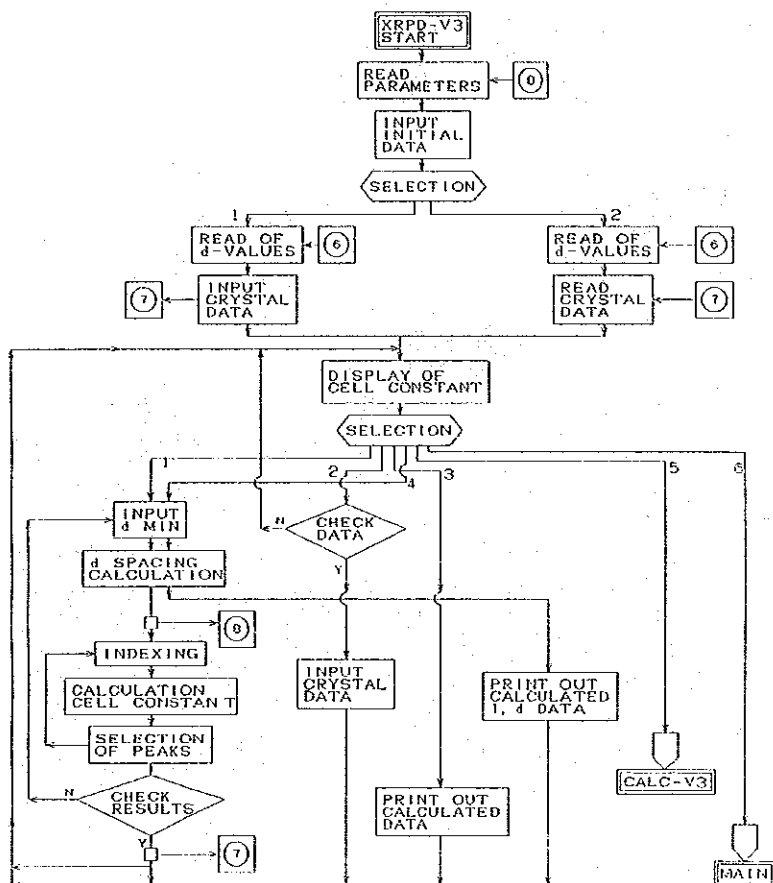


Fig. 6. Schematic flow chart of the "XRPD-V3" program. Number of data file is same as Fig. 8. 7: "...DAT"

crystal system, symbol of space group, Z-number, approximate cell parameters and other comments. At this moment, the symbol of space group is listed in Appendix 1, and is checked in the program.

- (4) Indexed d-spacing having greater than the given minimum value are calculated by the cell parameters according to the extinction rule of the space group given as symmetry code (Appendix 1). Then, these calculated values are arranged in larger order.
- (5) Indexing for the observed d-spacing are carried out in comparison with observed and calculated d-values.
- (6) Cell parameters are refined using all indexed data by the least squares calculation according to the crystal system.
- (7) After that, print out all given crystallographic data, refined cell parameters, observed and calculated d and 2θ values with both differences.

5. Arrangements using the software

The Guinier film reading and calculation programs are performed on condition of using some initial parameters for reading and calculation which are selected by the JOB No.=4, 5 and 6 in the "OPENING MENU". Then these JOBS are carried out as first procedure when using the software.

5.1. Setting of initial parameters

When the program starts, the following message is displayed:

OPENING MENU

JOB LIST

- 1: FILM READING
- 2: CALCULATION OF READING DATA
- 3: CELL PARAMETER CALCULATION
- 4: SETTING OF INITIAL PARAMETERS
- 5: FORMAT & DISKCOPY
- 6: FUNCTION OF CALCULATION
- 7: END

JOB No. =

4: SETTING OF INITIAL PARAMETERS

SETTING DATA ARE AS FOLLOWS
0: DIGITAL M = YEM7551
1: DATA DISK = B:
2: VERSION = 1.20
3: MEASUREMENT = GUINIER
4: CAMERA R = 200.00mm
5: SCAN SPEED = 0.1 mm/sec
6: RADIATION = CuK α 1
7: RAMDA = 1.540598
8: STANDARD = SILICON

mm DATA FOR STANDARD

a= 5.43088 A
1 28.443 49.9
2 47.303 83.1
3 56.123 98.6
4 69.131 121.6
5 76.377 134.4
6 88.032 155.0

READING STEP=1000
DATA OK (Y/N) =

Fig. 7. Message for setting on initial parameters using reading and calculation programs.

After selecting JOB No.=4 (input "4"), the initial parameters stored as "SETTING.DAT" file in the program disk are newly displayed as the message shown in Fig. 7. The setting data is no change, input "Y" and goes to the next setting after these data is saved in the program disk with same file name.

If setting data as initial parameters will be reformed to another data, input "N" and input desired numeral according to the asking message. After that, the message (Fig. 7) reappears and repeat in the same way.

Initial setting data like asking message correspond to the following parameters.

- (0) Type of digital multimeter
 - 1: Takeda TR 8652 used at Tohoku Univ.
 - 2: Yokogawa YEW 7551 used at Concepcion Univ.
- (1) Floppy disk drive for data disk
 - 1: B, 2: C, 3: D drive
- (2) Version number
In this program, it does not set.
- (3) Measurement method of X-ray diffraction
 - 1: Guinier camera.
 - 2: Gandolfi camera.
 - 3: manually input of intensity and d-values.
- (4) Diameter of camera
 - 1: 114.59 mm (Gandolfi camera).
 - 2: 57.30 mm (Gandolfi camera).
 - 3: 200.00 mm (Guinier camera).
- (5) Scanning speed of microphotometer
Set only 0.1 mm/sec (no choice).
- (6) Measurement X-ray radiation
 - 1: CuK α radiation.
 - 2: CrK α radiation.
 - 3: FeK α radiation.
- (7) Wave length as Angstrom for measurement radiation
- (8) Internal standard using for Guinier camera
 - 1: Silicon (a=5.43088 Å).
 - 2: Fluorite (a=5.4637 Å).

After the setting of initial parameters, previous values of the reflection data for the internal standard stored in the data disk as "SILICON.DAT" or "FLUORITE.DAT" as file name are displayed. If they do not change, input "Y" and program returns to "OPENING MENU".

To select a change (input "N"), input new data measured in mm for 6 reflections of the internal standard and repeat in the same way mentioned above.

5.2. Choice of the fitting function

This JOB consists of selecting the fitting function for the line profile measured by some cameras. In the "OPENING MENU", choice of No.=6, and then previous data as "FUNCTION.DAT" file are newly displayed. If these data are going to be changed, input numerals according to the selection messages.

The menus correspond to next procedures:

1: PROFILE FUNCTION

1: PEARSON VII function

Used for profile fitting of reflection lines obtained by the Guinier method.

2: GAUSSIAN function

Using for profile fitting for the data measured by the Gandolfi or Debye-Scherrer cameras.

2: CALCULATION MODE

1: ALL DATA FIX (NORMAL MODE)

In the case of peak doublet or more, values for the full-width at half maximum (FWHM) and asymmetry factor (ASFC) for the reflection and number of the Pearson VII function (PM) for each reflection are fixed in the least-squares calculation for fitting of the line profile.

2: FWHM VARIABLE (BAD CRYSTALLINE MODE)

In the above case, FWHM and ASFC values for each reflection can be calculated as variable component.

3: FWHM & PM VARIABLE

At above peaks, all components are calculated as variable parameters.

3: PROFILE DRAWING

This menu corresponds to printing out both of the profiles observed and calculated for all reflections at the computing time. In the case of "YES", program stops during the drawing time and calculation time is long, therefore usually "NO" is selected.

5.3. Format of data disk

When a new floppy disk is used for the first time, this procedure is needed. This JOB is used for initializing the new unformatted data disk. In the "OPENING MENU", select JOB No.=5 (input "5"), then follow the messages are newly displayed.

5: FORMATING AND DISKCOPY PROGRAM

DATA DISK = X
DISK = 2HD

- 1: FORMATING FOR DATA DISK
- 2: FORMATING AND DISKCOPY FOR SOURCE DISK

No. =

Input "1" in above message, then display continuously next asking.
NEW DISK INSERTS TO X : DRIVE
SYSTEM OK (Y/N) =

At this time, a new unformatted floppy disk of 2HD type having 1.25 MB memories is inserted into the X: floppy disk drive and answer as "YES" (input "Y"). Then "FORMAT version 4.0" program in MS-DOS system runs immediately displaying some Japanese and English messages and "FILE.NAM" file is made on this new data disk in X: drive. After that, the program returns to "OPENING MENU". The disk drive name "X" can be changed by JOB No.=4 described above.

5.4. Copy of program

Do selection of JOB No.=5 in the "OPENING MENU", then above "5 : FORMATTING AND DISKCOPY" message is displayed. In this message, input "2" and next asking are displayed continuously.

DISKCOPY PROGRAM
SOURCE DRIVE = A:
COPY DRIVE = X:
DRIVE OK (Y/N) =

A original program disk inserts into the A: drive, and a new unformatted floppy disk of 2HD type inserts into the X: drive. Then input "Y". The "FORMAT version 4.0" program in MS-DOS system runs displaying some Japanese and English message. After that, the "DISKCOPY" program in MS-DOS system runs and carries out the copy of all programs and data from A : drive to X : drive displaying some Japanese and English messages. After finishing the "DISKCOPY", the program returns to "OPENING MENU".

6. Instruction for preparation of the sample

The measured mineral sample of less than 10 mg for the X-ray powder diffraction by the Guinier method is finely ground in an agate mortar. The sample is mixed with finely powdered internal standard (metal silicon or fluorite) to proportion of approximately 3 to 1 as volume ratio, and then ground sufficiently in the agate mortar.

The specimen is supported by thin tape mounted over 6 mm holes in circular disk that are placed in the rotation disk holder. The finely powdered sample mixed with internal standard is dusted on to the adhesive part of the tape in the hole of the specimen disk holder. If a "Scotch" mending tape with a thin base is used, good diffraction data are generally obtained.

The X-ray film of 20 mm wide and 195 mm long is used for the Guinier camera, cutting from the original sheet film (25.4 x 30.5 cm) of industrial double coated X-ray film of ASA 150. This cut film is loaded on the film holder of camera under the safety light for the X-ray.

The primary beam (15 kV, 2 mA) exposes on the X-ray film about 1 to 2 seconds recording a position of the camera. After that, the X-ray film exposes for 10 to 12 hours under the condition of 35 kV and 15 mA. Finally, the X-ray film is only developed its inside side by a developer for the X-ray film.

According to above precedures, the X-ray powder diffraction film by the Guinier method as given in Fig. 8 is obtained.



Fig. 8. Photograph of the Guinier film for scheelite with silicon, $\text{CuK}\alpha_1$ radiation.

7. Using the programs

7.1. Start of the program (MAIN)

- (1) Switch on the personal computer.
- (2) Insert the program disk into A : floppy disk driver (No.1 floppy disk driver).
- (3) Push "RESET" key.
- (4) Following messages are displayed, after some Japanese and English message.

OPENING MENU
 JOB LIST
 1: FILM READING
 2: CALCULATION OF READING DATA
 3: CELL PARAMETER CALCULATION
 4: SETTING OF INITIAL PARAMETERS
 5: FORMAT & DISKCOPY
 6: FUNCTION OF CALCULATION
 7: END
 JOB No. =

- (5) Usually "1 : FILM READING" JOB corresponding to READ-V3 program is selected. Then input "1".

7.2. Guinier film reading program (READ-V3)

The data of concentration of a Guinier film are collected using the Guinier film reading system mentioned above. After that, all data are stored into data disk as "...FLM" data file in the "X : " floppy disk driver which is selected using JOB No.=4 in the "OPENING MENU", and continues automatically to CALC-V3 program. This program runs following the procedures.

- (1) If JOB No.=1 in "OPENING MENU" is selected, this program runs immediately, and some messages are displayed.
- (2) Input "FILE NAME" within 8 characters without ".", ",", ":", "...".
- (3) Set a Guinier film on the microphotometer, and adjust the 0-position of the Guinier film using Y screw and scanning of the stage.
- (4) Adjust the scanning speed of microphotometer to 0.1mm/sec.
- (5) Push "<" key in the microphotometer, and press any key (usually "RETURN" key). After that, data collection for the concentration of the Guinier film starts immediately.
- (6) After reading during 27 minutes, file name and all collecting data are stored into data disk as named "...FLM" in X : disk driver. In this case, ** is the file name given by procedure (2).
- (7) Automatically goes to "CALC-V3" program.

7.3. Calculation program (CALC-V3)

After film data reading, this program starts immediately, and the following procedures are performed.

- (1) Collected data are inputted to personal computer from the "...FLM" file in the data disk as channel data.

- (2) Back ground correction is carried out automatically.
- (3) Diminishing the intensity of the data can be performed using the Gaussian method and the data are stored into the data disk as "...SMT" file.
- (4) Calculation of peak search parameter is carried out using the digital filter method, and approximate peak positions are calculated.
- (5) After these calculation, peak positions, line profiles and some messages as shown in Fig. 9 are displayed. In this time, peak selection is done according to the message changing a cursor position and using "-" or "+" keys until final page (in this case "DATA PAGE = 11/11").
- (6) If "1" key is pushed to the final page, data of peak positions searched and selected above procedures are stored in data disk as "...CH" file and next calculation is start.
- (7) The calculation parameters for profile function such as peak intensity (I), peak position (X), full-width at half maximum of the reflection (FWHM), asymmetry parameter (AS), back ground (BG) for profile function are calculated using the least-squares fitting, and the results are displayed as seen in Fig. 10 with comparisons between measured and calculated peak profiles and deviation of both, but normally this disappears after several msec.
- (8) After the computation of the profile fitting for all reflections, channel data are corrected to length in mm considering position of direct beam, and line profile parameters such as peak intensity (NET-I), integral intensity (INT-I), peak position as distance from 0-position to each reflection as channel data (CH) and mm data, value of FWHM as channel (CH) and length in mm, asymmetry parameter (ASF) are printed out (Table 1).

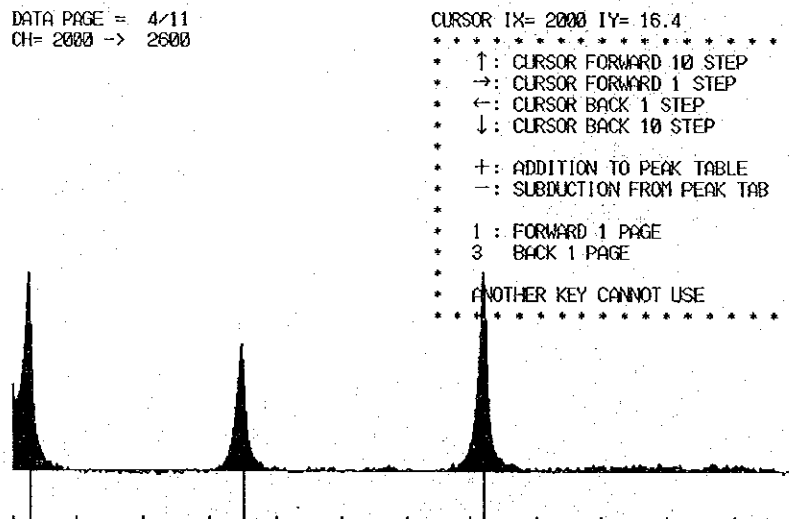


Fig. 9. Line profiles and peak positions performed back ground subduction, smoothing and peak search calculations.

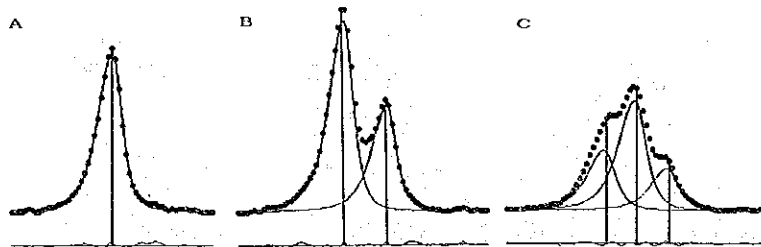


Fig. 10. Comparison of measured diffraction patterns (black circle) with calculated line profiles and deviation of both values using Pearson VII function. A: single peak, B: double peak, C: triple peaks.

- (9) The message for the peak selection of the internal standard is displayed as seen in Fig. 11. Input the delete number until 6 reflections, for example, No.4, 6 and 8 reflection in the figure because their D-MM and RATIO values are different from another 6 reflections. If average of difference (D-MM) between observed (OBS) and calculated (TRUE) values is less than 0.005 in 2θ , the program goes to the next procedure continuously.
- (10) The data for the internal standard (Table 2) are printed out together with the correction formulas for conversion from length (mm) to 2θ and their reverse. These constants for later formula are saved into data disk as "***.FNC" file.
- (11) After that, calculation result for intensity, 2θ and d-values are printed out (Table 3) and stored into data disk as "***.ID" data file.
- (12) When this program ends, "XRPD-V3" is automatically called.

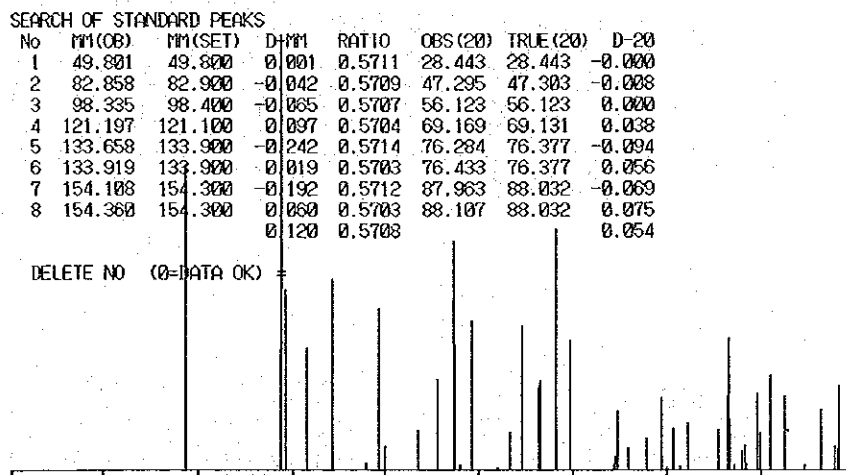


Fig. 11. Selection message for reflection lines of the internal standard compared with line position of the measured sample.

7.4. Cell parameter calculation program (XRPD-V3)

- (1) At the starting time of this program, some messages (Fig. 12) are displayed. Then usually input "1" as DATA TYPE = 1, and also "1" as ID DATA TYPE.
- (2) Messages (Fig. 13) are immediately displayed, and then, input the crystal data for sample as data of some numerals or descriptions according to the asked messages from 1 to 11. At this step, the space group is previously stored in the program with the name described in appendix 1. Therefore another name for space group cannot be used and inputted.
- (3) Input minimum d-value for the d-spacing is calculated by given cell parameters. If precision of cell parameters is not so good, input values of 2 or 1.5 as d-min firstly.

Table 1. Calculation results of line profile fitting for scheelite

```

*****
RESULT OF GUINIER FILM READING
FILE NAME = SCH-1
*****
SMOOTHING      : GAUSSIAN FUNCTION
FUNCTION       : PEARSON VII
CALCULATION   : ALL DATA FIX
    
```

No	NET-I	INT-I	CH	FWHM	PM	ASFC	mm	FWHM	R
1	65.83	449.62	1261.49	5.602	2.000	0.596	32.61	0.145	6.74
2	26.18	233.60	1926.25	7.323	2.000	0.759	49.80	0.189	7.72
3	93.48	840.47	1944.26	7.372	2.000	0.759	50.27	0.191	7.72
4	38.80	351.29	1966.18	7.429	2.000	0.759	50.83	0.192	7.72
5	26.37	207.19	2128.04	6.450	2.000	0.815	55.02	0.167	7.60
6	40.99	299.14	2314.51	5.989	2.000	0.777	59.84	0.155	5.44
7	1.52	13.21	2557.21	7.152	2.000	0.898	66.11	0.185	47.58
8	34.77	263.81	2854.89	6.232	2.000	0.803	68.64	0.161	5.65
9	4.97	28.30	2703.72	4.675	2.000	0.900	69.90	0.121	28.61
10	8.41	55.16	2935.23	5.383	2.000	0.704	75.89	0.139	11.62
11	19.49	143.30	3079.16	6.034	2.000	0.782	79.61	0.156	6.75
12	49.36	353.43	3192.09	5.873	2.000	0.722	82.53	0.152	3.29
13	27.00	193.63	3204.85	5.882	2.000	0.722	82.86	0.152	3.29
14	32.36	259.05	3327.17	6.572	2.000	0.851	86.02	0.170	6.77
15	0.62	9.73	3509.71	13.000	2.000	0.907	90.74	0.336	57.78
16	8.16	57.18	3590.02	5.746	2.000	0.739	92.82	0.149	13.35
17	31.26	288.98	3680.15	7.597	2.000	0.882	95.15	0.196	7.44
18	17.88	144.53	3803.49	6.635	2.000	0.879	98.33	0.172	7.37
19	19.39	156.97	3816.25	6.644	2.000	0.879	98.66	0.172	7.37
20	51.86	482.86	3923.40	7.643	2.000	0.805	101.44	0.198	2.96
21	8.48	79.05	3937.22	7.658	2.000	0.805	101.79	0.198	2.96
22	28.16	280.50	4031.35	8.192	2.000	0.909	104.23	0.212	5.42
23	12.04	81.43	4376.87	5.548	2.000	0.744	113.16	0.143	16.33
24	4.78	35.36	4448.52	6.066	2.000	0.916	115.01	0.157	17.85
25	6.78	63.66	4579.14	7.715	2.000	0.842	118.39	0.199	13.49
26	15.69	134.14	4687.79	7.023	2.000	0.823	121.20	0.182	7.36
27	9.05	83.07	4777.14	7.593	2.000	0.851	123.51	0.196	9.99
28	0.83	6.57	4822.44	6.480	2.000	0.919	124.68	0.168	67.74
29	10.33	99.39	4880.84	7.913	2.000	0.887	126.19	0.205	10.05
30	8.84	108.32	5093.19	10.106	2.000	1.013	131.68	0.261	10.92
31	15.49	146.54	5160.55	7.766	2.000	0.806	133.42	0.201	2.82
32	28.29	267.93	5169.81	7.772	2.000	0.806	133.66	0.201	2.82
33	10.78	102.14	5179.74	7.780	2.000	0.807	133.92	0.201	2.82
34	3.99	62.68	5265.67	13.000	2.000	1.236	136.14	0.336	15.74
35	4.93	77.59	5283.90	13.000	2.000	1.236	136.61	0.336	15.74
36	16.39	175.60	5375.58	8.811	2.000	0.907	138.98	0.228	6.11
37	8.18	87.76	5386.89	8.822	2.000	0.907	139.27	0.228	6.11
38	20.28	236.33	5469.51	9.603	2.000	0.945	141.41	0.248	5.53
39	16.01	204.85	5570.69	10.566	2.000	1.109	144.02	0.273	9.44
40	12.97	144.54	5840.70	9.182	2.000	0.961	151.00	0.237	6.68
41	5.03	48.20	5945.22	7.872	2.000	0.884	153.71	0.204	4.78
42	4.47	42.95	5960.75	7.883	2.000	0.884	154.11	0.204	4.78
43	18.03	173.27	5970.48	7.889	2.000	0.884	154.36	0.204	4.78

Table 2. Observed reflection position for the internal standard compared with calculated and recommended 2θ values

```

*****
      RESULT OF GUINIER FILM READING
      FILE NAME = SCH-1
*****

INTERNAL STANDARD = SILICON(a=5.43088 A)
WAVE LENGTH CuK $\alpha$ 1 (1.540600 A)

      DATA OF INTERNAL STANDARD
-----
No      mm      OBS      TRUE     OBS-TRUE
-----
  1    49.801    28.444    28.443    0.000
  2    82.858    47.304    47.303    0.001
  3    98.335    56.120    56.123   -0.003
  4   121.197    69.134    69.131    0.003
  5   133.916    76.376    76.377   -0.002
  6   154.360    88.032    88.032    0.000
-----
                         $\sigma$  = 0.002

2 $\theta$  = .570272 *mm-1  4.00144E-05 *mm2 -5.45066E-07 *mm3  1.8604E-09 *mm4
mm     = 1.75457 *2 $\theta$ -1 -2.71452E-04 *2 $\theta$ 2  6.09144E-06 *2 $\theta$ 3 -3.58294E-08 *2 $\theta$ 4

```

- (4) The calculation of d-spacing is performed using given cell parameters according to the symmetry operation by given space group, ordering of d-values in large order, and indexing for the observed d- values. Then cell parameter is calculated by least-squares method using indexed data and the results are displayed (Fig. 14).
- (5) At first time of cell parameter calculation, input "N" and "Y" for asking messages of "DATA CORRECT" and then "REINDEXING", respectively.

```

CELL PARAMETER CALCULATION PROGRAM
XRPD-V3 PROGRAM

      FILE NAME = SCH-1      ICALC=5

READ OF CRYSTAL DATA FROM
  1 : NEW DATA   NO   *.DAT FILE
  2 : STORED DATA AS   *.DAT FILE

DATA TYPE = 1

READ OF ID FILE
  1 : ID-DATA FILE   *.ID
  2 : MANUAL INPUT OF ID-DATA

FILE TYPE =

```

Fig. 12. The message of data type selection for XRPD-V3 program.

Table 3. X-ray powder diffraction data obtained by the Guinier film reading and calculation systems

 RESULT OF GUINIER FILM READING
 FILE NAME = SCH-1

 DIFFRACTION DATA OF SAMPLE

No	I/10	mm	2θ	FWHM	d(obs.)	
1	70.4	32.61	18.62	0.083	4.7603	
2	16.1	49.80	28.44	0.108	3.1354	STD
3	100.0	50.27	28.71	0.109	3.1070	
4	41.5	50.83	29.03	0.110	3.0731	
5	28.2	55.02	31.42	0.096	2.8446	
6	43.9	59.84	34.17	0.089	2.6216	
7	1.6	66.11	37.76	0.106	2.3808	
8	37.2	68.64	39.20	0.092	2.2965	
9	5.3	69.90	39.92	0.069	2.2567	
10	9.0	75.89	43.33	0.080	2.0865	
11	20.8	79.61	45.45	0.089	1.9939	
12	52.8	82.53	47.12	0.087	1.9273	
13	17.8	82.86	47.30	0.087	1.9201	STD
14	34.6	86.02	49.11	0.097	1.8538	
15	0.7	90.74	51.79	0.193	1.7637	
16	8.7	92.82	52.98	0.085	1.7271	
17	33.4	95.15	54.30	0.113	1.6879	
18	15.0	98.33	56.12	0.098	1.6376	STD
19	20.7	98.66	56.31	0.098	1.6325	
20	55.5	101.44	57.89	0.113	1.5917	
21	9.1	101.79	58.09	0.113	1.5867	
22	30.1	104.23	59.47	0.121	1.5530	
23	12.9	113.16	64.56	0.082	1.4424	
24	5.1	115.01	65.61	0.090	1.4217	
25	7.3	118.39	67.54	0.114	1.3859	
26	16.1	121.20	69.13	0.104	1.3577	STD
27	9.7	123.51	70.45	0.112	1.3355	
28	0.9	124.68	71.12	0.096	1.3246	
29	11.0	126.19	71.98	0.117	1.3109	
30	9.5	131.68	75.10	0.150	1.2639	
31	16.6	133.42	76.09	0.115	1.2499	
32	30.3	133.66	76.23	0.115	1.2480	
33	10.6	133.92	76.38	0.115	1.2460	STD
34	4.3	136.14	77.64	0.193	1.2288	
35	5.3	136.61	77.91	0.193	1.2252	
36	17.5	138.98	79.26	0.131	1.2077	
37	6.7	139.27	79.43	0.131	1.2056	
38	21.7	141.41	80.64	0.142	1.1904	
39	17.1	144.02	82.13	0.157	1.1726	
40	13.9	151.00	86.12	0.136	1.1282	
41	5.4	153.71	87.66	0.117	1.1123	
42	4.8	154.11	87.89	0.117	1.1100	
43	17.6	154.36	88.03	0.117	1.1086	STD

- Then the program returns to procedure (3), and repeats the procedure (4).
- (6) If indexing, cell parameter calculation, and differences between observed and calculated d or 2θ values are not problem, input "N" and next "N" in procedure (5). These data are stored in the data disk as "***.DAT" file.
 - (7) The refined cell parameters and another data inputted previously are displayed with some messages (Fig. 15).
 - (8) In this message, if No.3 JOB (DATA PRINT BY PRINTER) is selected, the refined cell parameters, another crystal data and information for the measured sample, intensities, indexes and both of calculated and observed d-spacing and 2θ values with their difference for each reflections are printed out (Table 4). Then, the program returns to the message seen in Fig. 15.
 - (9) The reading and calculation programs are finished. Select No.6 to send "program end".

FILE NAME = SCH-1

ID DATA= 49

```

1: MINERAL NAME =
2: CHEMICAL FORMULA =
3: CRYSTAL SYSTEM =          0
4: SPACE GROUP =            0
5: Z-NUMBER = 0
6: CELL PARAMETER
   a = 0.00000( 0)  b = 0.00000( 0)  c = 0.00000( 0)
   α = 0.000( 0)  β = 0.000( 0)  γ = 0.000( 0)
7: MEASUREMENT METHOD = GUINIER
8: INTERNAL STANDARD = SILICON
9: RADIATION = CuKα1 (1.540598 Å)
10: SPECIMEN =
11: REMARK =
  
```

Fig. 13. The message inputted crystal data and some measurement condition of cell parameter refinement for the measured sample.

```

SCH-1 SCHEELITE Tetragonal 141/a
a = 5.24323( 19)  b = 5.24323( 19)  c = 11.37468( 59)
α = 90.00000( 0)  β = 90.00000( 0)  γ = 90.00000( 0)
DATA CORRECT ? (y/n) =
 1 70 1 0 1 4.7606 -11 4 21 5 0 0 8 1.4217 -1 5
 2 100 1 1 2 3.1071 12 -11 22 7 3 0 5 1.3859 -1 4
 3 42 1 0 3 3.0731 7 -7 23 16 3 2 3 1.3577 -1 5
 4 28 0 0 4 2.8447 10 -11 24 10 2 1 7 1.3355 -1 4
 5 44 2 0 0 2.6216 -0 0 25 11 4 0 0 1.3109 1 -7
 6 2 2 0 2 2.3808 -1 2 26 9 4 1 1 1.2639 1 -9
 7 37 2 1 1 2.2965 -1 1 27 17 2 0 8 1.2499 1 -4
 8 5 1 1 4 2.2567 3 -6 28 30 3 1 6 1.2480 -1 4
 9 9 1 0 5 2.0865 -5 10 29 5 1 0 9 1.2286 -0 3
10 21 2 1 3 1.9939 -4 9 30 6 3 2 5 1.2251 -1 11
11 53 2 0 4 1.9273 -2 5 31 18 3 3 2 1.2077 1 -4
12 35 2 2 0 1.8537 -0 1 32 9 4 1 3 1.2056 -1 6
13 9 3 0 1 1.7270 -4 14 33 22 0 4 1.1904 0 -1
14 33 1 1 6 1.6879 0 -0 34 3 0 7 1.1904 4 -30
15 21 2 1 5 1.6325 -2 9 35 4 2 0 1.1726 1 -12
16 55 3 1 2 1.5917 -0 2 36 14 2 2 8 1.1283 1 -5
17 9 3 0 3 1.5867 -6 23 37 5 2 1 9 1.1123 -2 22
18 30 2 2 4 1.5530 0 -1 38 5 4 1 5 1.1100 -0 1
19 - 1 0 7 1.5530 8 -35
20 14 3 2 1 1.4424 -1 3
  
```

Fig. 14. Results of cell parameter calculation with index, observed d values, differences between observed and calculated d (x 0.0001) and 2θ (x 0.001) values.

FILE NAME = SCH-1

ID DATA= 36

```

1: MINERAL NAME = SCHEELITE
2: CHEMICAL FORMULA = CaWO4
3: CRYSTAL SYSTEM = Tetragonal
4: SPACE GROUP = 141/a
5: Z-NUMBER = 2
6: CELL PARAMETER
   a = 5.24324( 13)  b = 5.24324( 13)  c = 11.37376( 42)
   α = 90.000( 0)  β = 90.000( 0)  γ = 90.000( 0)
7: MEASUREMENT METHOD = GUINIER
8: INTERNAL STANDARD = SILICON
9: RADIATION = CuKα1 (1.540598 Å)
10: SPECIMEN = SYNTHETIC SAMPLE
11: REMARK = REF JCPDS 7-210
  
```

```

1: INDEXING AND CALCULATION
2: CHANGE OF INITIAL DATA
3: DATA PRINT BY PRINTER
4: TYPE OF d-LIST
5: RECALCULATION OF PEAKS
6: PROGRAM END
   JOB NO =
  
```

Fig. 15. Refined cell parameters and given crystal data, and the selection messages for procedure in XRPD-V3 program.

Table 4. Cell parameter calculation result with crystal data and X-ray powder diffraction data compared with observed and calculated d - and 2θ values

CELL PARAMETER CALCULATION PRG = VER-3

FILE NAME * SCH-1
 MINERAL NAME * SCHEELITE FORMULA = CaWO₄
 MEASUREMENT * GUINIER (STD: SILICON)
 RADIATION * CuK α 1 (1.540588 A)
 SPECIMEN * SYNTHETIC SAMPLE
 REMARK * REF JCPDS 7-210

CRYSTAL SYSTEM = Tetragonal SPACE GROUP = I41/a Z = 2
 CELL PARAMETERS
 $a = 5.24324(13)$ A $b = 5.24324(13)$ A $c = 11.37376(42)$ A
 $\alpha = 90.00000(0)^\circ$ $\beta = 90.00000(0)^\circ$ $\gamma = 90.00000(0)^\circ$ $V = 312.682(27)$

No	h	k	l	d(obs)	d(calc)	Δd	2θ obs	2θ calc	$\Delta 2\theta$	
1	70.4	1	0	1	4.7606	4.7616	-0.0010	18.623	18.820	0.004
2	100.0	1	1	2	3.1071	3.1058	0.0013	28.709	28.721	-0.012
3	41.5	1	0	3	3.0731	3.0722	0.0009	29.033	29.041	-0.009
4	28.2	0	0	4	2.8447	2.8434	0.0012	31.422	31.438	-0.014
5	43.9	2	0	0	2.6216	2.6216	-0.0000	34.175	34.174	0.001
6	1.6	2	0	2	2.3808	2.3808	-0.0001	37.758	37.755	0.001
7	37.2	2	1	1	2.2965	2.2966	-0.0001	39.197	39.196	0.001
8	5.3	1	1	4	2.2567	2.2563	0.0004	39.917	39.925	-0.008
9	9.0	1	0	5	2.0865	2.0868	-0.0003	43.331	43.323	0.007
10	20.9	2	1	3	1.9939	1.9942	-0.0003	45.452	45.444	0.008
11	52.8	2	0	4	1.9273	1.9274	-0.0001	47.116	47.113	0.003
12	34.8	2	2	0	1.8537	1.8538	-0.0000	49.106	49.106	0.001
13	8.7	3	0	1	1.7270	1.7275	-0.0004	52.978	52.963	0.014
14	33.4	1	1	6	1.6879	1.6878	0.0001	54.305	54.309	-0.004
15	20.7	2	1	5	1.6325	1.6327	-0.0002	56.308	56.301	0.007
16	55.5	3	1	2	1.5917	1.5918	-0.0000	57.885	57.884	0.002
17	9.1	3	0	3	1.5867	1.5872	-0.0006	58.089	58.066	0.023
18	30.1	2	2	4	1.5530	1.5529	0.0001	59.474	59.477	-0.002
19	13.5	3	2	1	1.4424	1.4425	-0.0001	64.557	64.554	0.003
20	5.1	0	0	8	1.4217	1.4217	0.0000	65.613	65.614	-0.001
21	7.3	3	0	5	1.3859	1.3859	-0.0000	67.534	67.533	0.002
22	16.1	3	2	3	1.3577	1.3578	-0.0001	69.133	69.129	0.005
23	9.7	2	1	7	1.3355	1.3355	0.0000	70.448	70.448	-0.000
24	11.1	4	0	0	1.3109	1.3108	0.0001	71.974	71.981	-0.007
25	9.5	4	1	1	1.2639	1.2638	0.0001	75.100	75.108	-0.009
26	18.8	2	0	8	1.2499	1.2498	0.0001	76.080	76.100	-0.010
27	30.4	3	1	6	1.2480	1.2480	-0.0000	76.228	76.227	0.001
28	4.6	1	0	9	1.2286	1.2286	0.0001	77.653	77.657	-0.004
29	5.8	3	2	5	1.2251	1.2252	-0.0001	77.916	77.907	0.009
30	17.5	3	3	2	1.2077	1.2077	0.0001	79.259	79.263	-0.004
31	8.8	4	1	3	1.2056	1.2057	-0.0001	79.426	79.420	0.005
32	21.7	4	0	4	1.1904	1.1904	0.0000	80.643	80.645	-0.002
33	17.1	4	2	0	1.1726	1.1724	0.0001	82.133	82.145	-0.012
34	13.9	2	2	8	1.1293	1.1281	0.0001	86.116	86.126	-0.011
35	5.4	2	1	9	1.1123	1.1125	-0.0002	87.659	87.644	0.015
36	4.8	4	1	5	1.1100	1.1100	0.0000	87.868	87.890	-0.001

$\sigma 2\theta = 0.008$

8. Reading and measurement errors

Estimations of measurement errors in this system are carried out using same Guinier films, and Guinier films obtained by same sample but different treatments.

8.1. Reading errors

Guinier films for scheelite and quartz samples obtained by the same method mentioned above. Same X-ray films for scheelite and quartz are reading and calculation by this system. Results for 5 times reading of scheelite are shown in Table 5. Value for a and c axis is in the range from 5.2431 to 5.2433 and from 11.3736 to 11.3738, respectively. These differences are within ± 0.0002 corresponding to stan-

Table 5. Cell parameters calculated from same film for scheelite

Reading	a(Å)	c(Å)
SCH-1 A	5.2431 (1)	11.3736 (2)
SCH-1 B	5.2432 (1)	11.3736 (2)
SCH-1 C	5.2432 (1)	11.3738 (2)
SCH-1 D	5.2433 (1)	11.3736 (3)
SCH-1 E	5.2431 (1)	11.3737 (2)
Average	5.2432 (2)	11.3737 (3)

Table 6. Cell parameters calculated from same film for quartz sample

Reading	a(Å)	c(Å)
BZ-1 A	4.9122 (1)	5.4034 (2)
BZ-1 B	4.9121 (1)	5.4033 (2)
BZ-1 C	4.9121 (1)	5.4032 (2)
BZ-1 D	4.9121 (1)	5.4033 (2)
BZ-1 E	4.9123 (1)	5.4033 (2)
Average	4.9122 (1)	5.4033 (2)

standard deviations for each result. Those for quartz given in Table 5 are about same result for scheelite. Then, the reading error is negligible because it is thought to be about same value of the standard deviations for each reading.

8.1. Measurement errors

The X-ray powder diffraction films for same sample prepared with another treatment are obtained to estimation the errors caused by the taking, reading and calculation method. Results for 5 time treatment of same quartz sample as given Table 6 are shown in Table 7.

Values for a and c axis are almost same to different reading values given in Table 6, and these values are included in standard errors for each measurement.

From these results mentioned above, errors caused by sample preparation, film treatment, reading and calculation methods consider to be negligible, and accuracy of cell parameters obtained by one time measurement is within its standard deviations.

Table 7. Cell parameters calculated from different films for same quartz sample

Film No	a(Å)	b(Å)
BZ-1	4.9122 (1)	5.4033 (2)
BZ-2	4.9120 (1)	5.4033 (2)
BZ-3	4.9122 (1)	5.4034 (3)
BZ-4	4.9121 (1)	5.4031 (3)
BZ-5	4.9122 (1)	5.4035 (3)
Average	4.9122 (2)	5.4033 (2)

References

- Howard, S. A. and Preston, K. D. (1989) Profile fitting of powder diffraction patterns. In *Modern Powder Diffraction*, ed. Bish, D. L. & Post, J. E.; *Reviews in Mineralogy Vol. 20*, Miner. Soc. Amer., Washington, pp. 217-275.
- Jenkins, R. (1989) Instrumentation. In *Modern Powder Diffraction*, ed. Bish, D. L. & Prost, J. E.; *Reviews in Mineralogy Vol. 20*, Miner. Soc. Amer., Washington, pp. 19-45.
- Malmros, G. and Thomas, J. O. (1977) Least-squares structure refinement based on profile analysis of powder film intensity data measured on an automatic microdensitometer. *Jour. Appl. Cryst.*, **10**, 7-11.
- Sonneveld, E. and Visser, J. W. (1975) Automatic collection of powder data from photographs. *Jour. Appl. Cryst.*, **8**, 1-7.
- Smith, D. K. (1989) Computer analysis of diffraction data. In *Modern Powder Diffraction*, ed. Bish, D. L. & Prost, J. E.; *Reviews in Mineralogy Vol. 20*, Miner. Soc. Amer., Washington, pp. 183-216.

Appendix

The name of space group and its symmetry operation code of the cubic, tetragonal, hexagonal, and orthorhombic, monoclinic and triclinic systems stored in the "XRPD-V3" program is Appendix 1. Another space group names are not stored. If using another space group name, "XRPD-V3" program should be necessary changed.

Appendix 1. Symbol for the space group using the "XRPD-V3"
program and their symmetry code

CUBIC SYSTEM						
P,	0,0,0,0	I,	2,3,3,1	F,	3,4,3,1	
P23,	0,0,0,0	Fm3,	0,0,0,0			
P213,	0,0,0,1					
Pn3,	0,3,0,1					
Pa3,	0,0,0,1					
I23,	2,3,0,1	Im3,	2,3,0,1			
I213,	2,3,0,1					
Ia3,	2,4,0,1					
F23,	3,4,0,1	Fm3,	3,4,0,1			
Fd3,	3,5,0,2					
P4-3m,	0,0,0,0	P432,	0,0,0,0	Fm3m,	0,0,0,0	
P4132,	0,0,0,2	P4332,	0,0,0,2			
P4232,	0,0,0,1					
P4-3n,	0,0,1,1	Fm3n,	0,0,1,1			
Pn3n,	0,3,0,1					
Pn3n,	0,3,1,1					
I4-3m,	2,3,1,1	I432,	2,3,1,1	Im3m,	2,3,1,1	
I4132,	2,3,1,2					
I4-3d,	2,3,2,2					
Ia3d,	2,4,2,2					
F4-3m,	3,4,3,1	F432,	3,4,3,1	Fm3m,	3,4,3,1	
F4132,	3,4,3,2					
F4-3c,	3,4,4,1	Fm3c,	3,4,4,1			
Fd3m,	3,5,3,2					
Fd3c,	3,5,4,2					
TETRAGONAL SYSTEM						
P,	0,0,0,0,0,0	I,	2,3,3,1,1,1			
P4-	4,4,4,4,1,1	P4,	0,0,0,0,0,0	P4/m,	0,0,0,0,0,0	
P42,	0,0,0,0,0,1	P42/m,	0,0,0,0,0,1			
P41,	0,0,0,0,0,2	P43,	0,0,0,0,0,2			
P4/n,	0,3,0,0,1,0					
P42/N,	0,3,0,0,1,1					
I4-	2,3,3,0,1,1	I4,	2,3,3,0,1,1	I4/m,	2,3,3,0,1,1	
I41,	2,3,3,0,1,2					
I41/a,	2,4,3,0,1,2					
P4-2m,	0,0,0,0,0,0	P4-m2,	0,0,0,0,0,0	P4mm,	0,0,0,0,0,0	
P422,	0,0,0,0,0,0	P4/mmm,	0,0,0,0,0,0			
P4222,	0,0,0,0,0,1					
P4122,	0,0,0,0,0,2	P4322,	0,0,0,0,0,2			
P4-21m,	0,0,0,0,1,0	P4212,	0,0,0,0,1,0			
P42212,	0,0,0,0,1,1					
P41212,	0,0,0,0,1,2	P43212,	0,0,0,0,1,2			
P4-2c,	0,0,0,1,0,1					
P42mc,	0,0,0,1,0,1	P42/mmc,	0,0,0,1,0,1			
P4-21c,	0,0,0,1,1,1					
P4-b2,	0,0,1,0,1,0	P4bm,	0,0,1,0,1,0	P4/nbm,	0,0,1,0,1,0	
P42bc,	0,0,1,1,1,1	P42/nbc,	0,0,1,1,1,1			
P4-c2,	0,0,2,0,0,1					
P42cm,	0,0,2,0,0,1	P42/mcm,	0,0,2,0,0,1			
P4cc,	0,0,2,1,0,1	P4/mcc,	0,0,2,1,0,1			
P4-n2,	0,0,3,0,1,1					
P42nm,	0,0,3,0,1,1	P42/nmm,	0,0,3,0,1,1			
P4nc,	0,0,3,1,2,1	P4/mnc,	0,0,3,1,1,1			
P4/nmm,	0,3,0,0,1,0					
P42/nmc,	0,3,0,1,1,1					
P4/nbm,	0,3,1,0,1,0					
P42/nbc,	0,3,1,1,1,1					
P42/ncm,	0,3,2,0,1,1					
P42/ncc,	0,3,2,1,1,1					
P42/nnm,	0,3,3,0,1,1					
P4/nnc,	0,3,3,1,1,1					
I4-2m,	2,3,3,1,1,1	I4mm,	2,3,3,1,1,1			
I422,	2,3,3,1,1,1	I4/nmm,	2,3,3,1,1,1			
I4122,	2,3,3,1,1,2					
I4-2d,	2,3,3,2,1,2					
I41md,	2,3,3,2,1,2					
I4-c2,	2,3,4,1,1,1	I4cm,	2,3,4,1,1,1	I4/ncc,	2,3,4,1,1,1	
I41cd,	2,3,4,2,1,2					
I41amd,	2,4,3,2,1,2					
I41/acd,	2,4,4,2,1,2					

Appendix 1. (Continued)

HEXAGONAL SYSTEM

P	0,0,0	R	1,0,2		
P3	0,0,0	P3-	0,0,0		
P31	0,0,2	P32	0,0,2		
R3	1,0,2	R3-	1,0,2		
P3m1	0,0,0	P321	0,0,0	P3-m1	0,0,0
P3121	0,0,2	P3221	0,0,2		
P3c1	0,0,1	P3-c1	0,0,1		
P31m	0,0,0	P312	0,0,0	P3-1m	0,0,0
P31c	0,1,1	P3-1c	0,1,1		
R3m	1,2,2	R3-m	1,2,2	R32	1,2,2
R3c	1,2,3	R3-c	1,2,3		
P6	0,0,0	P6-	0,0,0	P6m	0,0,0
P61	0,0,3	P65	0,0,3		
P62	0,0,2	P64	0,0,2		
P63	0,0,1	P63/m	0,0,1		
P6-m2	0,0,0	P6-2m	0,0,0	P6mm	0,0,0
P622	0,0,0	P6/mmm	0,0,0		
P6122	0,0,3	P6522	0,0,3		
P6222	0,0,2	P6422	0,0,2		
P6322	0,0,1				
P6-c2	0,0,1	P63cm	0,0,1	P63/mcm	0,0,1
P6-2c	0,1,1	P63mc	0,1,1	P63/mmc	0,1,1
P6cc	0,1,1	P63/mcc	0,1,1		

TRICLINIC SYSTEM

P1	0,0,0,0,0,0,0	P1-	0,0,0,0,0,0,0		
----	---------------	-----	---------------	--	--

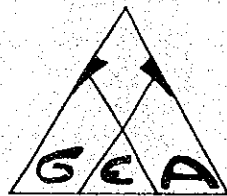
MONOCLINIC SYSTEM

Pm	0,0,0,0,0,0,0	P2	0,0,0,0,0,0,0	P2/m	0,0,0,0,0,0,0
P21	0,0,0,0,0,1,0	P21/m	0,0,0,0,0,1,0		
Pc	0,0,2,0,0,0,1	P2/c	0,0,2,0,0,0,1		
P21/c	0,0,2,0,0,1,1				
P21/a	0,0,1,0,1,1,0	C2	1,1,1,3,1,1,0	C2/m	1,1,1,3,1,1,0
Cm	1,1,1,3,1,1,0	C2/c	1,1,4,3,1,1,1		
Cc	1,1,4,3,1,1,1				

ORTHORHOMBIC SYSTEM

Pmm2	0,0,0,0,0,0,0	P222	0,0,0,0,0,0,0	Pmmm	0,0,0,0,0,0,0
P2221	0,0,0,0,0,0,1				
P21212	0,0,0,0,1,1,0				
P212121	0,0,0,0,1,1,1	Pbam	0,1,1,0,1,1,0		
Pba2	0,1,1,0,1,1,0				
Pban	0,1,1,3,1,1,0				
Pbca	0,1,2,1,1,1,1	Pcmm	0,2,0,0,0,0,1		
Pbcn	0,1,2,3,1,1,1				
Pc2m	0,2,0,0,0,0,1				
Pmma	0,0,0,1,1,0,0	Pccm	0,2,2,0,0,0,1		
Pcm21	0,2,0,0,0,0,1				
Pcam	0,2,1,0,1,0,1				
Pca21	0,2,1,0,1,0,1				
Pcc2	0,2,2,0,0,0,1				
Pcca	0,2,2,1,1,0,1				
Pccn	0,2,2,3,1,1,1				
Pmmm	0,3,0,0,0,1,1	Pncm	0,3,2,0,0,1,1		
Pnm21	0,3,0,0,0,1,1	Pnmm	0,3,3,0,1,1,1		
Pnam	0,3,1,0,1,1,1				
Pna21	0,3,1,0,1,1,1				
Pnc2	0,3,2,0,0,1,1				
Pbnm	0,1,3,0,1,1,0				
Pnn2	0,3,3,0,1,1,1				
Pnna	0,3,3,1,1,1,1				
Pnna	0,3,3,3,1,1,1				
Cmm2	1,1,1,3,1,1,0	Cm2m	1,1,1,3,1,1,0		
C222	1,1,1,3,1,1,0	Cmmm	1,1,1,3,1,1,0		
C2221	1,1,1,3,1,1,1				
C2ma	1,1,1,4,1,1,0	Cmma	1,1,1,4,1,1,0		
C2cm	1,1,4,3,1,1,1	Cmca	1,1,4,3,1,1,1		
Cmc21	1,1,4,3,1,1,1				
C2ca	1,1,4,4,1,1,1	Cmca	1,1,4,4,1,1,1		
Ccc2	1,4,4,3,1,1,1	Cccm	1,4,4,3,1,1,1		
Ccca	1,4,4,4,1,1,1				
Imm2	2,3,3,3,1,1,1	I222	2,3,3,3,1,1,1	Immm	2,3,3,3,1,1,1
I212121	2,3,3,3,1,1,1				
Ima2	2,3,4,3,1,1,1	Immm	2,3,4,3,1,1,1		
Iba2	2,4,4,3,1,1,1	Ibam	2,4,4,3,1,1,1		
Ibca	2,4,4,4,1,1,1				
Fmm2	3,4,4,4,1,1,1	F222	3,4,4,4,1,1,1	Fmmm	3,4,4,4,1,1,1
Fdd2	3,5,5,4,2,2,2				
Fddd	3,5,5,5,2,2,2				

Esta publicación
se terminó de imprimir
en los talleres de
EDITORA ANIBAL PINTO S.A.,
Maipú 768, Concepción,
Chile.



EDITORIA ANIBAL PINTO S.A. Maipú 769, Concepción, Chile

